The Thesis Committee for Ashley Darius Biria
certifies that this is the approved version of the following thesis:

Analytical Approach to the Design of Optimal Satellite Constellations for Space-Based Space Situational Awareness Applications

APPROVED BY

SUPERVISING COMMITTEE:

Belinda G. Marchand, Supervisor

E. Glenn Lightsey

Analytical Approach to the Design of Optimal Satellite Constellations for Space-Based Space Situational Awareness Applications

by

Ashley Darius Biria, B.S.

THESIS

Presented to the Faculty of the Graduate School of

The University of Texas at Austin

in Partial Fulfillment

of the Requirements

for the Degree of

MASTER OF SCIENCE IN ENGINEERING

THE UNIVERSITY OF TEXAS AT AUSTIN

December 2011

To my family.

Acknowledgments

First and foremost, I wish to thank my parents. The encouragement and support that they gave during my studies has proven invaluable. I am also grateful to my grandmother for her undying positive attitude and understanding. She has shaped me in innumerable ways.

I also extend my gratitude to my advisor, Dr. Belinda Marchand. Under her supervision, I gained significant experience both in the capacity of a teaching assistant and of a researcher. I have learned many life lessons from my experience working with her, and she has allowed me to cultivate many skills that I am sure will prove essential to my career and long-term goals.

I am especially grateful to those who have provided substantial candid advice over the last few years. Professor Mason Peck has lent considerable guidance and expertise that has inspired me to come as far as I have. I am also thankful to Aaron Stehura for his continual friendship and support. He has always managed to present a unique perspective on life's adversities that has invariably gotten me through many rough patches.

Additionally, I wish to thank my officemates and friends for making graduate school a more enjoyable experience. Ben Hanna and Bonnie Prado made excellent company in our little office. My thanks also go to Kevin Eckes, Ken Pesyna, John Valenta, Sarah Villarreal, and Kyle Wesson for being good friends and making life

more entertaining.

Lastly, I wish to thank a number of organizations that have funded my research. I have had the fortune of being supported by the University of Texas at Austin Department of Aerospace Engineering and Engineering Mechanics, the C. W. W. Cook Endowed Graduate Fellowship in Engineering, and by the Air Force Office of Scientific Research through the Air Force Young Investigator Award, contract #FA9550-09-1-0227.

Analytical Approach to the Design of Optimal Satellite Constellations for Space-Based Space Situational Awareness Applications

Ashley Darius Biria, M.S.E.
The University of Texas at Austin, 2011

Supervisor: Belinda G. Marchand

In recent years, the accumulation of space debris has become an increasingly pressing issue, and adequately monitoring it is a formidable task for designated ground-based sensors. Supplementing the capabilities of these ground-based networks with orbiting sensing platforms would dramatically enhance the ability of such systems to detect, track, identify, and characterize resident space objects — the primary goals of modern space situational awareness (SSA). Space-based space situational awareness (SBSSA), then, is concerned with achieving the stated SSA goals through coordinated orbiting sensing platforms. To facilitate the design of satellite constellations that promote SSA goals, an optimization approach is selected, which inherently requires a pre-defined mathematical representation of a cost index or measure of merit. Such representations are often analytically available, but when considering optimal constellation design for SBSSA applications, a closed-form expression for the cost index is only available under certain assumptions. The present

study focuses on a subset of cases that admit exact representations. In this case, geometrical arguments are employed to establish an analytical formulation for the coverage area provided as well as for the coverage multiplicity. These analytical results are essential in validating numerical approximations that are able to simulate more complex configurations.

Table of Contents

Acknowledgments **v**

Abstract **vii**

List of Tables **xii**

List of Figures **xiii**

Chapter 1. Introduction **1**

1.1 Background 3

1.1.1 Properties of Constellations 3

1.1.2 ATH Coverage 4

1.1.2.1 Single-Altitude Band Coverage 7

1.1.2.2 Dual-Altitude Band Coverage 8

1.2 Present Study 12

1.3 Thesis Organization 14

Chapter 2. Coverage Area Methodology for Constellation Design **16**

2.1 Coverage Provided by a Single Satellite 17

2.2 Computing the Total Coverage Area 20

2.3 Key Intersection Points 23

2.3.1 Type I Intersections 29

2.3.2 Type II Intersections 30

2.3.2.1 Intersections of Two Range Shells 30

2.3.2.2 Intersections of Two Tangent Lines 32

2.3.2.3 Intersections of Tangent Lines with Range Shells . . . 36

2.4 Geometrical Elements of Regions Subject to 2-fold Coverage 37

2.4.1 Composite Triangles 38

2.4.2 Convex Quadrilaterals 40

2.4.3 Composite Quadrilaterals 41
2.5 Above-the-Horizon 2-fold Coverage Area for a Constellation in a Circular Orbit 42
2.6 The Existence of Arbitrary Coverage Multiplicities 48
2.6.1 Partial Conditions on the Existence of p-fold Coverage 48
2.6.1.1 Necessary Conditions for Existence 55
2.6.1.2 Derivation of the Fundamental Necessary Condition for Existence 56
2.6.1.3 Necessary and Sufficient Conditions for Existence . . 66
2.6.1.4 Determining the Location of Q_p 67
2.6.2 Partial Conditions on the Existence of 2-fold Coverage 71

Chapter 3. Results and Validation **74**
3.1 Constraints on the Parameter Space 74
3.2 Parameter Space and Validation of Numerical Methods 75
3.3 Optimal Constellation Design 82
3.4 Multiple Independent Variables 87

Chapter 4. Conclusion **90**

Appendices **91**

Appendix A. Modified Single Satellite ATH Coverage Model **92**
A.1 Type I Shell Intersections 92
A.1.1 Intersections of Altitude Shells with the Range Shell 93
A.1.2 Intersections of Tangent Lines with Altitude Shells 93
A.1.3 Intersections of Tangent Lines with the Range Shell 94
A.2 Fundamental Geometrical Elements 94
A.2.1 Triangles 95
A.2.2 Circular Segments 95
A.2.3 Circular Sectors 95
A.2.4 Composite Teardrop Sectors 96
A.2.5 Composite Triangles 97
A.2.6 Overlap Region of Two Circles 97
A.3 Piecewise Differentiable Representation of Coverage Area $\mathbf{A}_{1\times,1}$ . . . 98

Appendix B. Details of the 22 Shape Types for $\mathbf{A}'_{2\times,12}$ **101**

Appendix C. Derivation: Determining the Location of Q_p **124**

Appendix D. Relating the 22 Shape Types to Satellite Altitude **140**

Bibliography **151**

Vita **154**

List of Tables

2.1 Definitions of Five Types of Intersections for a Single Satellite 18
2.2 Subscripts Used to Label Intersections for a Single Satellite 18
2.3 Notation for the Area of Fundamental Geometrical Elements 19
2.4 Relation between the Number of Vertices and Number of Unique Shapes for $C'_{2\times,12}$ 38
2.5 Conditions for Identifying the Overlap Region Polygon $C'_{2\times,12}$ 44
2.6 Piecewise Formulation for 2-fold Coverage Area $\mathbf{A}'_{2\times,12}$ 45
2.7 Flow Chart — Conditions for Determining the Location of Q_p, Odd $p \geq 2$ 70
2.8 Flow Chart — Conditions for Determining the Location of Q_p, Even $p \geq 2$ 71
2.9 Flow Chart — Conditions for Determining the Location of Q_p, $p = 2$ 73

A.1 Coverage Region $C_{1\times,1}$ Subcases for $r_t \leq r_s < r_l$ 98
A.2 Coverage Region $C_{1\times,1}$ Subcases for $r_l \leq r_s < r_u$ 99
A.3 Coverage Region $C_{1\times,1}$ Subcases for $r_u \leq r_s < r_{s_3}$ 99
A.4 Coverage Area $\mathbf{A}_{1\times,1}$ for $r_t \leq r_s < r_l$ 99
A.5 Coverage Area $\mathbf{A}_{1\times,1}$ for $r_l \leq r_s < r_u$ 100
A.6 Coverage Area $\mathbf{A}_{1\times,1}$ for $r_u \leq r_s < r_{s_3}$ 100

List of Figures

1.1 Differences between single- and dual-altitude band coverage[1] 6
1.2 Coverage problem for a single satellite on a circular orbit with above-the-horizon coverage area shaded yellow 10
1.3 Seven-satellite constellation on a circular orbit 13

2.1 Shell intersections for a single satellite on a circular orbit with ATH coverage area shaded yellow 17
2.2 Key shell intersections for a satellite constellation on a circular orbit 25
2.3 Collinear tangent lines for $n = 4$, $D_{\rho_j \rho_k, jk} \equiv M_{jk}$ 34
2.4 Parallel but not collinear tangent lines for $n = 8$ and $r_s = r_t$ 35
2.5 A general convex quadrilateral 40
2.6 Taxonomy of Overlap Areas $\mathbf{A}'_{2\times,12}$ 46
2.7 Taxonomy of Overlap Areas $\mathbf{A}'_{2\times,12}$ 47
2.8 Only 1-fold coverage exists: $d_{12} > 2R$ 49
2.9 Upper limit of 1-fold coverage; threshold of creation of 2-fold coverage: $d_{12} = 2R$ 50
2.10 1-fold and 2-fold coverage exist: $d_{12} < 2R$ 51
2.11 Case 1 — $|\overline{OD_{12,12}}| \geq r_u$ with $r_s < r_u$ 52
2.12 Case 2 — $|\overline{OD_{12,12}}| \geq r_u$ with $r_s > r_u$ 53
2.13 Parallel but not collinear tangent lines for $n = 2$ and $r_s = r_t$ 54
2.14 Lower limit (threshold) for $p = 2$ 58
2.15 Lower limit (threshold) for $p = 3$ 60
2.16 Lower limit (threshold) for $p = 4$ 62
2.17 Lower limit (threshold) for $p = 5$ 63

3.1 Total coverage area vs. satellite altitude (Example 1) is a continuous smooth curve: Optimal altitude corresponds to maximum coverage area 75

3.2 Total coverage area vs. satellite altitude (Example 2) is a continuous smooth curve: Maximum coverage area saturation observed at low altitudes 76
3.3 Total coverage area vs. satellite altitude (Example 3) is a continuous non-smooth curve: Global maximum exists only at the start of the altitude range considered 77
3.4 Example 4: Total coverage area vs. satellite altitude 78
3.5 Total coverage area vs. satellite altitude 79
3.6 Total coverage area vs. satellite altitude 80
3.7 Total coverage area vs. satellite altitude 81
3.8 Minimum number of satellites vs. satellite altitude 83
3.9 Maximum total coverage area vs. satellite altitude for the minimum number of satellites 85
3.10 Percent relative error in maximum total coverage area vs. satellite altitude for the minimum number of satellites 86
3.11 Example 1: $h_t = 100$ km, $h_l = 1400$ km, $R = 100$ km, $n = 6$ 88
3.12 Example 2: $h_t = 100$ km, $h_l = 1400$ km, $h_u = 1500$ km, $n = 6$ 89

B.1 Case 2 102
B.2 Case 3.i 103
B.3 Case 3.ii 104
B.4 Case 3.iii.a 105
B.5 Case 3.iii.b 106
B.6 Case 4.i.a 107
B.7 Case 4.i.b 108
B.8 Case 4.ii 109
B.9 Case 4.iii.a 110
B.10 Case 4.iii.b 111
B.11 Case 5.i.a 112
B.12 Case 5.i.b 113
B.13 Case 5.ii.a 114
B.14 Case 5.ii.b 115
B.15 Case 5.iii 116
B.16 Case 6.i.a 117

B.17 Case 6.i.b 118
B.18 Case 6.ii 119
B.19 Case 6.iii 120
B.20 Case 7.i 121
B.21 Case 7.ii 122
B.22 Case 8 123

C.1 For odd p, shows tangent lines associated with $D_{21,\iota\kappa}$, which moves first down the $\hat{\mathbf{y}}$-axis and then up the $\hat{\mathbf{y}}$-axis as p increases ($n = 25$) 125
C.2 Evidence that $D_{21,\iota\kappa}$ does not monotonically increase along the $\hat{\mathbf{y}}$-axis as p increases ($n = 25$, odd p) 127
C.3 Depiction of point $P_{2,12}$ with $y_{P_{2,12}} \geq r_s$ and $|\overline{P_{2,12}S_2}| < |\overline{S_1S_2}| < R$. 132
C.4 Depiction of point $P_{2,12}$ with $y_{P_{2,12}} < r_s$ and $|\overline{P_{2,12}S_2}| < R < |\overline{S_1S_2}|$. 133

D.1 Total coverage area vs. satellite altitude, five new cases: 3.iii.b, 5.ii.b, 6.i.b, 4.ii, 3.i 141
D.2 Total coverage area vs. satellite altitude, two new cases: 6.i.a, 3.ii . . 142
D.3 Total coverage area vs. satellite altitude, three new cases: 4.i.a, 6.ii, 8 143
D.4 Total coverage area vs. satellite altitude, two new cases: 4.iii.a, 2 . . 144
D.5 Total coverage area vs. satellite altitude, one new shape: 4.i.b 145
D.6 Total coverage area vs. satellite altitude, three new cases: 3.iii.a, 5.iii, 7.i 146
D.7 Total coverage area vs. satellite altitude, two new cases: 4.iii.b, 5.i.b 147
D.8 Total coverage area vs. satellite altitude, two new cases: 5.i.a, 6.iii . 148
D.9 Total coverage area vs. satellite altitude, one new shape: 7.ii 149
D.10 Total coverage area vs. satellite altitude, one new shape: 5.ii.a . . . 150

Chapter 1

Introduction

Since 1957, the ground-based Space Surveillance Network (SSN) has been monitoring near-Earth space objects in an effort to provide a sense of space situational awareness (SSA). Unfortunately, the increasingly cluttered state of this region of space is taxing the already limited capabilities of these ground-based sensors. ~~They fail under a number of circumstances, such as under poor atmospheric conditions or when viewing small or distant objects.~~ As currently envisioned, space-based space situational awareness (SBSSA) overcomes these inadequacies by employing a network of space-based sensors to supplement ground sensing capabilities in the detection, tracking, identification, and characterization (DTI&C) of active or passive resident space objects (RSOs). ~~Such a group of artificial satellites working in concert to achieve some common goal is also called a satellite constellation, of which there are many types and applications.~~

Satellite constellations that meet SBSSA objectives are markedly different from traditional ones. Early on, constellations were designed to act as Earth communication networks and were thus concerned with providing partial or complete Earth coverage. The widely-used streets-of-coverage technique, proposed by David Lüders, was developed with this objective in mind, and is one of the first documented methods for constellation design.[2] The Earth coverage problem falls under

the purview of below-the-horizon (BTH) coverage — the term used to describe the type of coverage provided by a constellation for which the region of interest lies below the horizon of each satellite. It also implies that the region of interest is viewed against an Earth background. For example, any space-based global navigation satellite system (GNSS), such as the Global Positioning System (GPS), is concerned with BTH coverage. But applications of BTH coverage are not limited to navigation. The Tracking and Data Relay Satellite System (TDRSS) is a communications network designed for continuous global coverage, but it is used to relay information between Earth and spacecraft in low Earth orbit (LEO), which is different from traditional networks that simply link points on Earth. The novel contribution of TDRSS is its capability to increase the window of communication between Earth and other spacecraft. With TDRSS, a spacecraft can communicate with Earth for approximately 85 to 100 percent of its orbit, whereas before TDRSS, communication was only possible for less than 15 percent of each orbit.[3]

But what if, instead of providing continuous global coverage, TDRSS were designed to provide continuous coverage of the region in LEO in which the satellites of interest reside? What if a constellation's objective were to provide coverage of a region in space instead of a region on the ground? Such a constellation would be especially useful if atmospheric interference prevented the sensors from looking toward the Earth or if they were used to sense objects that were too small or far away for a ground-based sensor to detect. This alternative type of coverage is called above-the-horizon (ATH) coverage — that provided by a constellation for which the region of interest lies above the horizon of each satellite. ATH coverage implies

that the region of interest is viewed against a space background, in contrast to BTH coverage, where the region of interest is viewed against an Earth background. Above-the-horizon coverage is the focus of this work.

1.1 Background

This thesis examines a specific ATH coverage problem, and to make it tractable analytically, a number of simplifying assumptions must be made. To put these in context, it is necessary to become acquainted with common constellation design variables before discussing different types of ATH coverage.

1.1.1 Properties of Constellations

Constellation design is subject to considerations both regarding the individual constituent satellite trajectories and also the collective performance of the group of satellites. The number of satellites and their relative orbital arrangements are clear design parameters, but their ideal values are unique to a given application. Indeed, a constellation designed to meet the goals of one mission may prove to be inadequate in meeting the goals of another. Russia's geographic location necessitated particularly high elliptical orbits for their desired communications network to have good coverage, leading to the Molniya satellites.[4] For its application to navigation, GPS was required to have four satellites visible to any object on the ground at any time in order to determine the target's position and velocity — an entirely different design objective that stemmed an entirely different constellation.[5] Such a desired coverage multiplicity — the number of satellites that can simultaneously

view a particular region — is an essential design specification for any constellation, usually ensured for some high-level mission requirement.

There are copious considerations to make in the design of a constellation, and many trade-offs. The total number of satellites is the primary cost and coverage driver.[4] But other design variables significantly impact coverage as well, such as the constellation pattern, the number of orbital planes, and the satellite altitudes. Altitude, naturally, directly affects individual satellite design, too, because with higher altitude comes increased harmful radiation from the space environment. In contrast, the drag associated with a low-altitude orbit may be undesirable.[4] Furthermore, an orbit's inclination, which is one aspect of a constellation pattern, can be tuned to achieve particular latitude coverage requirements. For BTH coverage, Draim showed that using elliptical orbits can greatly reduce the number of satellites required to achieve continuous Earth coverage,[6,7] and even for arbitrary coverage multiplicity,[8] but a benefit of elliptical orbits is yet to be demonstrated for ATH coverage.

1.1.2 ATH Coverage

For this study and earlier ones on ATH coverage, the local horizon is defined differently as compared to the traditional BTH coverage problem, where the horizon is drawn tangent to the Earth's surface. Instead, the horizon is defined relative to the so-called tangent height shell (THS), which loosely represents the atmosphere. The THS is actually sensor-specific, and is defined by a tangent height, at which the sensor to target line-of-sight (LOS) penetration of the atmosphere causes some maximum allowable sensor degradation. In this context, poor sensor performance

is caused by atmospheric interference like airglow, Earth limb, aurora, and albedo phenomena.[9] The THS serves thus as a reference surface, a sphere concentric with the Earth and whose radius exceeds the Earth's by the tangent height. The local horizon, henceforth referred to as the tangent line (TL), is an imaginary line extending from the satellite sensor and tangent to any point on the THS, so that the locus of TLs traces out a cone, termed the tangent height cone (THC). Therefore, the region of interest in BTH coverage becomes the region inside the THC, while for ATH coverage it becomes the region outside the THC. Per this definition, and as mentioned in the discussion of TDRSS, BTH coverage is not limited to ground coverage. For this reason, objects that may be visible to a satellite sensor but which lie within the THC are outside the satellite's region of regard in the ATH coverage problem. This does not mean that such an object would be invisible to the entire constellation, though, because an object below the horizon of one satellite could be above the horizon of another.

Two types of ATH coverage problems have been proposed and studied in the literature. Single-altitude band coverage is concerned with the region between the THS and some user-specified upper target altitude shell (UTAS) that is some distance above the THS. Any objects above this target altitude would be of no interest to the satellites in the constellation. Dual-altitude band coverage, which is the focus of this study, defines a second target altitude shell between the THS and UTAS, and then considers the region of interest as lying between this lower target altitude shell (LTAS) and the UTAS. Evidence of fundamental differences between single- and dual-altitude band coverage are apparent in Figure 1.1, which uses the

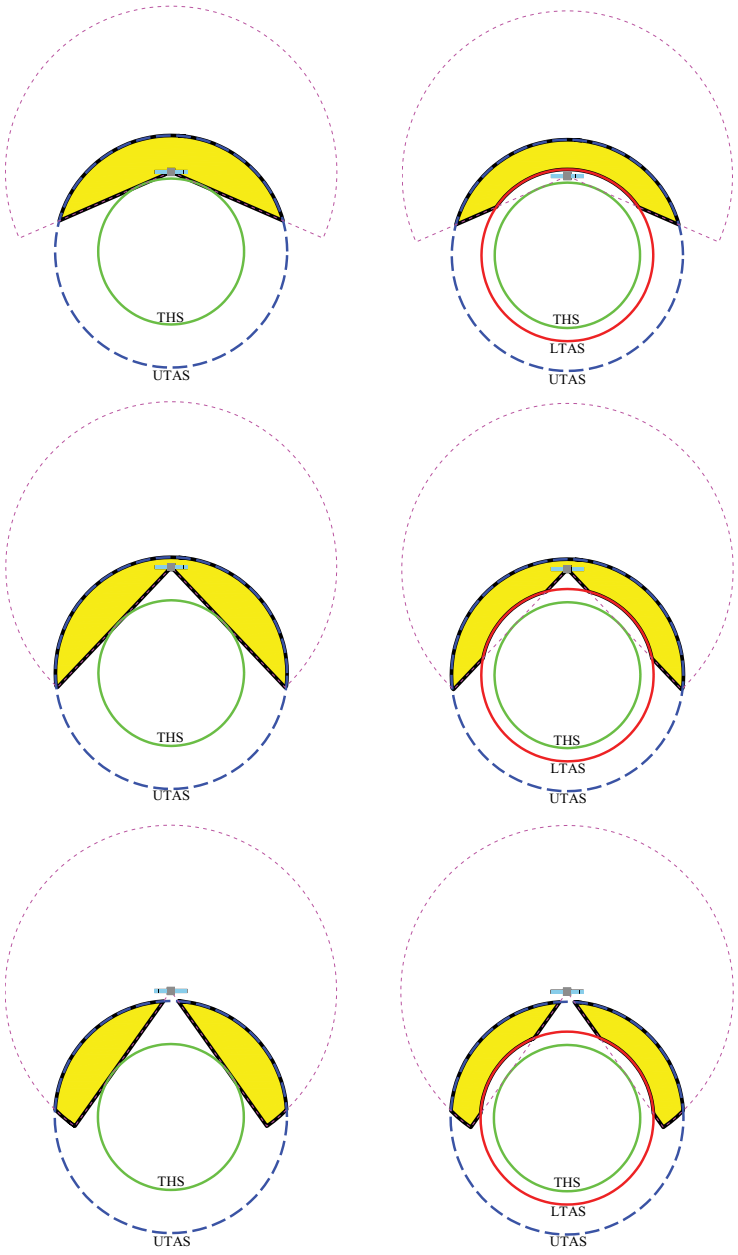

(a) Single-Altitude Band (b) Dual-Altitude Band

Figure 1.1: Differences between single- and dual-altitude band coverage[1]

example of a single satellite equipped with an omnidirectional sensor to quantify coverage as a cross-sectional area.

1.1.2.1 Single-Altitude Band Coverage

All literature examining the single-altitude band ATH coverage problem considers only satellites in circular orbits with a purely analytical approach to the constellation design process.[9–11] Most studies also restrict their analysis to symmetric orbits, in which satellites and orbital planes are equally spaced, though some results can be found on nonsymmetric satellite distributions. Many implement and discuss the effects of latitude constraints as well.

Beste[12] is the first to solve a constellation design problem where the desired coverage region is of some spherical shell concentric with the Earth, specified by some altitude range. It is similar to the single-altitude band ATH coverage problem in terms of the geometry of the region to be covered, except it appears that his solution used BTH coverage in a fashion akin to that of TDRSS.

Rider's[9] treatment only considers single and double continuous global coverage with satellites symmetrically distributed along a circular orbit in the equatorial plane. In the study requiring at least single coverage, Rider presents an optimal six-satellite and an optimal eight-satellite constellation, each with continuous single coverage on the equator and increasing coverage multiplicity with increasing latitude. These constellations are optimal in the sense that for a fixed number of satellites, the constellation has minimal values of target altitude and satellite altitude.

Hanson and Linden[10] restrict their investigation to single ATH coverage, where the satellites are constrained to circular orbits at the same altitude and inclination. Their approach examined the meshing of coverage circles of satellites in one orbital plane or between multiple orbital planes, forming "streets of coverage" — essentially lanes of continuous coverage. By using a streets-of-coverage approach,[2,13] they show that constellations with nonsymmetric satellite placement can also be modeled analytically. As such, this work is an extension of that put forth by Adams and Rider.[13] One interesting finding of this study was that the Walker delta constellations[14] serve as a good benchmark for single ATH coverage constellation design, even though the delta constellation is optimized for double BTH coverage. In several but not all examples, Hanson and Linden were able to improve on the delta constellation for single ATH coverage in the sense that fewer satellites were actually necessary than a delta constellation would suggest.

1.1.2.2 Dual-Altitude Band Coverage

Very little research has been published on the dual-altitude band coverage problem. It was first studied by Rider,[15] who considers constellations in low to medium altitudes with multiple orbital planes, where the satellites lie within or above the dual-altitude band. In his approach, Rider uses spherical geometry and the streets-of-coverage method[2,13] to derive formulas that determine coverage multiplicity from geometrical parameters. Rider then relates coverage multiplicity to the required number of orbital planes, required number of satellites per orbital plane, and latitude constraints. Thus, given a desired coverage multiplicity, the required

number of sensors for global coverage is completely determined.

Marchand and Kobel[16] proposed an entirely different approach that actually quantifies the coverage provided by a constellation analytically, so that the ultimate constellation that provides the desired coverage is designed by a numerical optimization process instead of by a set of specialized equations. One of the most difficult aspects of this problem is the definition of the cost index, namely the coverage provided by the sensors. As demonstrated by Marchand and Kobel[16] in their initial study, even under extremely simplified assumptions, such as omnidirectional sensors, obtaining a closed-form representation of the cost index is a complex process. Figure 1.2 illustrates the relevant problem geometry in the single satellite case studied by Marchand and Kobel.[16]

The three concentric circles that surround the Earth in Figure 1.2 represent reference boundaries. The region of interest to the sensors lies outside the THC, within the sensor range shell (RS), and inside the region between the UTAS and LTAS. This region represents a three-dimensional volume, and the constellation's goal is to maximize coverage of this region. Due to the inherent symmetry introduced by the omnidirectional sensor assumption, maximizing the ATH coverage volume is equivalent to maximizing the cross-sectional coverage area.[16] This cross-sectional area of coverage appears shaded yellow in Figure 1.2. Under these assumptions, a nonlinear piecewise differentiable objective function fully describes the coverage area for all possible satellite altitudes constrained to be above the tangent height and below r_{s_3}, which is associated with the critical altitude at which no ATH coverage is provided.[16]

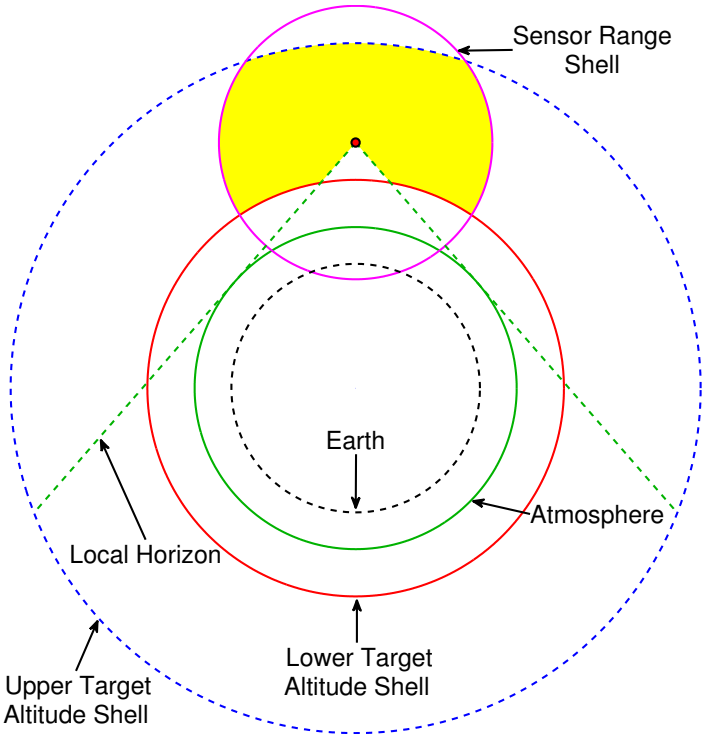

Figure 1.2: Coverage problem for a single satellite on a circular orbit with above-the-horizon coverage area shaded yellow

This initial work by Marchand and Kobel[16] is a powerful approach for the dual-altitude band problem as compared to previous research on the subject largely because their approach can be implemented numerically. Takano and Marchand[1,17] demonstrate this by using geometrical arguments similar to those first introduced by Marchand and Kobel[16] but with techniques from computational geometry. There are many advantages to this computational approach. For example, the algorithms used to solve the symmetric problem numerically are inherently valid for computing coverage area when asymmetry is introduced. A good analogy that conveys the value of computational geometry versus analytical geometry is that of numerical integration versus analytical integration. But this by no means implies that Marchand and Kobel's investigation is the end-all to the analytical method. Indeed, numerical schemes are always computationally more expensive than analytical ones, plus the work of Takano and Marchand[1,17] benefits from analytical validation. Significant insight can also be gleaned from developing the theory to analytically model the ATH coverage area provided by a constellation.

First, it is useful to understand the fundamental differences between the last three examples of previous work. Rider's approach uses purely analytical geometry to design a constellation that provides the desired coverage. Marchand and Kobel's uses purely analytical geometry to determine the quality of a given constellation, and then uses numerical optimization to design it to specifications, where a given constellation, in this case, would be an initial guess. Takano and Marchand[1,17] employ computational geometry to facilitate the determination of ATH coverage area, a process that can then be integrated with numerical optimization techniques in

a closed-loop design process. All three techniques represent important perspectives on the problem, each with its own contribution, advantages, and varying degrees of insight.

1.2 Present Study

As stated previously, this thesis presents research in the topic of SBSSA, an application of ATH coverage. The present investigation focuses specifically on a constellation of space-based sensors, uniformly distributed along a circular orbit, and is an extension of the work previously presented by Marchand and Kobel[16] for a single satellite. Consistent with the assumptions of this earlier study, the present investigation considers only the coverage of a region that exists above the horizon of the satellites and within a pre-specified altitude band. The objective is to maximize the coverage provided by the constellation sensors within the region of interest. An example of such a constellation is depicted in Figure 1.3. While a similar constellation could be designed for ATH coverage using Rider's method, the goal here is to establish a foundation for an alternative analytical approach that offers much greater flexibility and the potential to carry that flexibility through to the three-dimensional case. That is to say that in the planar case, using constellation coverage area as a design metric allows for the accommodation of a greater variety of problem specifications and constraints. First, Rider[15] did not consider satellites located between the THS and LTAS. If for some reason the satellite altitude were restricted to be below the LTAS, the coverage area approach offers a solution. Secondly, this coverage area can be used as a cost index in an optimization process that can more

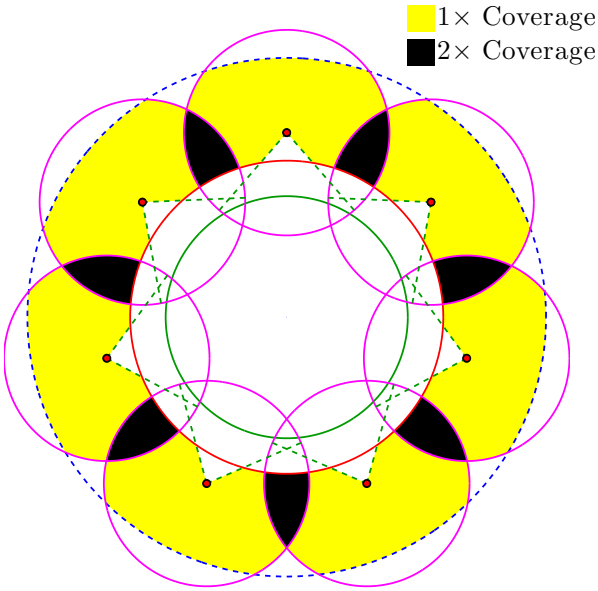

Figure 1.3: Seven-satellite constellation on a circular orbit

clearly describe and lend insight to the quality of a solution.

Of course, there are limitations to any analytical approach. If, for example, more complex sensor profiles are desired, the loss of symmetry makes an analytical solution especially difficult. For such scenarios, a more suitable approach is the numerical method proposed by Takano and Marchand.[1,17] Since their method approximates the coverage area, it benefits from validation by an analytical approach, which is demonstrated in this investigation as a secondary goal.

To maintain continuity relative to the initial work of Marchand and Kobel,[16] the methodology presented is based on geometrical arguments. First, key shell intersections are determined. Then, based on the spatial interaction of these

intersections, geometrical elements are identified for a unique region of each coverage multiplicity considered. Finally, a non-unique, nonlinear piecewise differentiable objective function is developed that characterizes the coverage area for $r_t \leq r_s < r_{s_3}$ and maximum coverage multiplicity of $p_{max} = 2$ — alternatively referred to as 2-fold or double coverage — provided by two adjacent satellites. This restriction is imposed for now because analysis becomes prohibitively complex if greater coverage multiplicities and coverage by non-adjacent satellites are permitted.

1.3 Thesis Organization

Chapter 2 begins with a brief overview of the method used by Marchand and Kobel to solve the ATH coverage problem for a single satellite. The remainder of Chapter 2 develops the theory for extending their result to constellations along with supplementary theory on coverage multiplicity, identifying 22 possible shape types of the 2-fold coverage region in the process.

The goal of Chapter 3 is two-fold: to convey clearly the capabilities of the analytical model developed thus far as well as to validate the numerical results of Takano and Marchand.[1,17] This is done primarily by comparing plots of total coverage area versus satellite altitude and the results of a simple optimal constellation design problem, though an introduction to larger parameter spaces is presented as well.

Finally, Chapter 4 presents some concluding remarks. It re-iterates important assumptions and puts findings in the context of long-term goals, ending with some suggestions for a future research direction.

The appendices provide important material that is either based on previous work or simply not inserted in the main body in the interest of being concise. Appendix A reformulates the single satellite analytical model for ATH coverage in favor of a simple objective function that is also easily compared to the original cost index proposed by Marchand and Kobel.[16] This is precisely what was implemented for this research. A collection of 22 figures corresponding to the 2-fold coverage regions with labeled vertices is given in Appendix B as a reference. Next, Appendix C contains a thorough derivation of conditions discussed in Chapter 2 regarding the existence of certain coverage multiplicities. Finally, Appendix D provides figures of analytical results illustrating how total coverage area varies with satellite altitude while indicating the 2-fold coverage region shape type at each data point.

Chapter 2

Coverage Area Methodology for Constellation Design

This chapter develops the theory and analysis required for designing constellations using ATH coverage area as a metric. The single satellite case will be presented first because the techniques employed for constellation design build on the framework developed for determining the coverage area provided by a single satellite. Since this scenario was studied extensively by Marchand and Kobel,[16] it is discussed in only enough detail so as to clearly convey the process of generalizing the single satellite analysis to a multiple satellite analysis.

Next, the coverage area model is developed for constellations, beginning with a discussion of total coverage area and assumptions on coverage multiplicity. Then, new shell intersections are defined, followed by an introduction to new geometrical elements, the development culminating in the establishment of a piecewise-smooth function for strictly 2-fold coverage area provided by multiple adjacent satellites in a single orbit. These results are used in conjunction with those of Marchand and Kobel[16] to compute the total coverage area provided by the constellation.

Finally, conditions are derived for determining the existence of arbitrary coverage multiplicities, providing a convenient way to test whether certain coverage multiplicities of interest exist. Results given here are subject to the assumption that coverage is provided only by adjacent satellites.

2.1 Coverage Provided by a Single Satellite

The simplest analyzable scenario is a single satellite on a circular orbit. Although this was thoroughly investigated by Marchand and Kobel,[16] the reader will find that reviewing this topic will facilitate the understanding of how coverage area can be computed for constellations. Figure 2.1 depicts all 14 shell intersections

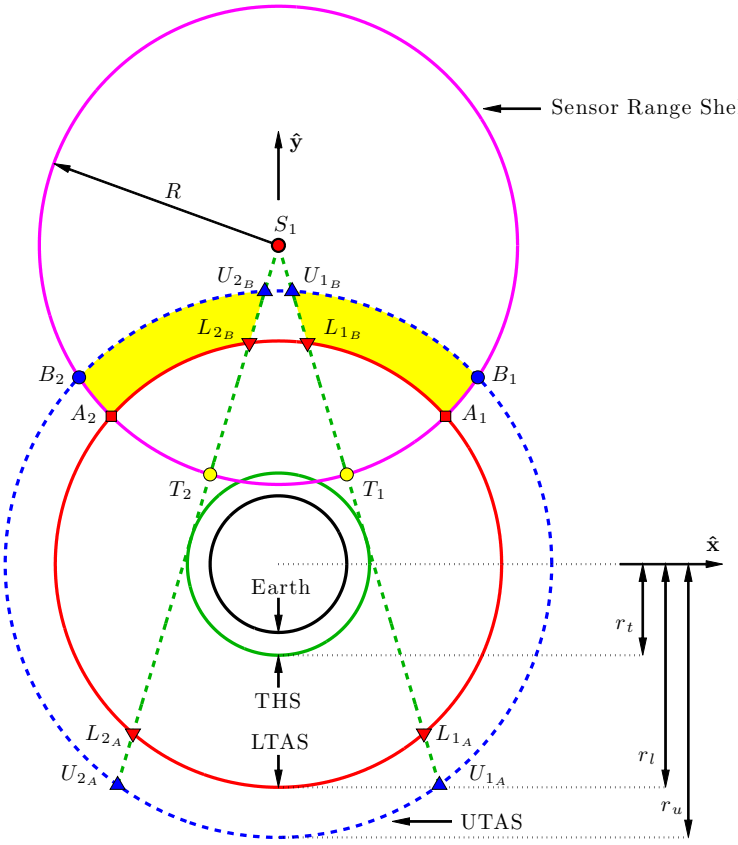

Figure 2.1: Shell intersections for a single satellite on a circular orbit with ATH coverage area shaded yellow

associated with satellite S_1, using the original notation adopted by Marchand and

Kobel, as well as the coverage area, which is shaded yellow. Each intersection point is denoted with A, B, L, U, or T, depending on the type of intersection. Table 2.1 defines each of the five types of intersections and Table 2.2 defines the possible subscripts. Notice in Figure 2.1 that each intersection point has a subscript in order to give each one a unique label. The coordinates of all 14 intersection points were

Table 2.1: Definitions of Five Types of Intersections for a Single Satellite

Name	Definition
A	Intersections of RS and LTAS
B	Intersections of RS and UTAS
L	Intersections of TL and LTAS
U	Intersections of TL and UTAS
T	Intersections of TL and RS

defined analytically by Marchand and Kobel, and are given in Appendix A in Eqs. (A.1–A.14) for easy reference.

Table 2.2: Subscripts Used to Label Intersections for a Single Satellite

Subscript	Definition
1	Intersection to the right of S_1
2	Intersection to the left of S_1
A	Intersection between a target shell and TL that is farthest from S_1
B	Intersection between a target shell and TL that is closest to S_1

Another set of results from Marchand and Kobel that are essential for the development in this thesis pertain to the fundamental shapes that comprise the coverage area: the triangle, circular segment, circular sector, composite teardrop sector, two types of composite triangle, and overlap region of two circles. These shapes are fundamental in the sense that the coverage area $\mathbf{A}_{1\times,1}$ (originally referred

to by Marchand and Kobel as "**A**" for the single satellite case) can be expressed as the area of a combination of these shapes. In other words, the region visible to the satellite can be decomposed into different sets of these geometrical elements. Table 2.3 shows the notation used for each shape, while the actual equations for calculating these areas are given in Eqs. (A.15–A.30). The subscript "AS" is an

Table 2.3: Notation for the Area of Fundamental Geometrical Elements

Name	Definition
$\mathbf{A}_{\triangle}$	Area of a triangle
$\mathbf{A}_{\Sigma}$	Area of a circular segment
$\mathbf{A}_{\pi_1}$	Area of a circular sector
$\mathbf{A}_{\pi_2}$	Area of a composite teardrop sector
$\mathbf{A}_{\Lambda_1}$	Area of a type 1 composite triangle
$\mathbf{A}_{\Lambda_2}$	Area of a type 2 composite triangle
$\mathbf{A}_{\mathrm{AS}\cap\mathrm{RS}}$	Area of an overlap region of two circles

abbreviation of "altitude shell", which can refer to the LTAS or UTAS. Effectively, this subscript, which was first proposed by Takano and Marchand,[1,17] allows for a compact way of describing the areas $\mathbf{A}_{\mathrm{LTAS}\cap\mathrm{RS}}$ and $\mathbf{A}_{\mathrm{UTAS}\cap\mathrm{RS}}$ in one function.

Ultimately, as mentioned in Chapter 1, Marchand and Kobel showed that the ATH coverage area provided by a single satellite can be expressed as a continuous piecewise differentiable function. But their representation — comprised of 18 cases — is not unique, and in fact was simplified by Takano and Marchand,[1,17] who offered a revised ATH coverage model consisting of only 12 cases. Explicit conditions for identifying each case are provided in Tables A.1–A.3. The model employed in this thesis for computing $\mathbf{A}_{1\times,1}$ is then given in Tables A.4–A.6, using a combination of the revised 12-case structure presented by Takano and Marchand[1,17] and the equations developed by Marchand and Kobel with minor adjustments.

2.2 Computing the Total Coverage Area

The computational methods employed for determining the total coverage area provided by multiple satellites build upon the work of Marchand and Kobel[16] while taking advantage of the inherent symmetry in the constellation. Recall that for the single satellite problem, the area computed for S_1 was denoted as $\mathbf{A}$ and referred to a region of 1-fold coverage. For a constellation, an analogous area exists for each satellite j subject to a coverage multiplicity $p \geq 1$, so the notation is modified to $\mathbf{A}_{1\times,j}$ and computed according to the methods described in Marchand and Kobel.[16]

Next, this notation is generalized by first defining $C_{p\times}$ as the collection of regions of coverage multiplicity greater than or equal to p that lie within the "region of interest" — that is, within the dual-altitude band, outside the THC, and within the RS. Similarly, define $C'_{p\times}$ as the collection of regions of coverage multiplicity strictly equal to p that lie within the region of interest. Then, let $\mathbf{A}_{p\times}$ refer to the area of $C_{p\times}$ and $\mathbf{A}'_{p\times}$ refer to the area of $C'_{p\times}$. In fact, $\mathbf{A}_{1\times}$ is the desired total area covered by the entire constellation within the region of interest, but computing it analytically is especially challenging.

As shown by Marchand and Kobel,[16] shell intersections are used to define the vertices of polygons, the areas of which are computed analytically by completely surveying all possible geometries that the intersections of shells could form. For a multi-satellite constellation, even though all shell intersections can be analytically determined with a few equations, the polygon identification process becomes much more cumbersome. Marchand and Kobel[16] showed that it is advantageous to compute the areas of complex geometries by adding up areas of elementary components

— triangles, composite triangles, circular sectors and segments — that are easily determined analytically. But for computing coverage area, as the single satellite case requires explicit conditions and equations for each shell configuration, the multi-satellite case requires explicit conditions and equations for each shell configuration and for each coverage multiplicity. This reasoning suggests that $\mathbf{A}_{p_c\times}$, for any coverage multiplicity p_c of interest, could be expressed as a composition of $\mathbf{A}'_{p\times}$ for all $p \in [p_c, p_{max}]$:

$$\mathbf{A}_{p_c\times} \equiv \sum_{p=p_c}^{p_{max}} \mathbf{A}'_{p\times} \tag{2.1}$$

The quantity $\mathbf{A}_{p_c\times}$ actually has many uses in formulating optimization schemes. Suppose, for example, that it is desired to have continuous 2-fold coverage of the annular region bounded by the dual-altitude band shell, termed DABS. This area is simply expressed as

$$\mathbf{A}_{\text{DABS}} = \pi(r_u^2 - r_l^2) \tag{2.2}$$

In this case, $\mathbf{A}_{2\times}$ should be as close to $\mathbf{A}_{\text{DABS}}$ as possible. For the scope of this thesis, only the total coverage area is of interest, so Eq. (2.1) would be used with $p_c = 1$. However, Eq. (2.1) does not take advantage of the results of Marchand and Kobel,[16] so an alternative approach is presented here that uses $\mathbf{A}_{1\times,j}$.

Consider summing all $\mathbf{A}_{1\times,j}$. By this action, each region $C'_{p\times}$ would be counted p times for all $p \in [2, p_{max}]$. Thus, $\mathbf{A}'_{p\times}$ must be subtracted $p-1$ times from the sum to obtain the actual total coverage area:

$$\mathbf{A}_{1\times} = \sum_{j=1}^{n} \mathbf{A}_{1\times,j} - \sum_{p=2}^{p_{max}} (p-1)\mathbf{A}'_{p\times} \tag{2.3}$$

Also, observe in Eq. (2.3) that in general, $\mathbf{A}_{1\times,j}$ could be different for each j, but since the satellites have equal range shells and are uniformly distributed along a circular orbit, the area $\mathbf{A}_{1\times,j}$ is equal for each satellite:

$$\mathbf{A}_{1\times,j} = \mathbf{A}_{1\times,1} \quad \forall\, j \tag{2.4}$$

Recall that this thesis limits the discussion of coverage area calculations to maximum coverage multiplicity $p_{max} = 2$. Let $\mathbf{A}'_{2\times,jk}$ refer to the region formed by the intersection of the range shells of S_j and S_k that is also within the region of interest and subject to strictly 2-fold coverage. Then, $\mathbf{A}'_{2\times}$ is obtained from adding up $\mathbf{A}'_{2\times,jk}$ for all j and k, leading to the following result:

$$\mathbf{A}'_{2\times} \equiv \frac{1}{2}\sum_{j=1}^{n}\sum_{\substack{k=1\\k\neq j}}^{n}\mathbf{A}'_{2\times,jk} = \sum_{j=1}^{n-1}\sum_{k=j+1}^{n}\mathbf{A}'_{2\times,jk} \tag{2.5}$$

However, due to the significant symmetry of the problem, strictly 2-fold coverage typically only occurs for pairs of adjacent satellites. As such, this observation is restated as a constraint for further simplicity. Thus, Eq. (2.5) can be re-expressed as

$$\mathbf{A}'_{2\times} = \mathbf{A}'_{2\times,1n} + \sum_{j=1}^{n-1}\mathbf{A}'_{2\times,j(j+1)} \tag{2.6}$$

or more compactly as

$$\mathbf{A}'_{2\times} = \sum_{j=1}^{n}\mathbf{A}'_{2\times,j(1+j \bmod n)} \tag{2.7}$$

Notice that for $n = 2$ or 3, satellites are adjacent for all possible pairs. As for Eq. (2.4), since the satellites have equal range shells and are uniformly distributed along a circular orbit, the overlap area $\mathbf{A}'_{2\times,jk}$ is equal for each pair of adjacent satellites. Thus, the derivation arbitrarily focuses on S_1 and S_2 without loss of

generality. Furthermore, the number of satellite pairs is equal to the number of satellites, so Eq. (2.6) becomes

$$\mathbf{A}'_{2\times} = n\mathbf{A}'_{2\times,12} \tag{2.8}$$

where

$$\mathbf{A}'_{2\times,12} = \begin{cases} \frac{1}{2}\left(\mathbf{A}_{1\times,1} \cap \mathbf{A}_{1\times,2}\right) & n = 2 \\ \mathbf{A}_{1\times,1} \cap \mathbf{A}_{1\times,2} & n > 2 \end{cases} \tag{2.9}$$

The first case in Eq. (2.9) is degenerate and differentiated from the second in order for it to function properly with Eq. (2.3). Finally, by substituting Eq. (2.8) and Eq. (2.4) into Eq. (2.3) and simplifying, Eq. (2.3) reduces to

$$\mathbf{A}_{1\times} = n\left(\mathbf{A}_{1\times,1} - \mathbf{A}'_{2\times,12}\right) \tag{2.10}$$

which in conjunction with Eq. (2.9) is used to compute the total coverage area of the constellation. In fact, much of the following discussion focuses on obtaining analytical formulas for the area defined by Eq. (2.9). The method for determining $\mathbf{A}_{1\times,1}$ is given in Appendix A.

2.3 Key Intersection Points

With the extension to satellite constellations, the original 14 key intersections derived by Marchand and Kobel[16] are still valid and are defined by the five problem parameters r_s, r_u, r_l, r_t, and R. It is useful to label the original 14 intersections as Type I, defined as those that are associated with only one satellite, occurring between the range shell and a reference boundary or between a tangent line and a reference boundary. However, the analysis is complicated by the manifestation of new intersection points associated with regions of coverage multiplicity

$p > 1$. As is evident from Figure 1.3, when multiple satellites are introduced, each satellite has associated with it these same 14 intersection points rotated through appropriate multiples of the satellite separation angle,

$$\theta_s = \frac{2\pi}{n} \tag{2.11}$$

where n, a sixth problem parameter, is the number of satellites in the constellation. In addition to these $14n$ Type I intersections, surfaces associated with one satellite intersecting those of another create new intersections denoted as Type II, which are of a variety that cannot exist in the single satellite case. These changes in geometry necessitate a modified system for labeling intersection points that is illustrated in Figure 2.2.

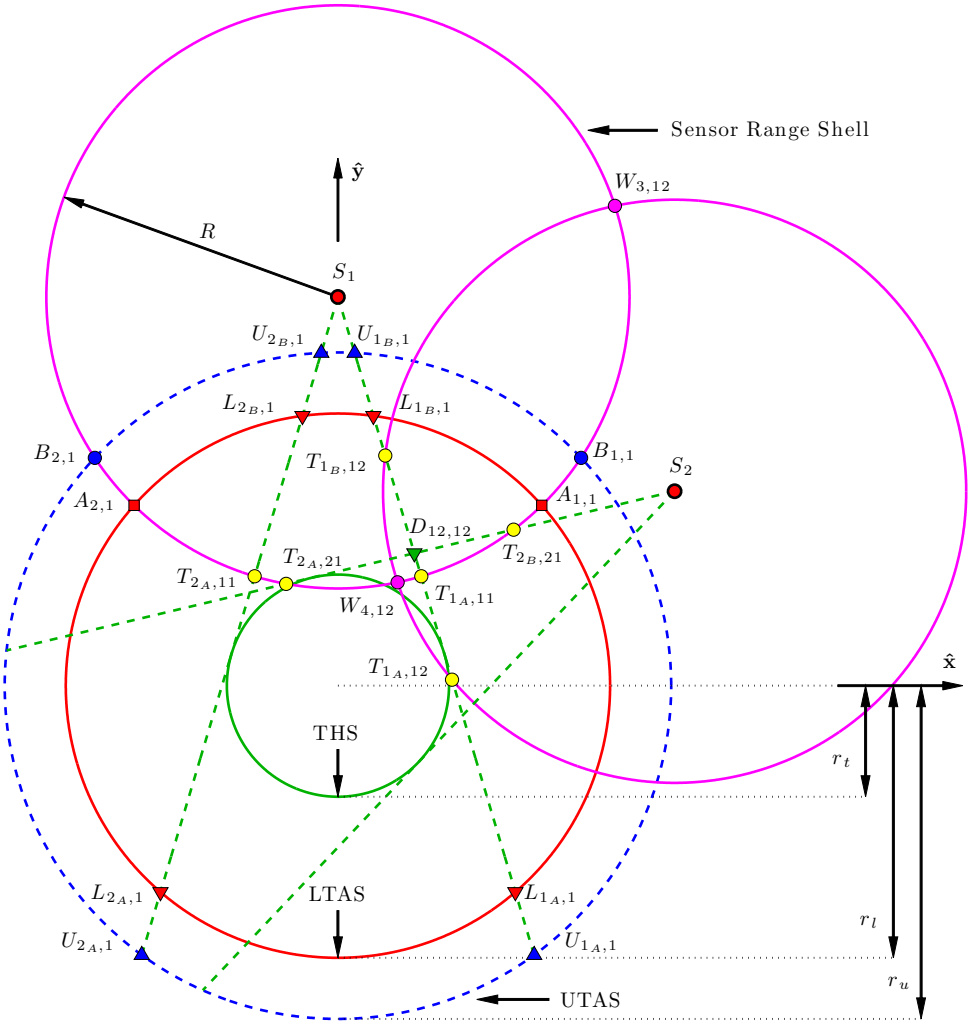

Figure 2.2: Key shell intersections for a satellite constellation on a circular orbit

The labels for Type I intersections are unchanged with two exceptions. First, at least one subscript is appended after a comma to denote the associated satellite. For example, point $B_{2,3}$ refers to point B_2 of S_3. Secondly, Type I T intersections, which involve the intersection of the TL and RS of one satellite, have a modified first

subscript to accommodate the complexity of Type II intersections. The following are sample transformations from the notation of Marchand and Kobel[16] for Type I intersections of S_1:

$$B_2 \longrightarrow B_{2,1}$$

$$T_1 \longrightarrow T_{1_A,11}$$

Unlike points A, B, L, and U, T intersections can involve two satellites, thus requiring two numbers after the comma to precisely describe which satellites are associated with that intersection. The first number after the comma refers to the satellite from which the TL originates, and the second number refers to the satellite whose RS intersects that TL. For subscripts *before* the comma, "1" and "2" still indicate intersections to the right and left of a satellite, respectively. To be precise, n rotating coordinate frames $\mathcal{E}_j$, for $j = 1, \ldots, n$, are defined as follows: $\hat{\mathbf{e}}_{2,j}$ is the unit vector directed from the center of the Earth to S_j; $\hat{\mathbf{e}}_{3,j}$ is the unit vector normal to the plane of motion of the satellite constellation, along the angular momentum vector; and $\hat{\mathbf{e}}_{1,j} = \hat{\mathbf{e}}_{2,j} \times \hat{\mathbf{e}}_{3,j}$. The origin of $\mathcal{E}_j$, indicated with an O, is located at the center of the Earth for all j. In fact, the $\mathcal{E}_1$ frame is identical to the rotating coordinate system used by Marchand and Kobel[16] and all intersections are determined relative to this coordinate system. To facilitate comparison to Marchand and Kobel,[16] a shorthand notation is therefore defined for the $\mathcal{E}_1$ unit vectors: $\hat{\mathbf{x}} = \hat{\mathbf{e}}_{1,1}$, $\hat{\mathbf{y}} = \hat{\mathbf{e}}_{2,1}$, and $\hat{\mathbf{z}} = \hat{\mathbf{e}}_{3,1}$. Thus, for all intersection points, subscript "1" refers to intersections with a positive $\hat{\mathbf{e}}_{1,j}$ component and subscript "2" refers to intersections with a negative $\hat{\mathbf{e}}_{1,j}$ component. The "A" and "B" subscripts have a similar interpretation to that used by Marchand and Kobel,[16] where "A" refers to intersections between a TL of

S_j and target shell that are farthest from S_j and "B" refers to intersections between a TL of S_j and target shell that are closest to S_j. Mathematically, these subscripts are used to distinguish between the two solutions produced by a quadratic equation, and they are added to the subscript of the T intersections because with the inclusion of Type II intersections, the quadratic equation associated with T intersections can have two valid solutions. For convenience, define the following subscripts for intersections A, B, L, U, T, W, and D:

$$\begin{aligned} \rho &\in \{1, 2\} \\ \sigma &\in \{1_A, 1_B, 2_A, 2_B\} \\ \tau &\in \{3, 4\} \end{aligned} \tag{2.12}$$

Their use is described throughout the remainder of this section. Should ρ and σ appear in the same equation, then they must be coupled and have the following special relationship:

$$\sigma \in \{\rho_A, \rho_B\} \tag{2.13}$$

In the single satellite case, the only T intersections are the result of the satellite's TL intersecting its own RS; the TL can only exit the RS because the satellite from which the TL originates is within the RS. However, with Type II intersections in a constellation, a satellite's TL can both enter and exit another's RS. Observe in Figure 2.2 that if R is increased until S_1 is within the RS of S_2, point $T_{1_B,12}$ disappears while point $T_{1_A,12}$ remains. This is a concrete scenario showing that if only one T intersection truly exists, it must have subscript "A". From this result, a convention for ambiguous cases is defined. For example, if the intersection

of a TL emanating from S_j intersects its own RS, that intersection must be $T_{1_A,jj}$ or $T_{2_A,jj}$.

There are two other intersection points to define: intersections of two range shells and intersections of two tangent lines. The former is indicated with a W and three numbers in the subscript. If the $W_{\tau,jk}$ intersection is farthest from the origin, then $\tau = 3$; if the $W_{\tau,jk}$ intersection is closest to the origin, then $\tau = 4$. The two subscripts after the comma indicate the satellites associated with the intersection, where $j < k$ by convention. The intersection of two tangent lines is marked with $D_{\rho_j\rho_k,jk}$. The ρ_j and ρ_k subscripts are equal to 1 or 2 and respectively indicate which TL of satellite j and k is associated with the intersection. For example, the intersection of the left TL of S_1 with the right TL of S_3 would be denoted as $D_{21,13}$. Again, even though $D_{12,12}$ and $D_{21,21}$ are identical, a convention is imposed such that $j < k$. Thus, $D_{12,12}$ is used to label Figure 2.2.

As in the single satellite case, the locations of these intersection points are integral to the computation of satellite coverage area. To simplify the determination of intersection points, this approach uses the same rotating coordinate system as implemented by Marchand and Kobel.[16] As depicted in Figure 2.2, the $\hat{\mathbf{y}}$-axis extends from the Earth to S_1, and the $\hat{\mathbf{x}}$-axis is perpendicular to the $\hat{\mathbf{y}}$-axis and in the plane of the orbit. This rotating coordinate system gives a simple formula for the location of the jth satellite in Cartesian coordinates as

$$(x_{s_j}, y_{s_j}) = (r_s \sin(j-1)\theta_s, r_s \cos(j-1)\theta_s) \tag{2.14}$$

where the satellites are numbered clockwise in increasing order. Thus, for a constel-

lation with positive angular momentum, S_1 can be viewed as the leading satellite.

2.3.1 Type I Intersections

Let Z be an auxiliary intersection point in the sense that

$$Z_\zeta \in \left\{ A_{\rho,j}, B_{\rho,j}, L_{\sigma,j}, U_{\sigma,j}, T_{\rho_A,jj}, T_{\sigma,jk}, W_{\tau,jk}, D_{\rho_j\rho_k,jk} \right\} \tag{2.15}$$

This definition of Z is convenient in Section 2.4 for labeling vertices of overlap areas, where its subscript ζ is simply a number for counting vertices. Then, let Z^* be an auxiliary Type I intersection point in the sense that

$$Z_j^* \in \{ A_{\rho,j}, B_{\rho,j}, L_{\sigma,j}, U_{\sigma,j}, T_{\rho_A,jj} \} \tag{2.16}$$

Since the original 14 intersections were defined relative to S_1, the correct rotation that gives the remaining $14(n-1)$ Type I intersections is analogous to that used in Eq. (2.14), which describes the location of each satellite. Thus, all Type I intersections of the constellation can be identified in the $\mathcal{E}_1$ frame as

$$\begin{bmatrix} x_{Z_j^*} \\ y_{Z_j^*} \end{bmatrix} = \begin{bmatrix} \cos(j-1)\theta_s & \sin(j-1)\theta_s \\ -\sin(j-1)\theta_s & \cos(j-1)\theta_s \end{bmatrix} \begin{bmatrix} x_{Z_1^*} \\ y_{Z_1^*} \end{bmatrix} \tag{2.17}$$

which is essentially a clockwise rotation of the input vector. For example, using the coordinates of $A_{2,1}$ as the input to Eq. (2.17), the output coordinates would be those of $A_{2,j}$. In fact, Eq. (2.14) is absorbed by Eq. (2.17) by letting $Z_j^* = S_j$. If symmetry is lost, either by uneven satellite spacing or unequal range shells, then Z_j^* locations can be determined for all j from Eqs. (A.1–A.14).

2.3.2 Type II Intersections

The remaining intersection points for a constellation of n satellites are of Type II. Recall that these include W and D intersections as well as certain T intersections. Since these intersections can be computed for an arbitrary satellite pair, there is no need to use Eq. (2.17) for Type II intersections.

2.3.2.1 Intersections of Two Range Shells

The intersections of the RS of S_j with the RS of S_k ($W_{3,jk}, W_{4,jk}$) are denoted as $W_{\tau,jk}$, and are most easily computed via the use of coordinate transformations. First, realize that the midpoint of a line connecting S_j and S_k is

$$M_{jk} = \left(\frac{x_{s_j} + x_{s_k}}{2}, \frac{y_{s_j} + y_{s_k}}{2} \right) \tag{2.18}$$

The midpoint is used in the definition of a new reference frame $\mathcal{R}_{jk}$: $\hat{\mathbf{r}}_{2,jk}$ is the unit vector directed from the center of the Earth to M_{jk}; $\hat{\mathbf{r}}_{3,jk}$ is the unit vector normal to the plane of motion of the satellite constellation, along the angular momentum vector; and $\hat{\mathbf{r}}_{1,jk} = \hat{\mathbf{r}}_{2,jk} \times \hat{\mathbf{r}}_{3,jk}$. The origin of $\mathcal{R}_{jk}$ is chosen to be at M_{jk} because this greatly simplifies the math. For W intersections, S_j has a negative $\hat{\mathbf{r}}_{1,jk}$ component and S_k has a positive $\hat{\mathbf{r}}_{1,jk}$ component by convention. A shorthand for the distance between two satellites is also defined as

$$d_{jk} = |\overline{S_j S_k}| \tag{2.19}$$

Interpreting Fewell's[18] result, the general formula for the positive solution of the intersection of two range shells with arbitrary radii is

$$\begin{aligned} x_{W_{3,jk}} &= \frac{R_j^2 - R_k^2 + d_{jk}^2}{2d_{jk}} \\ y_{W_{3,jk}} &= \frac{1}{2d_{jk}}\sqrt{2d_{jk}^2\left(R_j^2 + R_k^2\right) - \left(R_j^2 - R_k^2\right)^2 - d_{jk}^4} \end{aligned} \tag{2.20}$$

when viewed in a frame identical to the $\mathcal{R}_{jk}$ frame, but with the origin placed at S_j. Recall that the $\mathcal{R}_{jk}$ frame is defined with equal range shells in mind, so it is known that a line connecting the W intersections must pass through M_{jk}. If the range shells were to have arbitrary radii, then it would be easier to make the coordinates of the $\mathcal{R}_{jk}$ frame identical to those used by Fewell, but this generalization is not presented here. For the purposes of this study, $R_j = R_k$, so Eq. (2.20) becomes

$$^{\mathcal{R}}x_{W_{3,jk}} = 0; \qquad ^{\mathcal{R}}y_{W_{3,jk}} = \frac{1}{2}\sqrt{4R^2 - d_{jk}^2} \tag{2.21}$$

where the superscript $\mathcal{R}$ indicates that the coordinates are given in the $\mathcal{R}_{jk}$ frame. It is important to note that Eq. (2.21) is only valid if $d_{jk} \leq 2R$ so that the coordinates are real numbers. Furthermore, symmetry implies that

$$^{\mathcal{R}}x_{W_{4,jk}} = {}^{\mathcal{R}}x_{W_{3,jk}}; \qquad ^{\mathcal{R}}y_{W_{4,jk}} = -{}^{\mathcal{R}}y_{W_{3,jk}} \tag{2.22}$$

Transforming these intersections to the $\mathcal{E}_1$ frame requires both a rotation by angle η and a translation, where η is the angle between the $\hat{\mathbf{y}}$ and $\hat{\mathbf{r}}_{2,jk}$ unit vectors. Using a fundamental property of the dot product, the magnitude of this angle is given by

$$\eta = \cos^{-1}\left(\hat{\mathbf{y}} \cdot \hat{\mathbf{r}}_{2,jk}\right) \tag{2.23}$$

which enforces the condition that $0 \leq \eta \leq \pi$; however, this does not distinguish between clockwise and counterclockwise rotations and is undesirable. Thus, Eq. (2.23) is corrected by adding the following convention: $\eta > 0$ if $\hat{\mathbf{r}}_{2,jk}$ has a positive $\hat{\mathbf{x}}$ component and $\eta < 0$ if $\hat{\mathbf{r}}_{2,jk}$ has a negative $\hat{\mathbf{x}}$ component, which determines whether the appropriate rotation is clockwise or counterclockwise. Re-expressing Eq. (2.23) with this correction gives:

$$\eta = \begin{cases} +\cos^{-1}\left(\hat{\mathbf{y}} \cdot \hat{\mathbf{r}}_{2,jk}\right), & \text{if } \hat{\mathbf{x}} \cdot \hat{\mathbf{r}}_{2,jk} > 0 \\ -\cos^{-1}\left(\hat{\mathbf{y}} \cdot \hat{\mathbf{r}}_{2,jk}\right), & \text{if } \hat{\mathbf{x}} \cdot \hat{\mathbf{r}}_{2,jk} < 0 \end{cases} \tag{2.24}$$

Lastly, the translation, which is associated with the displacement between the origin of each frame, must be properly handled by shifting $x_{M_{jk}}$ in the $\hat{\mathbf{x}}$ direction and $y_{M_{jk}}$ in the $\hat{\mathbf{y}}$ direction. Then, the total transformation from the $\mathcal{R}_{jk}$ frame to the $\mathcal{E}_1$ frame is

$$^{\mathcal{E}_1}\begin{bmatrix} x_{W_{\tau,jk}} \\ y_{W_{\tau,jk}} \end{bmatrix} = \begin{bmatrix} \cos\eta & \sin\eta \\ -\sin\eta & \cos\eta \end{bmatrix} {}^{\mathcal{R}_{jk}}\begin{bmatrix} x_{W_{\tau,jk}} \\ y_{W_{\tau,jk}} \end{bmatrix} + {}^{\mathcal{E}_1}\begin{bmatrix} x_{M_{jk}} \\ y_{M_{jk}} \end{bmatrix} \tag{2.25}$$

For $\eta > 0$, the direction cosine matrix gives a counterclockwise rotation of the frame. Should $d_{jk} = 2R$, then the two range shells intersect at only one point, which is the midpoint M_{jk}.

2.3.2.2 Intersections of Two Tangent Lines

The intersections of a TL of S_j and a TL of S_k are denoted as $D_{\rho_j\rho_k,jk}$ in the most general form. This gives four possible D intersections per satellite pair, collectively identified as ($D_{11,jk}$, $D_{12,jk}$, $D_{21,jk}$, $D_{22,jk}$). For certain geometries, it is possible that less than four intersections exist, such as when two TLs are parallel or when they diverge. First, some results from Marchand and Kobel[16] must be

generalized for constellations. One result states that the TL of S_1 is tangent to the THS when

$$\theta_t = \cos^{-1}\left(\frac{r_t}{r_s}\right) \tag{2.26}$$

which actually holds for any TL, where θ_t is the above-the-horizon coverage angle at the point of tangency. The slope of each TL of S_j can then be expressed in terms of the satellite location and the points of tangency as follows:

$$m_{\rho,j} = \frac{y_{t_{\rho,j}} - y_{s_j}}{x_{t_{\rho,j}} - x_{s_j}} \tag{2.27}$$

for

$$\begin{aligned} x_{t_{\rho,j}} &= \begin{cases} r_t \sin\left[(j-1)\theta_s + \theta_t\right] & \text{if } \rho = 1 \\ r_t \sin\left[(j-1)\theta_s - \theta_t\right] & \text{if } \rho = 2 \end{cases} \\ y_{t_{\rho,j}} &= \begin{cases} r_t \cos\left[(j-1)\theta_s + \theta_t\right] & \text{if } \rho = 1 \\ r_t \cos\left[(j-1)\theta_s - \theta_t\right] & \text{if } \rho = 2 \end{cases} \end{aligned} \tag{2.28}$$

Each intersection is given by the solution to the following system of equations:

$$y_{D_{\rho_j\rho_k,jk}} = m_{\rho_j,j} x_{D_{\rho_j\rho_k,jk}} + b_{\rho_j,j}; \qquad y_{D_{\rho_j\rho_k,jk}} = m_{\rho_k,k} x_{D_{\rho_j\rho_k,jk}} + b_{\rho_k,k} \tag{2.29}$$

where b is the y-coordinate of the point at which the TL intersects the $\hat{\mathbf{y}}$-axis, determined as

$$b_{\rho_j,j} = y_{s_j} - m_{\rho_j,j} x_{s_j}; \qquad b_{\rho_k,k} = y_{s_k} - m_{\rho_k,k} x_{s_k} \tag{2.30}$$

Using Eq. (2.29) to solve for $x_{D_{\rho_j\rho_k,jk}}$ by substitution gives

$$x_{D_{\rho_j\rho_k,jk}} = \frac{b_{\rho_k,k} - b_{\rho_j,j}}{m_{\rho_j,j} - m_{\rho_k,k}} \tag{2.31}$$

Then, substituting Eq. (2.30) into Eq. (2.29) and Eq. (2.31) gives

$$\begin{aligned} x_{D_{\rho_j\rho_k,jk}} &= \frac{m_{\rho_j,j} x_{s_j} - m_{\rho_k,k} x_{s_k} - y_{s_j} + y_{s_k}}{m_{\rho_j,j} - m_{\rho_k,k}} \\ y_{D_{\rho_j\rho_k,jk}} &= m_{\rho_j,j}\left(x_{D_{\rho_j\rho_k,jk}} - x_{s_j}\right) + y_{s_j} \end{aligned} \tag{2.32}$$

Of course, Eqs. (2.31) and (2.32) are not valid if $m_{\rho_j,j} = m_{\rho_k,k}$ since the denominator would go to zero. Such a scenario implies that the intersection does not exist, which makes sense physically because two parallel lines cannot intersect, assuming they are not collinear. Should two TLs happen to be collinear, as in Figure 2.3, then $D_{\rho_j\rho_k,jk}$ becomes meaningless and adds no new information to the geometry. Under

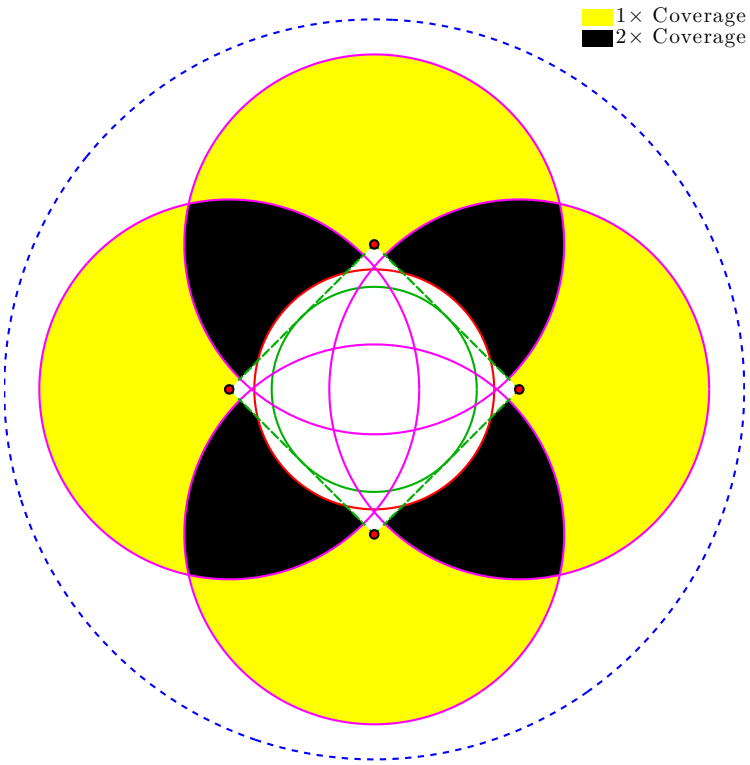

Figure 2.3: Collinear tangent lines for $n = 4$, $D_{\rho_j\rho_k,jk} \equiv M_{jk}$

such circumstances, let $D_{\rho_j\rho_k,jk}$ be equivalent to M_{jk}, which can be expressed as

$$D_{\rho_j\rho_k,jk} \equiv M_{jk} \quad \text{if } m_{\rho_j,j} = m_{\rho_k,k} \text{ and } b_{\rho_j,j} = b_{\rho_k,k} \tag{2.33}$$

If two TLs are parallel but not collinear, then $D_{\rho_j\rho_k,jk}$ does not exist, which can be expressed as

$$D_{\rho_j\rho_k,jk} = \varnothing \quad \text{if } m_{\rho_j,j} = m_{\rho_k,k} \text{ and } b_{\rho_j,j} \neq b_{\rho_k,k} \tag{2.34}$$

One situation in which this can occur is when $r_s = r_t$ and n is even, as in Figure

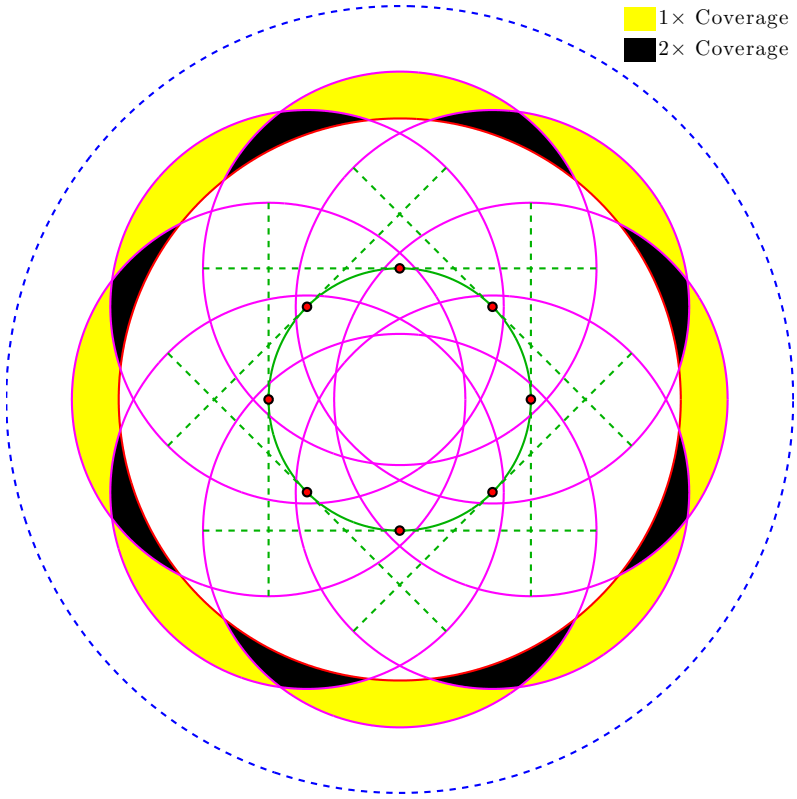

Figure 2.4: Parallel but not collinear tangent lines for $n = 8$ and $r_s = r_t$

2.4. Further observe that Eq. (2.32) assumes each TL is a line, though in reality the TL does not extend above the satellite from which it originates. Thus, care should be taken to ignore a solution given by Eq. (2.32) if the computed intersection is

located above the satellites from which each TL emanates.

2.3.2.3 Intersections of Tangent Lines with Range Shells

The intersection of a TL of S_j with the RS of S_k for $j \neq k$ is a Type II intersection denoted as $T_{\sigma,jk}$. There are at most four such T intersections per satellite pair, collectively identified as ($T_{1_A,jk}$, $T_{1_B,jk}$, $T_{2_A,jk}$, $T_{2_B,jk}$). Note the application of Eq. (2.13) to Eqs. (2.35–2.37). The coordinates are given by the solution to the following system of equations:

$$\left(x_{T_{\sigma,jk}} - x_{s_k}\right)^2 + \left(y_{T_{\sigma,jk}} - y_{s_k}\right)^2 = R^2; \qquad y_{T_{\sigma,jk}} = m_{\rho,j} x_{T_{\sigma,jk}} + b_{\rho,j} \tag{2.35}$$

where $b_{\rho,j}$ is interpreted as $b_{\rho,j} = y_{s_j} - m_{\rho,j} x_{s_j}$ from Eq. (2.30). In general, solving Eq. (2.35) for $x_{T_{\sigma,jk}}$ gives

$$x_{T_{\sigma,jk}} = \frac{-\left[m_{\rho,j}\left(b_{\rho,j} - y_{s_k}\right) - x_{s_k}\right] \pm \sqrt{\left(m_{\rho,j}^2 + 1\right)R^2 - \left(b_{\rho,j} - y_{s_k} + m_{\rho,j} x_{s_k}\right)^2}}{m_{\rho,j}^2 + 1} \tag{2.36}$$

which has at most two real solutions. It has no real solution if $(m_{\rho,j}^2 + 1)R^2 < (b_{\rho,j} - y_{s_k} + m_{\rho,j} x_{s_k})^2$. However, Eq. (2.36) has an issue analogous to that of Eq. (2.32), which is that if the TL originates within the RS, it will still give two real solutions even if only one T intersection exists. The term "exist", as used here, implies that the intersection exists if the RS does not intersect the TL above the altitude of the satellite from which the TL originates. Should only one T intersection exist, ignore the $T_{\rho_B,jk}$ intersection. However, it is useful to compute a nonexisting T intersection for certain purposes, such as for some of the conditions given in Section 2.5 that are used to identify the overlap region polygon $C'_{2\times,12}$.

Determining which solution corresponds to subscript "A" and which to subscript "B" is nontrivial and is summarized as

$$x_{T_{\rho_A,jk}} = \begin{cases} x^{+}_{T_{\sigma,jk}}, & \text{if } x_{s_j} < 0 \\ x^{-}_{T_{\sigma,jk}}, & \text{if } x_{s_j} = 0, y_{s_j} > 0, m_{\rho,j} > 0 \\ x^{+}_{T_{\sigma,jk}}, & \text{if } x_{s_j} = 0, y_{s_j} > 0, m_{\rho,j} < 0 \\ x^{+}_{T_{\sigma,jk}}, & \text{if } x_{s_j} = 0, y_{s_j} < 0, m_{\rho,j} > 0 \\ x^{-}_{T_{\sigma,jk}}, & \text{if } x_{s_j} = 0, y_{s_j} < 0, m_{\rho,j} < 0 \\ x^{-}_{T_{\sigma,jk}}, & \text{if } x_{s_j} > 0 \end{cases} \tag{2.37}$$

where $x^{+}_{T_{\sigma,jk}}$ corresponds to the solution of Eq. (2.36) with the positive square root term and $x^{-}_{T_{\sigma,jk}}$ corresponds to the solution of Eq. (2.36) with the negative square root term. Then, $x_{T_{\rho_B,jk}}$ is the other solution of Eq. (2.36) not defined by Eq. (2.37). The complete solution to the system of equations given in Eq. (2.35) is then formed by using Eqs. (2.36–2.37) in conjunction with the equation for the TL:

$$y_{T_{\sigma,jk}} = m_{\rho,j}\left(x_{T_{\sigma,jk}} - x_{s_j}\right) + y_{s_j} \tag{2.38}$$

2.4 Geometrical Elements of Regions Subject to 2-fold Coverage

As demonstrated by Marchand and Kobel[16] for the single satellite case, the coverage area is at best reduced to a continuous piecewise differentiable function, and the same holds for areas subject to 2-fold coverage in a constellation. The overlap area $\mathbf{A}'_{2\times,jk}$ refers to the area of a region $C'_{2\times,jk}$ between two satellites that is within view of both satellites. Recall that for 2-fold coverage restricted to pairs of adjacent satellites, $C'_{2\times,12}$ can be analyzed instead without loss of generality. This region is a polygon whose vertices are connected by lines and/or circular arcs, and which can have 16 unique shapes, categorized according to the number of vertices that the

overlap area has. Table 2.4 shows the relation between the number of vertices and number of unique shapes. Due to the geometry of the problem, $C'_{2\times,12}$ cannot have

Table 2.4: Relation between the Number of Vertices and Number of Unique Shapes for $C'_{2\times,12}$

Number of Vertices	Number of Unique Shapes
2	1
3	3
4	3
5	3
6	3
7	2
8	1

greater than eight vertices. The following discussion defines all of the fundamental geometrical elements necessary for creating a piecewise differentiable function for the 2-fold coverage area $\mathbf{A}'_{2\times,12}$, using a combination of triangles, quadrilaterals, and circular segments. The area $\mathbf{A}'_{2\times,12}$ is then computed by summing the areas of the appropriate fundamental shapes, though this step is reserved for Section 2.5.

2.4.1 Composite Triangles

Composite triangles are formed by adding to and/or subtracting from a base triangle one or more circular segments. The areas $\mathbf{A}_{\Lambda_1}$ and $\mathbf{A}_{\Lambda_2}$ denote the first two types of composite triangle, which were originally defined by Marchand and Kobel.[16] Their formulas are given in Eqs. (A.25) and (A.26).

For the 3-vertex shapes, new composite triangles must be defined. Shape 3.i

requires the definition of a new composite triangle, Λ_3, made up of three arcs:

$$\begin{aligned}\mathbf{A}_{\Lambda_3}(r_1,r_2,r_3,q_1,q_2,q_3) &= \mathbf{A}_{\triangle}(q_1,q_2,q_3) \\ &- \mathbf{A}_{\Sigma}(r_1,q_1) + \mathbf{A}_{\Sigma}(r_2,q_2) + \mathbf{A}_{\Sigma}(r_3,q_3)\end{aligned} \tag{2.39}$$

where r_ζ denotes a radial quantity and q_ζ denotes an edge length. $\mathbf{A}_{\triangle}$ refers to the area of a triangle computed using Heron's formula, where each argument is a side of the triangle.[16] $\mathbf{A}_{\Sigma}$ refers to the area of a circular segment, where the first argument is the circle's radius and the second is the associated chord.[16] The equation for $\mathbf{A}_{\Lambda_3}$ essentially adds an $\mathbf{A}_{\Sigma}$ term to the definition of $\mathbf{A}_{\Lambda_1}$.

For shape 3.ii, a new composite triangle, Λ_4, is defined, also made up of three arcs but with different convexity:

$$\begin{aligned}\mathbf{A}_{\Lambda_4}(r_1,r_2,r_3,q_1,q_2,q_3) &= \mathbf{A}_{\triangle}(q_1,q_2,q_3) \\ &+ \mathbf{A}_{\Sigma}(r_1,q_1) + \mathbf{A}_{\Sigma}(r_2,q_2) + \mathbf{A}_{\Sigma}(r_3,q_3)\end{aligned} \tag{2.40}$$

The equation for $\mathbf{A}_{\Lambda_4}$ is similar to that for $\mathbf{A}_{\Lambda_3}$ except all circular segment areas are added to the base triangle.

A new composite triangle, Λ_5, must be defined for case 3.iii.a and 3.iii.b. Λ_5 is pie-shaped, consisting of one arc and two line segments:

$$\mathbf{A}_{\Lambda_5}(r_1,q_1,q_2,q_3) = \mathbf{A}_{\triangle}(q_1,q_2,q_3) + \mathbf{A}_{\Sigma}(r_1,q_1) \tag{2.41}$$

The equation for $\mathbf{A}_{\Lambda_5}$ is similar to that for $\mathbf{A}_{\Lambda_2}$ except that the circular segment area is added to the base triangle. λ_5 is also used in the construction of other regions of overlap.

For overlap areas with greater than three vertices, it is helpful to define an additional composite triangle, Λ_6:

$$\mathbf{A}_{\Lambda_6}(r_1,r_2,q_1,q_2,q_3) = \mathbf{A}_{\triangle}(q_1,q_2,q_3) + \mathbf{A}_{\Sigma}(r_1,q_1) + \mathbf{A}_{\Sigma}(r_2,q_2) \tag{2.42}$$

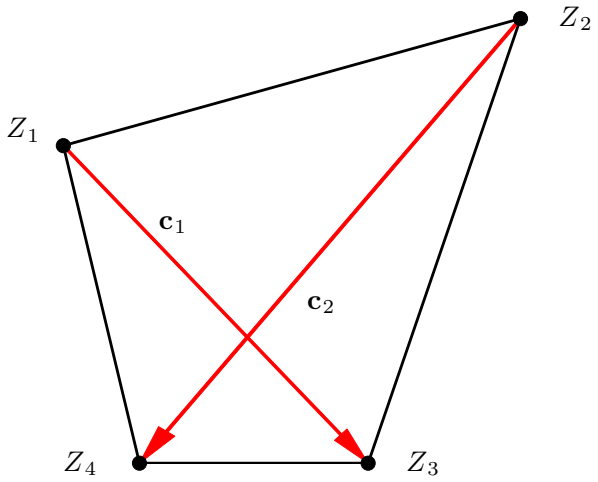

Figure 2.5: A general convex quadrilateral

Λ_6 is used in defining some of the regions with five, six, and seven vertices.

2.4.2 Convex Quadrilaterals

Formulas for the areas of composite quadrilaterals are derived from the general formula for the area of a convex quadrilateral based on its diagonals.[19] Each vertex is an intersection point Z_ζ, defined in Eq. (2.15), and which is numbered clockwise. For example, consider a convex quadrilateral $Z_1Z_2Z_3Z_4$, which is illustrated in Figure 2.5. If its diagonals are defined as the vectors

$$\begin{aligned} \mathbf{c}_1 &= (x_{Z_3} - x_{Z_1})\hat{\mathbf{x}} + (y_{Z_3} - y_{Z_1})\hat{\mathbf{y}} \\ \mathbf{c}_2 &= (x_{Z_4} - x_{Z_2})\hat{\mathbf{x}} + (y_{Z_4} - y_{Z_2})\hat{\mathbf{y}} \end{aligned} \tag{2.43}$$

then the area of quadrilateral $Z_1Z_2Z_3Z_4$ can be expressed as

$$\mathbf{A}_{\square}(Z_1, Z_2, Z_3, Z_4) = \frac{1}{2}|\mathbf{c}_1 \times \mathbf{c}_2| \tag{2.44}$$

An alternative means of determining the area of a convex quadrilateral is with Bretschneider's formula:[20]

$$\mathbf{A}_{\square}(q_1, q_2, q_3, q_4, c_1, c_2) = \frac{1}{4}\sqrt{4c_1^2c_2^2 - (q_2^2 + q_4^2 - q_1^2 - q_3^2)^2} \tag{2.45}$$

However, it is simpler to use Eq. (2.44) because the function has fewer arguments and requires less calculations. Thus, Eq. (2.44) is employed in this thesis for all computations of the area of convex quadrilaterals.

2.4.3 Composite Quadrilaterals

Composite quadrilaterals are formed by adding to and/or subtracting from a base convex quadrilateral one or more circular segments. Six types of composite quadrilaterals are introduced. For case 4.i.a, the area of overlap can be described as a composite quadrilateral $\mathbf{A}_{\Pi_1}$, defined as

$$\begin{aligned}\mathbf{A}_{\Pi_1}(r_1,r_2, Z_1, Z_2, Z_3, Z_4) &= \mathbf{A}_{\square}(Z_1, Z_2, Z_3, Z_4) \\ &+ \mathbf{A}_{\Sigma}(r_1, |\overline{Z_1Z_2}|) - \mathbf{A}_{\Sigma}(r_2, |\overline{Z_3Z_4}|)\end{aligned} \tag{2.46}$$

The five remaining types of composite quadrilaterals are defined in Eqs. (2.47–2.51).

$$\begin{aligned}\mathbf{A}_{\Pi_2}(r_1,r_2,r_3,r_4, Z_1, Z_2, Z_3, Z_4) &= \mathbf{A}_{\square}(Z_1, Z_2, Z_3, Z_4) + \mathbf{A}_{\Sigma}(r_1, |\overline{Z_1Z_2}|) \\ &- \mathbf{A}_{\Sigma}(r_2, |\overline{Z_3Z_4}|) + \mathbf{A}_{\Sigma}(r_3, |\overline{Z_2Z_3}|) + \mathbf{A}_{\Sigma}(r_4, |\overline{Z_4Z_1}|)\end{aligned} \tag{2.47}$$

$$\begin{aligned}\mathbf{A}_{\Pi_3}(r_1,r_2, Z_1, Z_2, Z_3, Z_4) &= \mathbf{A}_{\square}(Z_1, Z_2, Z_3, Z_4) \\ &+ \mathbf{A}_{\Sigma}(r_1, |\overline{Z_1Z_2}|) - \mathbf{A}_{\Sigma}(r_2, |\overline{Z_4Z_1}|)\end{aligned} \tag{2.48}$$

$$\begin{aligned}\mathbf{A}_{\Pi_4}(r_1,r_2,r_3, Z_1, Z_2, Z_3, Z_4) &= \mathbf{A}_{\square}(Z_1, Z_2, Z_3, Z_4) \\ &+ \mathbf{A}_{\Sigma}(r_1, |\overline{Z_1Z_2}|) + \mathbf{A}_{\Sigma}(r_2, |\overline{Z_2Z_3}|) + \mathbf{A}_{\Sigma}(r_3, |\overline{Z_4Z_1}|)\end{aligned} \tag{2.49}$$

$$\mathbf{A}_{\Pi_5}(r_1,Z_1,Z_2,Z_3,Z_4) = \mathbf{A}_{\square}(Z_1,Z_2,Z_3,Z_4) + \mathbf{A}_{\Sigma}(r_1,|\overline{Z_1Z_2}|) \tag{2.50}$$

$$\begin{aligned}\mathbf{A}_{\Pi_6}(r_1,r_2,r_3,Z_1,Z_2,Z_3,Z_4) &= \mathbf{A}_{\square}(Z_1,Z_2,Z_3,Z_4) \\ &- \mathbf{A}_{\Sigma}(r_1,|\overline{Z_1Z_2}|) + \mathbf{A}_{\Sigma}(r_2,|\overline{Z_2Z_3}|) + \mathbf{A}_{\Sigma}(r_3,|\overline{Z_4Z_1}|)\end{aligned} \tag{2.51}$$

2.5 Above-the-Horizon 2-fold Coverage Area for a Constellation in a Circular Orbit

The 2-fold coverage area computations are organized in a way that emphasizes the relationship expressed in Table 2.4. Table 2.5 identifies the conditions that must be satisfied for each of 22 possible cases, termed "shape types", and outlines the naming convention used. The first number denotes the number of vertices and the second number denotes the type. Thus, shape type 3.ii is a 3-vertex overlap area of the second kind. Shape types are labeled with an "a" or "b" when the shape is the same but some of the vertices are different intersection points. This is why there are 22 shape types for only 16 unique shapes.

Once the shape type is identified from Table 2.5, the appropriate formula for computing the 2-fold coverage area is found in Table 2.6. As mentioned previously, the way that each complex shape is divided into more fundamental shapes is not unique, and Table 2.6 merely shows one possible scheme. Effort is also made to describe the geometry in a systematic way. For example, quadrilaterals are labeled clockwise from the top-left corner, and fundamental areas are summed in the order in which they are stacked within the complex shape. Figures 2.6–2.7 contain clear

examples of all 22 shape types, zoomed in on the region $C'_{2\times,12}$. Greater detail on the coverage area for each of the 22 shape types, with labeled vertices, is given in Figures B.1–B.22.

Table 2.5: Conditions for Identifying the Overlap Region Polygon $C'_{2\times,12}$

Conditions	Shape Type
$r_l < \lvert\overline{OW_{4,12}}\rvert < \lvert\overline{OM_{12}}\rvert$, $\lvert\overline{OD_{12,12}}\rvert < \lvert\overline{OW_{4,12}}\rvert < \lvert\overline{OM_{12}}\rvert$, $\lvert\overline{OW_{3,12}}\rvert < r_u$, $\lvert\overline{OT_{1_B,12}}\rvert < \lvert\overline{OW_{4,12}}\rvert < \lvert\overline{OM_{12}}\rvert$	2
$\lvert\overline{OD_{12,12}}\rvert < r_l$, $x_{W_{4,12}} < r_l \sin(\theta_s/2)$, $r_l < \lvert\overline{OW_{3,12}}\rvert \leq r_u$, $\lvert\overline{OT_{1_B,12}}\rvert < r_l$	3.i
$r_l < \lvert\overline{OW_{4,12}}\rvert < \lvert\overline{OM_{12}}\rvert$, $\lvert\overline{OD_{12,12}}\rvert < \lvert\overline{OW_{4,12}}\rvert < \lvert\overline{OM_{12}}\rvert$, $r_u < \lvert\overline{OW_{3,12}}\rvert$, $\lvert\overline{D_{12,12}S_1}\rvert < \lvert\overline{T_{1_A,12}S_1}\rvert$, $\lvert\overline{D_{12,12}S_1}\rvert < \lvert\overline{T_{1_B,12}S_1}\rvert$	3.ii
$r_l \leq r_s$, $\lvert\overline{D_{12,12}S_1}\rvert < \lvert\overline{L_{1_B,1}S_1}\rvert$, $x_{W_{4,12}} < x_{D_{12,12}}$, $r_u \leq \lvert\overline{OT_{1_B,12}}\rvert$	3.iii.a
$\lvert\overline{L_{1_A,1}S_1}\rvert < \lvert\overline{D_{12,12}S_1}\rvert$, $x_{W_{4,12}} < x_{D_{12,12}}$, $r_u \leq \lvert\overline{OT_{1_A,11}}\rvert$	3.iii.b
$r_l \leq r_s$, $\lvert\overline{OD_{12,12}}\rvert < r_l$, $x_{W_{4,12}} < r_l \sin(\theta_s/2)$, $r_u \leq \lvert\overline{OT_{1_B,12}}\rvert$, $\lvert\overline{L_{1_B,1}S_1}\rvert < \lvert\overline{T_{1_A,12}S_1}\rvert$	4.i.a
$\lvert\overline{OD_{12,12}}\rvert < r_l$, $x_{W_{4,12}} < r_l \sin(\theta_s/2)$, $r_u \leq \lvert\overline{OT_{1_A,11}}\rvert$, $\lvert\overline{OT_{1_B,12}}\rvert < \lvert\overline{OT_{1_A,11}}\rvert$	4.i.b
$\lvert\overline{OD_{12,12}}\rvert < r_l$, $x_{W_{4,12}} < r_l \sin(\theta_s/2)$, $r_u < \lvert\overline{OW_{3,12}}\rvert$, $\lvert\overline{OT_{1_B,12}}\rvert < r_l$	4.ii
$r_l \leq r_s$, $\lvert\overline{D_{12,12}S_1}\rvert < \lvert\overline{L_{1_B,1}S_1}\rvert$, $x_{W_{4,12}} < x_{D_{12,12}}$, $\lvert\overline{OD_{12,12}}\rvert < \lvert\overline{OW_{3,12}}\rvert \leq r_u$	4.iii.a
$\lvert\overline{L_{1_A,1}S_1}\rvert < \lvert\overline{D_{12,12}S_1}\rvert$, $x_{W_{4,12}} < x_{D_{12,12}}$, $\lvert\overline{OD_{12,12}}\rvert < \lvert\overline{OW_{3,12}}\rvert \leq r_u$	4.iii.b
$r_l \leq r_s$, $\lvert\overline{OD_{12,12}}\rvert < r_l$, $x_{W_{4,12}} < r_l \sin(\theta_s/2)$, $\lvert\overline{OW_{3,12}}\rvert < r_u$, $r_l < \lvert\overline{OT_{1_B,12}}\rvert$, $\lvert\overline{OT_{1_A,11}}\rvert < \lvert\overline{OT_{1_B,12}}\rvert$, $\lvert\overline{L_{1_B,1}S_1}\rvert < \lvert\overline{T_{1_A,12}S_1}\rvert$	5.i.a
$\lvert\overline{OD_{12,12}}\rvert < r_l$, $x_{W_{4,12}} < r_l \sin(\theta_s/2)$, $\lvert\overline{OW_{3,12}}\rvert < r_u$, $r_l < \lvert\overline{OT_{1_A,11}}\rvert$, $\lvert\overline{OT_{1_B,12}}\rvert < \lvert\overline{OT_{1_A,11}}\rvert$	5.i.b
$r_l \leq r_s$, $\lvert\overline{D_{12,12}S_1}\rvert < \lvert\overline{L_{1_B,1}S_1}\rvert$, $x_{W_{4,12}} < x_{D_{12,12}}$, $r_u < \lvert\overline{OW_{3,12}}\rvert$, $\lvert\overline{OT_{1_B,12}}\rvert < r_u$	5.ii.a
$\lvert\overline{L_{1_A,1}S_1}\rvert < \lvert\overline{D_{12,12}S_1}\rvert$, $x_{W_{4,12}} < x_{D_{12,12}}$, $r_u < \lvert\overline{OW_{3,12}}\rvert$, $\lvert\overline{T_{1_A,11}S_1}\rvert < \lvert\overline{U_{1_A,1}S_1}\rvert$	5.ii.b
$r_l < \lvert\overline{OW_{4,12}}\rvert < \lvert\overline{OM_{12}}\rvert$, $\lvert\overline{OD_{12,12}}\rvert < \lvert\overline{OW_{4,12}}\rvert < \lvert\overline{OM_{12}}\rvert$, $r_u < \lvert\overline{OW_{3,12}}\rvert$, $r_l < \lvert\overline{OT_{1_A,12}}\rvert < r_u$, $r_l < \lvert\overline{OT_{1_B,12}}\rvert < r_u$	5.iii
$\lvert\overline{OD_{12,12}}\rvert < r_l$, $x_{W_{4,12}} < r_l \sin(\theta_s/2)$, $r_u < \lvert\overline{OW_{3,12}}\rvert$, $r_l < \lvert\overline{OT_{1_B,12}}\rvert < r_u$, $\lvert\overline{OT_{1_A,11}}\rvert < \lvert\overline{OT_{1_B,12}}\rvert$	6.i.a
$\lvert\overline{OD_{12,12}}\rvert < r_l$, $x_{W_{4,12}} < r_l \sin(\theta_s/2)$, $r_u < \lvert\overline{OW_{3,12}}\rvert$, $r_l < \lvert\overline{OT_{1_A,11}}\rvert < r_u$, $\lvert\overline{OT_{1_B,12}}\rvert < \lvert\overline{OT_{1_A,11}}\rvert$	6.i.b
$\lvert\overline{OD_{12,12}}\rvert < \lvert\overline{OW_{4,12}}\rvert < \lvert\overline{OM_{12}}\rvert$, $x_{W_{4,12}} < r_l \sin(\theta_s/2)$, $r_u < \lvert\overline{OW_{3,12}}\rvert$, $r_l < \lvert\overline{OT_{1_A,12}}\rvert < r_u$, $r_u < \lvert\overline{OT_{1_B,12}}\rvert$	6.ii
$r_l < \lvert\overline{OW_{4,12}}\rvert < \lvert\overline{OM_{12}}\rvert$, $\lvert\overline{OD_{12,12}}\rvert < \lvert\overline{OW_{4,12}}\rvert < \lvert\overline{OM_{12}}\rvert$, $\lvert\overline{OW_{3,12}}\rvert < r_u$, $\lvert\overline{OM_{12}}\rvert < \lvert\overline{OT_{1_B,12}}\rvert$	6.iii
$r_l < \lvert\overline{OW_{4,12}}\rvert < \lvert\overline{OM_{12}}\rvert$, $\lvert\overline{OD_{12,12}}\rvert < \lvert\overline{OW_{4,12}}\rvert < \lvert\overline{OM_{12}}\rvert$, $r_u < \lvert\overline{OW_{3,12}}\rvert$, $r_l < \lvert\overline{OT_{1_A,12}}\rvert < r_u$, $r_l < \lvert\overline{OT_{1_B,12}}\rvert < r_u$	7.i
$x_{W_{4,12}} < r_l \sin(\theta_s/2)$, $\lvert\overline{OD_{12,12}}\rvert < \lvert\overline{OW_{4,12}}\rvert < \lvert\overline{OM_{12}}\rvert$, $\lvert\overline{OW_{3,12}}\rvert < r_u$, $\lvert\overline{OM_{12}}\rvert < \lvert\overline{OT_{1_B,12}}\rvert$	7.ii
$x_{W_{4,12}} < r_l \sin(\theta_s/2)$, $\lvert\overline{OD_{12,12}}\rvert < \lvert\overline{OW_{4,12}}\rvert < \lvert\overline{OM_{12}}\rvert$, $r_u < \lvert\overline{OW_{3,12}}\rvert$, $r_l < \lvert\overline{OT_{1_A,12}}\rvert < r_u$, $r_l < \lvert\overline{OT_{1_B,12}}\rvert < r_u$	8

Table 2.6: Piecewise Formulation for 2-fold Coverage Area $\mathbf{A}'_{2\times,12}$

Shape Type	2-fold Coverage Area $\mathbf{A}'_{2\times,12}$
2	$\mathbf{A}'_{2\times,12} = 2\mathbf{A}_{\Sigma}(R, \lvert\overline{W_{3,12}W_{4,12}}\rvert)$
3.i	$\mathbf{A}'_{2\times,12} = \mathbf{A}_{\Lambda_3}(r_l, R, R, \lvert\overline{A_{1,1}A_{2,2}}\rvert, \lvert\overline{A_{1,1}W_{3,12}}\rvert, \lvert\overline{A_{2,2}W_{3,12}}\rvert)$
3.ii	$\mathbf{A}'_{2\times,12} = \mathbf{A}_{\Lambda_4}(r_u, R, R, \lvert\overline{B_{1,1}B_{2,2}}\rvert, \lvert\overline{B_{1,1}W_{4,12}}\rvert, \lvert\overline{B_{2,2}W_{4,12}}\rvert)$
3.iii.a	$\mathbf{A}'_{2\times,12} = \mathbf{A}_{\Lambda_5}(r_u, \lvert\overline{U_{1_B,1}U_{2_B,2}}\rvert, \lvert\overline{U_{1_B,1}D_{12,12}}\rvert, \lvert\overline{U_{2_B,2}D_{12,12}}\rvert)$
3.iii.b	$\mathbf{A}'_{2\times,12} = \mathbf{A}_{\Lambda_5}(r_u, \lvert\overline{U_{2_A,2}U_{1_A,1}}\rvert, \lvert\overline{U_{2_A,2}D_{12,12}}\rvert, \lvert\overline{U_{1_A,1}D_{12,12}}\rvert)$
4.i.a	$\mathbf{A}'_{2\times,12} = \mathbf{A}_{\Pi_1}(r_u, r_l, U_{1_B,1}, U_{2_B,2}, L_{2_B,2}, L_{1_B,1})$
4.i.b	$\mathbf{A}'_{2\times,12} = \mathbf{A}_{\Pi_1}(r_u, r_l, U_{2_A,2}, U_{1_A,1}, L_{1_A,1}, L_{2_A,2})$
4.ii	$\mathbf{A}'_{2\times,12} = \mathbf{A}_{\Pi_2}(r_u, r_l, R, R, B_{2,2}, B_{1,1}, A_{1,1}, A_{2,2})$
4.iii.a	$\mathbf{A}'_{2\times,12} = \mathbf{A}_{\Pi_3}(R, R, W_{3,12}, T_{2_B,21}, D_{12,12}, T_{1_B,12})$
4.iii.b	$\mathbf{A}'_{2\times,12} = \mathbf{A}_{\Pi_3}(R, R, W_{3,12}, T_{1_A,11}, D_{12,12}, T_{2_A,22})$
5.i.a	$\mathbf{A}'_{2\times,12} = \mathbf{A}_{\Pi_1}(R, r_l, W_{3,12}, T_{2_B,21}, L_{2_B,2}, L_{1_B,1})$ $+ \mathbf{A}_{\Lambda_5}(R, \lvert\overline{T_{1_B,12}W_{3,12}}\rvert, \lvert\overline{W_{3,12}L_{1_B,1}}\rvert, \lvert\overline{L_{1_B,1}T_{1_B,12}}\rvert)$
5.i.b	$\mathbf{A}'_{2\times,12} = \mathbf{A}_{\Pi_1}(R, r_l, W_{3,12}, T_{1_A,11}, L_{1_A,1}, L_{2_A,2})$ $+ \mathbf{A}_{\Lambda_5}(R, \lvert\overline{T_{2_A,22}W_{3,12}}\rvert, \lvert\overline{W_{3,12}L_{2_A,2}}\rvert, \lvert\overline{L_{2_A,2}T_{2_A,22}}\rvert)$
5.ii.a	$\mathbf{A}'_{2\times,12} = \mathbf{A}_{\Pi_4}(r_u, R, R, B_{2,2}, B_{1,1}, T_{2_B,21}, T_{1_B,12})$ $+ \mathbf{A}_{\triangle}(\lvert\overline{T_{2_B,21}D_{12,12}}\rvert, \lvert\overline{D_{12,12}T_{1_B,12}}\rvert, \lvert\overline{T_{1_B,12}T_{2_B,21}}\rvert)$
5.ii.b	$\mathbf{A}'_{2\times,12} = \mathbf{A}_{\Pi_4}(r_u, R, R, B_{2,2}, B_{1,1}, T_{1_A,11}, T_{2_A,22})$ $+ \mathbf{A}_{\triangle}(\lvert\overline{T_{1_A,11}D_{12,12}}\rvert, \lvert\overline{D_{12,12}T_{2_A,22}}\rvert, \lvert\overline{T_{2_A,22}T_{1_A,11}}\rvert)$
5.iii	$\mathbf{A}'_{2\times,12} = \mathbf{A}_{\Pi_5}(r_u, U_{1_B,1}, U_{2_B,2}, T_{2_A,21}, T_{1_A,12})$ $+ \mathbf{A}_{\Lambda_6}(R, R, \lvert\overline{T_{2_A,21}W_{4,12}}\rvert, \lvert\overline{W_{4,12}T_{1_A,12}}\rvert, \lvert\overline{T_{1_A,12}T_{2_A,21}}\rvert)$
6.i.a	$\mathbf{A}'_{2\times,12} = \mathbf{A}_{\Pi_1}(r_u, r_l, B_{2,2}, B_{1,1}, L_{2_B,2}, L_{1_B,1})$ $+ \mathbf{A}_{\Lambda_5}(R, \lvert\overline{B_{1,1}T_{2_B,21}}\rvert, \lvert\overline{T_{2_B,21}L_{2_B,2}}\rvert, \lvert\overline{L_{2_B,2}B_{1,1}}\rvert)$ $+ \mathbf{A}_{\Lambda_5}(R, \lvert\overline{T_{1_B,12}B_{2,2}}\rvert, \lvert\overline{B_{2,2}L_{1_B,1}}\rvert, \lvert\overline{L_{1_B,1}T_{1_B,12}}\rvert)$
6.i.b	$\mathbf{A}'_{2\times,12} = \mathbf{A}_{\Pi_1}(r_u, r_l, B_{2,2}, B_{1,1}, L_{1_A,1}, L_{2_A,2})$ $+ \mathbf{A}_{\Lambda_5}(R, \lvert\overline{B_{1,1}T_{1_A,11}}\rvert, \lvert\overline{T_{1_A,11}L_{1_A,1}}\rvert, \lvert\overline{L_{1_A,1}B_{1,1}}\rvert)$ $+ \mathbf{A}_{\Lambda_5}(R, \lvert\overline{T_{2_A,22}B_{2,2}}\rvert, \lvert\overline{B_{2,2}L_{2_A,2}}\rvert, \lvert\overline{L_{2_A,2}T_{2_A,22}}\rvert)$
6.ii	$\mathbf{A}'_{2\times,12} = \mathbf{A}_{\Pi_5}(r_u, U_{1_B,1}, U_{2_B,2}, T_{2_A,21}, T_{1_A,12})$ $+ \mathbf{A}_{\Pi_6}(r_l, R, R, A_{1,1}, A_{2,2}, T_{1_A,12}, T_{2_A,21})$
6.iii	$\mathbf{A}'_{2\times,12} = \mathbf{A}_{\square}(T_{2_B,21}, T_{2_A,21}, T_{1_A,12}, T_{1_B,12})$ $+ \mathbf{A}_{\Lambda_6}(R, R, \lvert\overline{T_{1_B,12}W_{3,12}}\rvert, \lvert\overline{W_{3,12}T_{2_B,21}}\rvert, \lvert\overline{T_{2_B,21}T_{1_B,12}}\rvert)$ $+ \mathbf{A}_{\Lambda_6}(R, R, \lvert\overline{T_{2_A,21}W_{4,12}}\rvert, \lvert\overline{W_{4,12}T_{1_A,12}}\rvert, \lvert\overline{T_{1_A,12}T_{2_A,21}}\rvert)$
7.i	$\mathbf{A}'_{2\times,12} = \mathbf{A}_{\Pi_4}(r_u, R, R, B_{2,2}, B_{1,1}, T_{2_B,21}, T_{1_B,12})$ $+ \mathbf{A}_{\square}(T_{2_B,21}, T_{2_A,21}, T_{1_A,12}, T_{1_B,12})$ $+ \mathbf{A}_{\Lambda_6}(R, R, \lvert\overline{T_{2_A,21}W_{4,12}}\rvert, \lvert\overline{W_{4,12}T_{1_A,12}}\rvert, \lvert\overline{T_{1_A,12}T_{2_A,21}}\rvert)$
7.ii	$\mathbf{A}'_{2\times,12} = \mathbf{A}_{\Lambda_6}(R, R, \lvert\overline{T_{1_B,12}W_{3,12}}\rvert, \lvert\overline{W_{3,12}T_{2_B,21}}\rvert, \lvert\overline{T_{2_B,21}T_{1_B,12}}\rvert)$ $+ \mathbf{A}_{\square}(T_{2_B,21}, T_{2_A,21}, T_{1_A,12}, T_{1_B,12})$ $+ \mathbf{A}_{\Pi_6}(r_l, R, R, A_{1,1}, A_{2,2}, T_{1_A,12}, T_{2_A,21})$
8	$\mathbf{A}'_{2\times,12} = \mathbf{A}_{\Pi_4}(r_u, R, R, B_{2,2}, B_{1,1}, T_{2_B,21}, T_{1_B,12})$ $+ \mathbf{A}_{\square}(T_{2_B,21}, T_{2_A,21}, T_{1_A,12}, T_{1_B,12})$ $+ \mathbf{A}_{\Pi_6}(r_l, R, R, A_{1,1}, A_{2,2}, T_{1_A,12}, T_{2_A,21})$

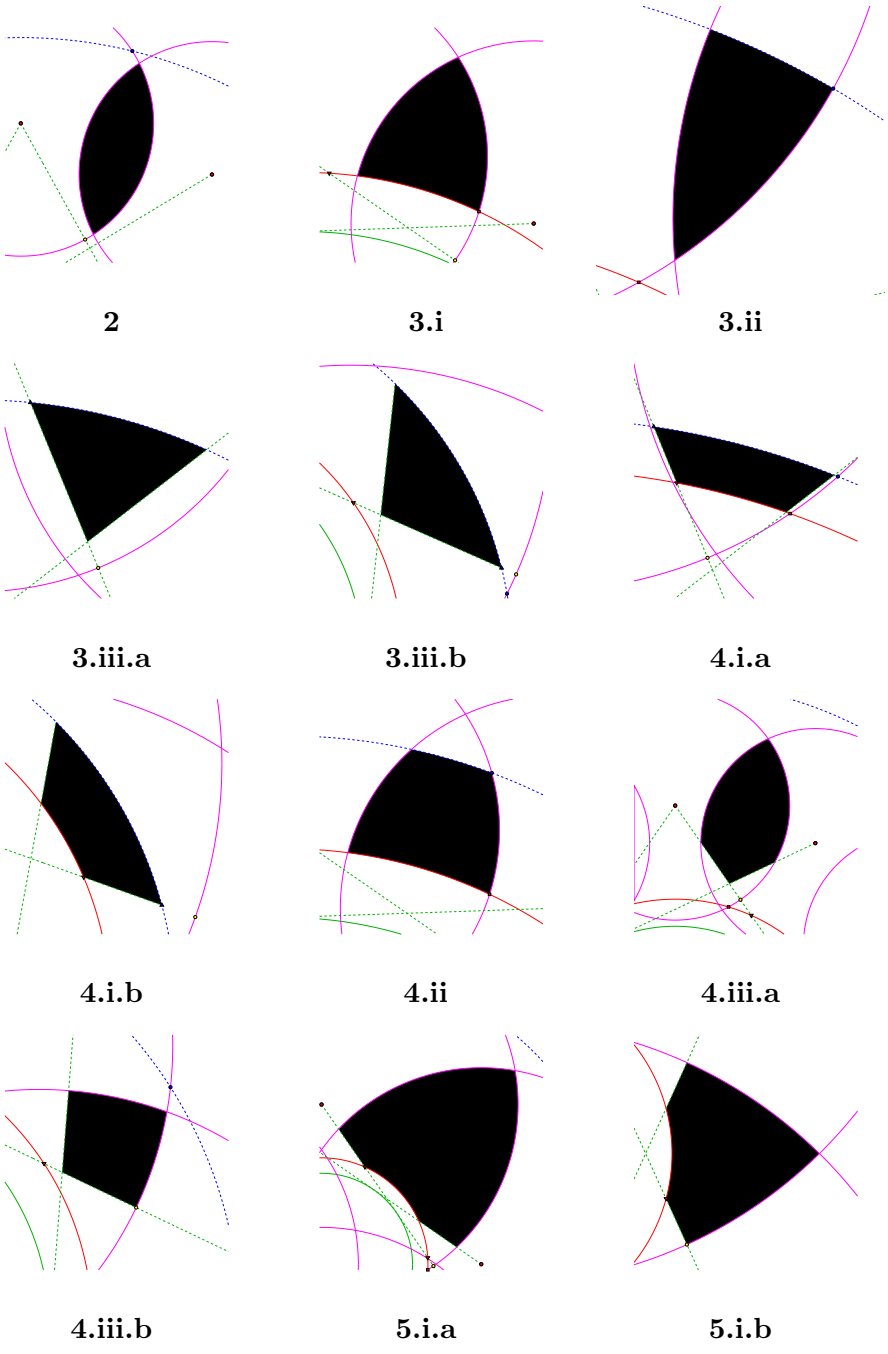

Figure 2.6: Taxonomy of Overlap Areas $\mathbf{A}'_{2\times,12}$

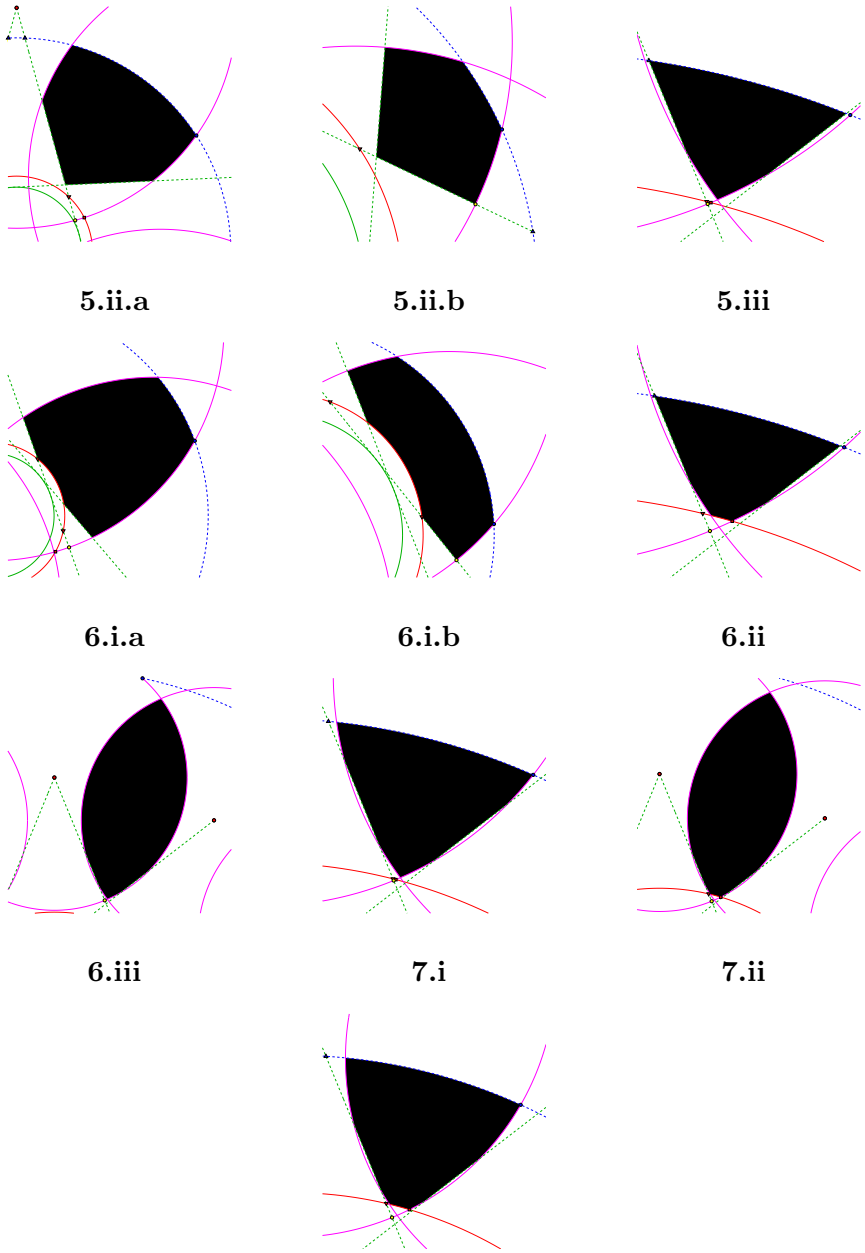

Figure 2.7: Taxonomy of Overlap Areas $\mathbf{A}'_{2\times,12}$

2.6 The Existence of Arbitrary Coverage Multiplicities

This section aims to determine explicitly the coverage multiplicities present for a given constellation at an instant in time using arguments based on shell intersections. Due to the complexity of this endeavor, exhaustive conditions are outside the scope of this thesis. However, partial conditions are provided to illustrate a basic approach that could be used to derive the remaining conditions.

In a sense, coverage multiplicities are created and destroyed systematically. There are several ways in which this can occur, but to adhere to previously made assumptions, the conditions presented here focus on only one of these ways in which coverage multiplicities are manifested — strictly between adjacent satellites. First, generalized conditions for the existence of p-fold coverage between adjacent satellites are derived. Then, conditions on the existence of 2-fold coverage are given separately since all results and validation presented in this thesis are subject to a maximum 2-fold coverage constraint and it is thus useful to have these conditions explicitly stated for this special case.

2.6.1 Partial Conditions on the Existence of p-fold Coverage

Recall that, according to previously mentioned assumptions that led to Eq. (2.10), strictly 2-fold coverage only occurs for pairs of adjacent satellites. This rule can be extended to 3-fold coverage by stating that strictly 3-fold coverage only occurs for triplets of adjacent satellites. Indeed, a fundamental argument in the derivation of conditions on the existence of p-fold coverage simply extends these observations to say that p-fold coverage only occurs for p adjacent satellites.

Using 2-fold coverage creation as an example, the sequence of Figures 2.8, 2.9, and 2.10 shows how additional coverage multiplicity for some region can be created. The ratio of the range shell to the distance between certain satellites turns out to be an important quantity in determining existence of coverage multiplicities. Notice that initially, in Figure 2.8, only single coverage or 1-fold coverage exists because $1 > \frac{2R}{d_{12}}$. As the radius of the range shell is increased, a threshold is

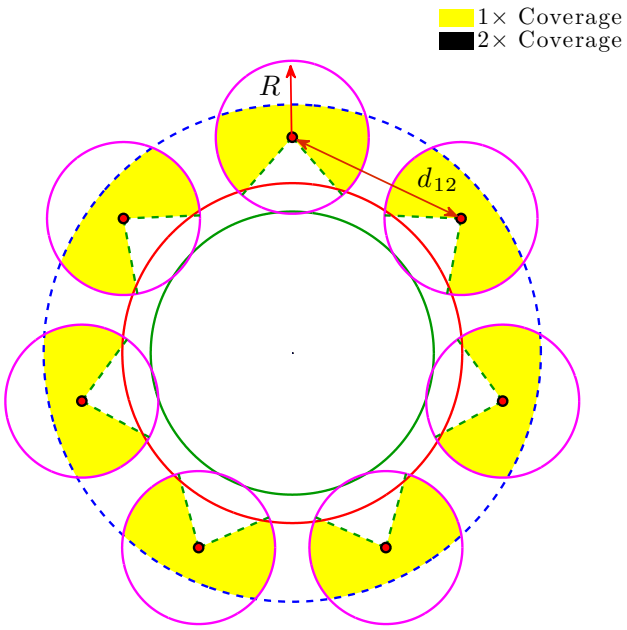

Figure 2.8: Only 1-fold coverage exists: $d_{12} > 2R$

reached, shown in Figure 2.9, beyond which 2-fold coverage exists. Thus, this state

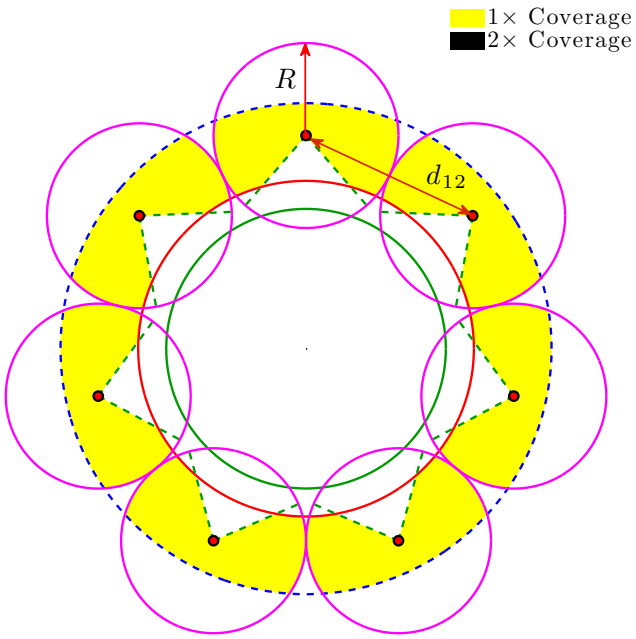

Figure 2.9: Upper limit of 1-fold coverage; threshold of creation of 2-fold coverage: $d_{12} = 2R$

can be considered as an upper limit of 1-fold coverage or a lower limit of 2-fold coverage, occurring when $1 = \frac{2R}{d_{12}}$. Hereinafter, the term "threshold" is used in the sense that the geometry is assumed fixed with $R = 0$, and then as R is increased, the threshold of p-fold coverage — represented as a point — is reached. Figure 2.10 illustrates the case where both 1-fold and 2-fold coverage exist, which gives one of

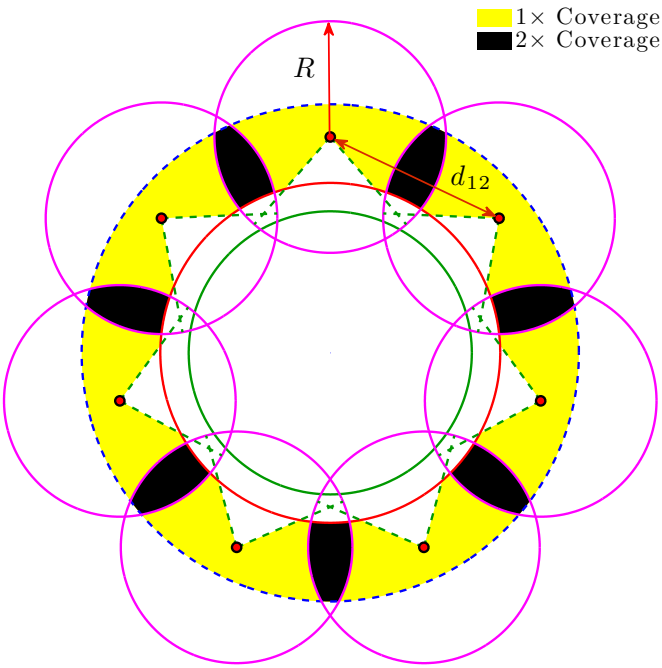

Figure 2.10: 1-fold and 2-fold coverage exist: $d_{12} < 2R$

the necessary conditions for the existence of 2-fold coverage:

$$1 < \frac{2R}{d_{12}} \tag{2.52}$$

Eq. (2.52) essentially states that a necessary condition for 2-fold coverage is that the range shells of S_1 and S_2 must intersect. For the second necessary condition on the existence of 2-fold coverage, consider the case where the intersection of two particular tangent lines, $D_{12,12}$, is outside the UTAS. Examples are given in Figures 2.11–2.12. These examples show that the condition

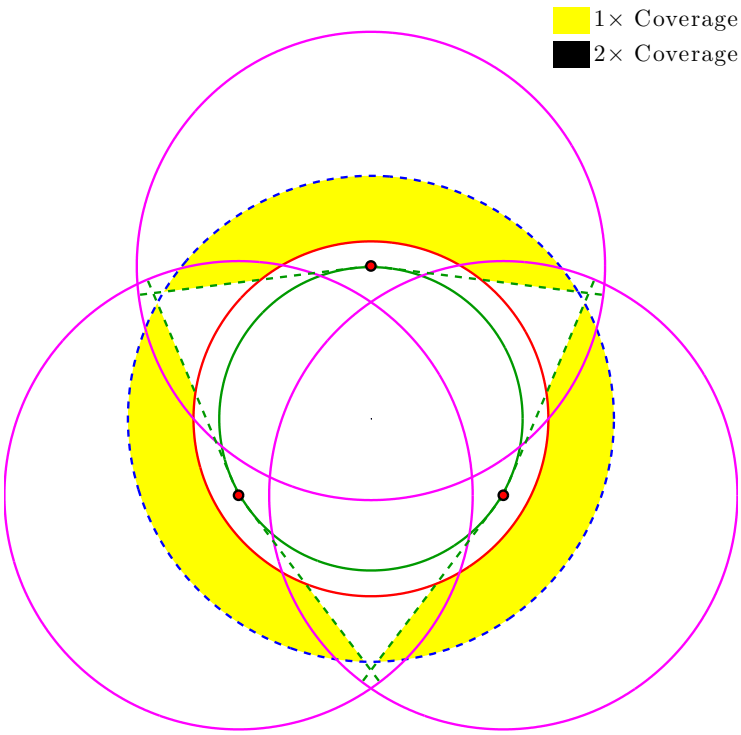

Figure 2.11: Case 1 — $|\overline{OD_{12,12}}| \geq r_u$ with $r_s < r_u$

$$|\overline{OD_{12,12}}| < r_u \tag{2.53}$$

must be satisfied for 2-fold coverage to exist, because otherwise the region above the horizon of the satellite pair is outside the region DABS. A final requirement for 2-fold coverage is that the intersection $D_{12,12}$ itself must exist, which is to say that

$$D_{12,12} \neq \varnothing \tag{2.54}$$

The only configuration for which Eq. (2.54) is violated is when the right TL of S_1

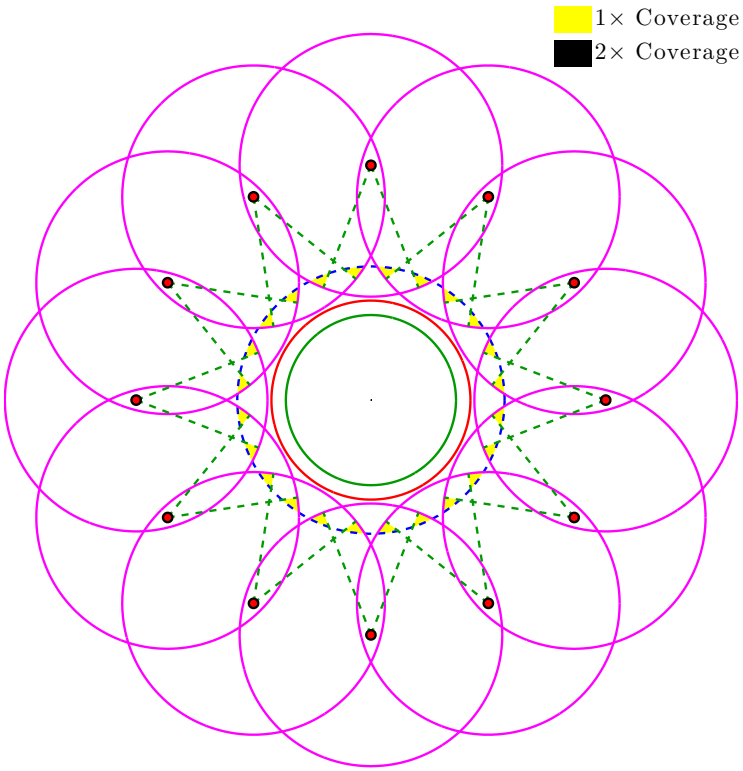

Figure 2.12: Case 2 — $|\overline{OD_{12,12}}| \geq r_u$ with $r_s > r_u$

and the left TL of S_2 are parallel but not collinear:

$$m_{1,1} = m_{2,2} \text{ and } b_{1,1} \neq b_{2,2} \tag{2.55}$$

which is derived from Eq. (2.34). Eq. (2.55) represents a rare scenario that ostensibly can only occur for unrealistic constellations in which $r_s = r_t$. An example is shown in Figure 2.13. Due to this special case, Eq. (2.54) is included as the third necessary condition for the existence of 2-fold coverage. Otherwise, $D_{12,12}$ is guaranteed to exist because the right TL of S_1 and the left TL of S_2 are usually only parallel

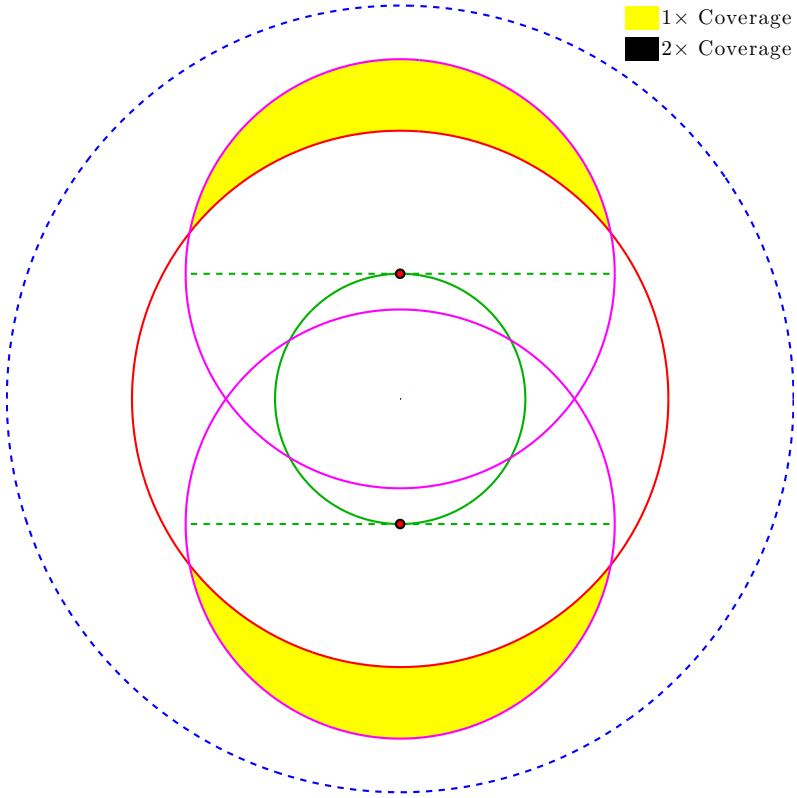

Figure 2.13: Parallel but not collinear tangent lines for $n = 2$ and $r_s = r_t$

if they are also collinear. In other words, $m_{1,1} = m_{2,2}$ is usually only satisfied if $b_{1,1} = b_{2,2}$ is satisfied as well. One could argue for additional necessary conditions, but they would not apply to all possible satellite configurations. These are the only three conditions that must hold for all possible satellite configurations in order for 2-fold coverage to exist.

Much of the derivation is performed using symmetry arguments, as in Eqs. (2.4) and (2.8). Essentially, by choosing to analyze appropriate groupings of adjacent

satellites, the threshold of even coverage multiplicities will always be associated with the bisector of a line segment connecting S_1 and S_2. Similarly, the threshold of odd coverage multiplicities will always be associated with the bisector of a line segment connecting S_2 and S_n or with both TLs of S_1, depending on the satellite altitude. Evidence of the even coverage case is in Figures 2.8–2.10, while evidence of the odd coverage case is in Figure 2.12. For the latter, if r_u were increased beyond r_s, then a region of triple coverage between three adjacent satellites would be associated with the bisector of a line segment connecting S_2 and S_n *and* with both TLs of S_1, since S_1 would be the threshold. This concept will become clearer in the subsequent derivation in Section 2.6.1.2.

2.6.1.1 Necessary Conditions for Existence

Now that the geometry of the problem is more clearly established, the necessary conditions given in Eqs. (2.52) and (2.53) for 2-fold coverage can easily be generalized to p-fold coverage, respectively, as

$$1 < \frac{2R}{d_{\iota\kappa}} \tag{2.56}$$

and

$$|\overline{OD_{21,\iota\kappa}}| < r_u \tag{2.57}$$

Similarly, Eqs. (2.54–2.55) are generalized to a third necessary condition for p-fold coverage as

$$D_{21,\iota\kappa} \neq \varnothing \quad \Longleftrightarrow \quad \text{if } m_{2,\iota} = m_{1,\kappa}, \text{ then } b_{2,\iota} = b_{1,\kappa} \tag{2.58}$$

Eq. (2.58) states that requiring $D_{21,\iota\kappa}$ to exist is equivalent to requiring that the right TL of S_κ and the left TL of S_ι are parallel only if also collinear. Two addi-

tional necessary conditions arise when considering odd p-fold coverage by adjacent satellites:

$$|\overline{OD_{21,1n}}| < r_u \quad \text{for } p \text{ odd} \tag{2.59}$$

$$|\overline{OD_{21,\iota 1}}| < r_u \quad \text{for } p \text{ odd} \tag{2.60}$$

Eqs. (2.59–2.60) are analogous to Eq. (2.57) except that they only apply for odd p. Their similarities should become apparent later in the derivation, specifically in Appendix C during discussions related to and including Eq. (C.33).

2.6.1.2 Derivation of the Fundamental Necessary Condition for Existence

Before beginning the derivation of the fundamental necessary condition on the existence of p-fold coverage, it is helpful to outline a different notation for labeling intersection points as well as some new variables. Specifically, the use of a different satellite numbering convention requires the use of different indices: $\iota = 2, 3, 4, \ldots$ and $\kappa = 1, n, n-1, \ldots$. It will be shown subsequently that the indices ι and κ never overlap. Thus, S_ι is clockwise from S_1 and S_κ is counterclockwise from S_1. It is also essential to define an auxiliary point Q_p for $p = 2, 3, 4, \ldots, p_{max}$, located along the bisector of a line segment connecting special satellite pairs, which are unique for each coverage multiplicity. Recall that p_{max} is some specified desired maximum coverage multiplicity that clearly cannot exceed the number of satellites in the constellation. The maximum coverage multiplicity also should not be less than a test value p since it is pointless to test for coverage multiplicities above some desired value. The need for such a test value would arise under certain circumstances. For example, consider

that p_{max}-fold coverage is required and does not exist for some constellation, say, some suboptimal design solution. Testing, then, for $(p_{max} - 1)$-fold coverage or less would reveal how close the coverage achieved by the constellation is to the desired coverage. Thus, p and p_{max} should presumably be restricted to the range $2 \leq p \leq p_{max} \leq n$, although it will be shown later that due to the way in which the fundamental necessary condition is derived, the case $p_{max} = n$ is treated separately.

With these considerations in mind, the initial step is not actually to define Q_p, but to determine what information Q_p gives about coverage multiplicity. First, as a convention for systematic analysis, it is arbitrarily decided to define the threshold of existence of some coverage multiplicity p as the *lower limit* of p-fold coverage. For example, as shown in Figures 2.8–2.10, the threshold of 2-fold coverage is $\frac{2R}{d_{12}} = 1$, which is the lower limit of 2-fold coverage. The term "lower limit" is used here because if the ratio $\frac{2R}{d_{12}}$ is less than unity, double coverage cannot exist and single coverage becomes the maximum coverage multiplicity that can exist ("can exist" is used because it is possible for no coverage to exist as well). While the existence of p-fold coverage could alternatively be formulated in terms of an *upper limit* of $(p-1)$-fold coverage, this would actually complicate the analysis.

Now, the derivation is done by considering the existence of coverage multiplicities 2 through 5 as four separate examples. From here, a pattern emerges that leads to the formulation of a key equation for determining the existence of coverage multiplicities. For even p, the lower limit of p-fold coverage is linked geometrically to changes in intersection points along the bisector of a line segment $\overline{S_1 S_2}$ connecting satellites S_1 and S_2. Notice that this does not contradict what was said previously,

even though now references to even or odd coverage multiplicities are in the context of lower limits. The geometry is depicted in Figure 2.14 for $p = 2$, where

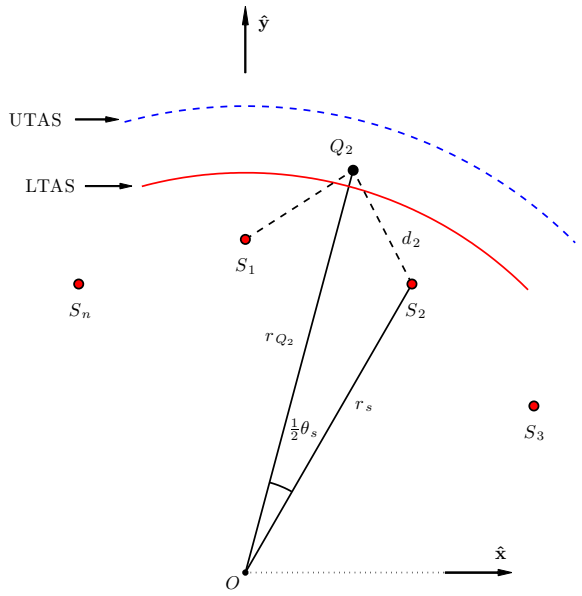

Figure 2.14: Lower limit (threshold) for $p = 2$

$$d_2 = |\overline{Q_2 S_2}| \tag{2.61}$$

The new quantity d_2 is used instead of d_{12} because d_{12} does not directly relate to the bisector of $\overline{S_1 S_2}$. Indeed, d_2 can be used to determine whether $W_{3,21}$ is above point Q_2 in the sense that $|\overline{OW_{3,21}}| > |\overline{OQ_2}|$. Alternatively, d_2 can be used to determine whether $W_{4,21}$ is below point Q_2 in the sense that $x_{W_{4,21}} < x_{Q_2}$ (this becomes important when $r_s > r_u$, as will be shown). Using d_2 in place of d_{12} is only permissible due to considerable symmetry in the constellation.

An alternative representation of the distance d_2 can be obtained by invoking the law of cosines. Letting l_1, l_2, and l_3 be the lengths of the legs of a triangle opposite angles ϕ_1, ϕ_2, and ϕ_3, respectively, the law of cosines states that

$$\begin{aligned} l_1 &= \sqrt{l_2^2 + l_3^2 - 2l_2 l_3 \cos\phi_1} \\ l_2 &= \sqrt{l_1^2 + l_3^2 - 2l_1 l_3 \cos\phi_2} \\ l_3 &= \sqrt{l_1^2 + l_2^2 - 2l_1 l_2 \cos\phi_3} \end{aligned} \tag{2.62}$$

In applying the law of cosines to the problem at hand, Figure 2.14 reveals that d_2 can also be written as

$$d_2 = \sqrt{r_s^2 + r_{Q_2}^2 - 2r_s r_{Q_2} \cos\frac{1}{2}\theta_s} \tag{2.63}$$

where

$$r_{Q_p} \equiv |\overline{OQ_p}| = \sqrt{x_{Q_p}^2 + y_{Q_p}^2} \tag{2.64}$$

Due to symmetry, Eq. (2.64) can also be written as

$$r_{Q_p} = \begin{cases} \sqrt{x_{Q_p}^2 + y_{Q_p}^2} & p \text{ even} \\ y_{Q_p} & p \text{ odd} \end{cases} \tag{2.65}$$

In an effort to relate the satellite indices to the coverage multiplicity of interest, it is useful to keep track of their values for each of the four example coverage multiplicities. For $p = 2$,

$$\begin{aligned} \iota &= \frac{1}{2}(2+2) = 2 \\ \kappa &= 1 \end{aligned} \tag{2.66}$$

For odd p, the lower limit of p-fold coverage is, in some cases, linked geometrically to changes in intersection points along the $\hat{\mathbf{y}}$-axis. The fact that this occurs along the $\hat{\mathbf{y}}$-axis is pure coincidence and a result of the chosen coordinate frames.

More importantly, the changes in intersection points occur along the bisector of a line segment $\overline{S_2S_n}$ connecting satellites S_2 and S_n. Under other circumstances, the lower limit of p-fold coverage is linked to changes in intersection points along both TLs of S_1, symmetric about the bisector of $\overline{S_2S_n}$. Due to symmetry, while these changes occur along both TLs, it is only necessary to analyze the geometry for one TL. As will be demonstrated later in the derivation, the left TL of S_1 is chosen to be consistent with Eq. (2.61), where Q_p is compared to S_ι. The relevant geometry for the first scenario mentioned is depicted in Figure 2.15 for $p = 3$, where

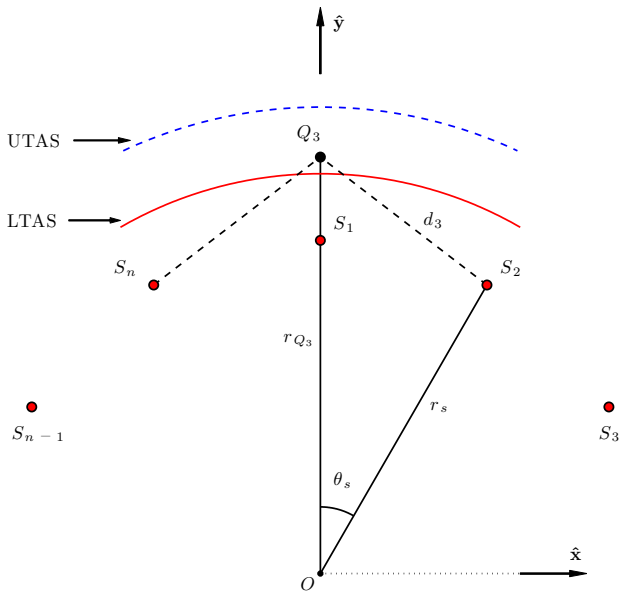

Figure 2.15: Lower limit (threshold) for $p = 3$

$$d_3 = |\overline{Q_3S_2}| \tag{2.67}$$

As should be evident already from Eqs. (2.61) and (2.67), d_2 and d_3 are actually d_p

for $p = 2$ and $p = 3$, respectively. In fact, for a general p (even or odd), Eq. (2.61) can be written as

$$d_p = |\overline{Q_p S_\iota}| \quad \text{for } p = 2, 3, 4, \ldots, n \tag{2.68}$$

when used with the correct formula for ι, which will be given shortly in Eq. (2.75). Thus, in some cases, d_p is used to determine whether $W_{3,\iota\kappa}$ is above point Q_p in the sense that $|\overline{OW_{3,\iota\kappa}}| > |\overline{OQ_p}|$. In other cases, d_p is used to determine whether $W_{4,\iota\kappa}$ is below point Q_p in the sense that $x_{W_{4,\iota\kappa}} < x_{Q_p}$. Note that the previous two statements hold true for even and odd p. Using the law of cosines, an alternative representation for the distance d_3 is

$$d_3 = \sqrt{r_s^2 + r_{Q_3}^2 - 2 r_s r_{Q_3} \cos \frac{2}{2}\theta_s} = \sqrt{r_s^2 + r_{Q_3}^2 - 2 r_s r_{Q_3} \cos \theta_s} \tag{2.69}$$

Lastly, note that for $p = 3$, satellite indices are given by

$$\begin{aligned} \iota &= \frac{1}{2}(3 + 1) = 2 \\ \kappa &= n + 2 - 2 = n \end{aligned} \tag{2.70}$$

Next, incrementing the coverage multiplicity to $p = 4$ gives new geometry shown in Figure 2.16. Notice that the geometry is similar to that in Figure 2.14 for $p = 2$, except that the critical distance is associated with a different satellite pair. The new pair is S_3 and S_n, which is the next closest pair to point Q_2 that is symmetric about the bisector of $\overline{S_1 S_2}$. From Figure 2.16, observe that an alternative representation for the distance d_4 is

$$d_4 = \sqrt{r_s^2 + r_{Q_4}^2 - 2 r_s r_{Q_4} \cos \frac{3}{2}\theta_s} \tag{2.71}$$

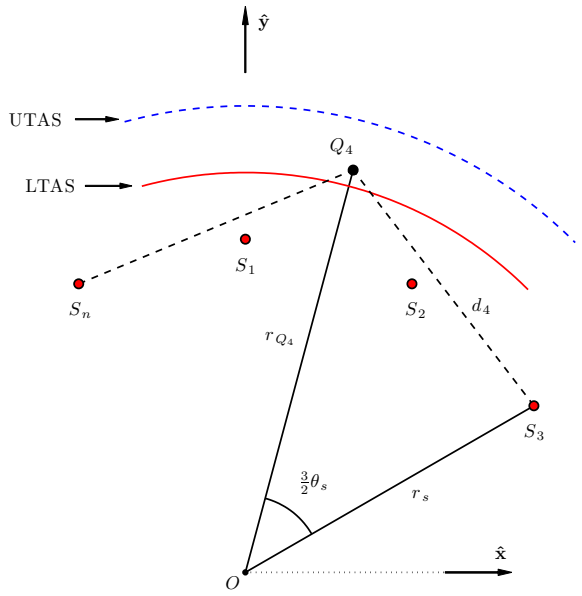

Figure 2.16: Lower limit (threshold) for $p = 4$

again obtained from the law of cosines. Satellite indices for $p = 4$ are

$$\begin{aligned} \iota &= \frac{1}{2}(4+2) = 3 \\ \kappa &= n + 3 - 3 = n \end{aligned} \tag{2.72}$$

Incrementing the coverage multiplicity to $p = 5$ again presents new but familiar geometry, where the geometry illustrated in Figure 2.17 is similar to that in Figure 2.15 for $p = 3$, except that the critical distance is associated with a different satellite pair. The new pair is S_3 and S_{n-1}, which is the next closest pair to point Q_3 that is symmetric about the bisector of $\overline{S_2 S_n}$. The distance d_5 is given by Eq. (2.68), or alternatively by

$$d_5 = \sqrt{r_s^2 + r_{Q_5}^2 - 2 r_s r_{Q_5} \cos\frac{4}{2}\theta_s} = \sqrt{r_s^2 + r_{Q_5}^2 - 2 r_s r_{Q_5} \cos 2\theta_s} \tag{2.73}$$

Satellite indices for $p = 5$ are found to be

$$\begin{aligned} \iota &= \frac{1}{2}(5+1) = 3 \\ \kappa &= n + 2 - 3 = n - 1 \end{aligned} \tag{2.74}$$

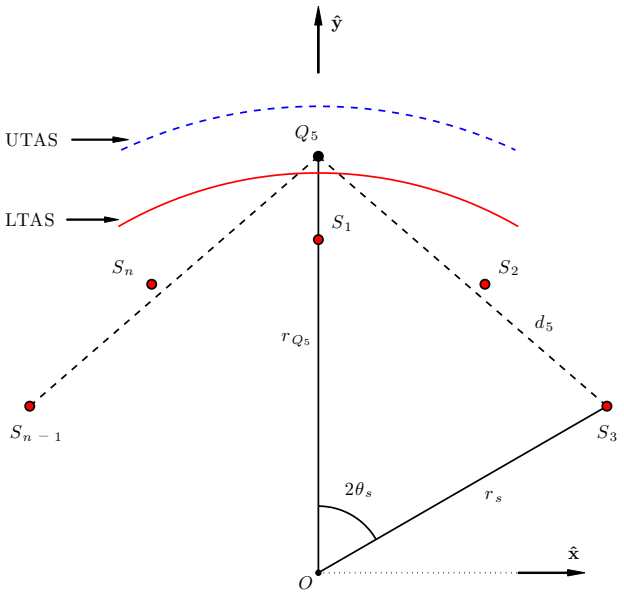

Figure 2.17: Lower limit (threshold) for $p = 5$

At this point, it is important to notice that the bisector of $\overline{S_\iota S_\kappa}$ is always equivalent to the bisector of $\overline{S_1 S_2}$ for even p and the bisector of $\overline{S_2 S_n}$ for odd p. This is a direct consequence of the aforementioned symmetry, which greatly simplifies the analysis because all coverage multiplicity thresholds are associated with changes in intersection points along only two distinct and clearly defined lines. Even when the constraint of only considering coverage between adjacent satellites is relaxed, cov-

erage multiplicity thresholds are still associated with changes in intersection points along the same two lines except that the link between even and odd p changes.

From the preceding four examples, a pattern emerges from Eqs. (2.66), (2.70), (2.72), and (2.74) suggesting that satellite indices can be expressed in terms of the coverage multiplicity p as

$$\iota = \begin{cases} \frac{1}{2}(p+2) & p \text{ even} \\ \frac{1}{2}(p+1) & p \text{ odd} \end{cases} \tag{2.75}$$

$$\kappa = \begin{cases} [(n+2-\iota) \bmod n] + 1 & p \text{ even} \\ n+2-\iota & p \text{ odd} \end{cases} \tag{2.76}$$

The equation for even p in Eq. (2.76) is obtained from simplifying the following more obvious expression:

$$\kappa = \begin{cases} 1 & \text{if } \iota = 2 \\ n+3-\iota & \text{if } \iota > 2 \end{cases} \tag{2.77}$$

A pattern also emerges from Eqs. (2.63), (2.69), (2.71), and (2.73), leading to the following alternative expression for d_p as compared to Eq. (2.68):

$$d_p = \sqrt{r_s^2 + r_{Q_p}^2 - 2r_s r_{Q_p} \cos\left(\frac{p-1}{2}\theta_s\right)} \quad \text{for } p = 2, 3, 4, \ldots, n \tag{2.78}$$

Note that Eq. (2.78) is valid for both even and odd p. Another nice aspect of this expression becomes apparent by substituting Eq. (2.11) into Eq. (2.78):

$$d_p = \sqrt{r_s^2 + r_{Q_p}^2 - 2r_s r_{Q_p} \cos\frac{\pi(p-1)}{n}} \quad \text{for } p = 2, 3, 4, \ldots, n \tag{2.79}$$

Eq. (2.79) shows more clearly the dependence of coverage multiplicity on the number of satellites in the constellation since n appears explicitly in the formula. However, a clear disadvantage to defining d_p with Eq. (2.79) instead of Eq. (2.68) is that Eq. (2.79) can only be used for odd p if Q_p is located on the bisector of $\overline{S_2 S_n}$.

Finally, the ultimate necessary condition for p-fold coverage becomes $d_p < R$, or

$$1 < \frac{R}{d_p} \quad \text{for } p = 2, 3, 4, \ldots, n \tag{2.80}$$

Next, it helps to paint a more complete picture of the bounds on the coverage multiplicity conditions. For example, if a maximum allowable coverage multiplicity p_{max} is to be imposed, this condition is simply expressed as $d_{p_{max}+1} \geq R$ or

$$1 \geq \frac{R}{d_{p_{max}+1}} \quad \text{for } p_{max} < n \tag{2.81}$$

The equality is imposed because p_{max+1}-fold coverage still does not exist when R and $d_{p_{max}+1}$ are equal; it only exists when R exceeds $d_{p_{max}+1}$. Furthermore, this does not mean that p_{max}-fold coverage must exist, simply that the maximum coverage multiplicity *allowed* is p_{max}. Observe that Eqs. (2.80) and (2.81) are always finite: $d_p \neq 0$ and $d_{p_{max}+1} \neq 0$ because the location of each satellite of a pair associated with p-fold coverage (S_ι and S_κ) is never equal to the location of Q_p. It could only occur if $S_\iota = S_\kappa$, which is impossible since the satellites are uniformly distributed.

If Eq. (2.81) is imposed, it may be helpful to write the inequalities in Eqs. (2.80) and (2.81) as one expression:

$$\frac{R}{d_{p_{max}+1}} \leq 1 < \frac{R}{d_p} \quad \text{for } p = 2, 3, 4, \ldots, p_{max} \tag{2.82}$$

Several comments and observations should be made about Eq. (2.80–2.82). For existence, the fundamental necessary condition for p-fold coverage is Eq. (2.80). If some maximum coverage multiplicity is to be *required*, then the condition

$$\frac{R}{d_{p_{max}+1}} \leq 1 < \frac{R}{d_{p_{max}}} \quad \text{for } p_{max} < n \tag{2.83}$$

must be satisfied. Also note that Eq. (2.81) is only valid if the coverage multiplicity p being tested satisfies the condition $p < n$, and more specifically, $p \leq p_{max} < n$. If $p = n$ or $p_{max} = n$, then the only condition for existence is, respectively, Eq. (2.80) or

$$1 < \frac{R}{d_{p_{max}}} \tag{2.84}$$

In either case, though, the actual condition is on the existence of n-fold coverage:

$$1 < \frac{R}{d_n} \tag{2.85}$$

2.6.1.3 Necessary and Sufficient Conditions for Existence

Compare Eq. (2.80) to Eq. (2.56) and note the differences. They are both necessary, but Eq. (2.56) is much more conservative. The fundamental idea behind this is that Eq. (2.56) is strictly concerned with the intersection of range shells, while Eq. (2.80) must ensure that the intersection region of range shells occurs entirely or partially above the horizon of the satellite pair (S_ι, S_κ) and all preceding pairs. This is the precise function of Q_p and is the very idea that leads to the series of conditions in Tables 2.7–2.8. The other necessary conditions given by Eqs. (2.57–2.60) ensure that the intersection region of range shells occurs entirely or partially within the dual-altitude band. Thus, coupling Eqs. (2.57–2.60) with the fundamental condition derived in this section creates a set of necessary and sufficient conditions for the existence of p-fold coverage provided by p adjacent satellites.

2.6.1.4 Determining the Location of Q_p

Before discussing the conditions in Tables 2.7–2.8, the reader might benefit from some observations about Q_p. First, notice that if $n = 2$, then Q_2 lies on the $\hat{\mathbf{x}}$-axis. Furthermore, Q_p is bounded by the LTAS and UTAS, and in many instances, the threshold occurs when Q_p coincides with a $M_{\iota\kappa}$ midpoint or a $D_{21,\iota\kappa}$ intersection. As mentioned before, different satellite indices (ι and κ) are used here and the index conventions adopted in the derivation of shell intersection point locations no longer apply. For this reason, $D_{21,21}$ appears in Table 2.8 instead of $D_{12,12}$. Also, recall that, in reality, Eq. (2.80) compares Q_p to $W_{\tau,\iota\kappa}$ for one of the two possible values of τ. Depending on the satellite altitude, τ takes on one of two values. Usually, $\tau = 3$ is relevant, but not when the satellite altitude exceeds the UTAS ($r_s > r_u$). In that case, $\tau = 4$ may be relevant. The basic strategy for deriving Tables 2.7–2.8 takes the dependence on satellite altitude into account by dividing the conditions into three cases, separately for even and odd p, where each case is a range of satellite altitude: $r_t \leq r_s < r_l$, $r_l \leq r_s < r_u$, and $r_u \leq r_s < r_{s_3}$. For a detailed derivation of how to determine the location of Q_p, see Appendix C.

In the process of locating Q_p, it is necessary to define a new point $P_{2,1\iota}$, which is similar to $M_{\iota\kappa}$ in that it is a special point on a line. $M_{\iota\kappa}$ is the midpoint of a line connecting S_ι and S_κ, while $P_{2,1\iota}$ is the point on the left TL of S_1 that is closest to S_ι. Neither $M_{\iota\kappa}$ nor $P_{2,1\iota}$ is an intersection point in the same sense as Type I and II intersections, because they do not result from the intersection of shells and/or tangent lines. Rather, these two points are geometric constructs. The derivation of $P_{2,1\iota}$, as well as an explanation of its significance, is included as

part of the derivation of Q_p in Appendix C, but the results are repeated here for convenience. The coordinates of $P_{2,1\iota}$ are

$$\begin{aligned} x_{P_{2,1\iota}} &= \frac{m_{2,1}}{m_{2,1}^2+1}\left(\frac{x_{s_\iota}}{m_{2,1}} + y_{s_\iota} - r_s\right) \\ y_{P_{2,1\iota}} &= m_{2,1}x_{P_{2,1\iota}} + r_s \end{aligned} \tag{2.86}$$

The necessary and sufficient conditions on the existence of p-fold coverage are partial — not complete — because they are valid only for p-fold coverage occurring between p adjacent satellites. In general, for satellites with omnidirectional sensors uniformly distributed along a circular orbit, above-the-horizon p-fold coverage can occur between non-adjacent satellites as well, which includes coverage by combinations of adjacent and non-adjacent satellites. Note that generalized conditions would not replace the partial conditions just derived; rather, they would augment the partial conditions and lead to the creation of more tables similar to Tables 2.7–2.8. For example, then, to fully test for the existence of 3-fold coverage would require examining Table 2.7 and another one that accounts for the possibility of 3-fold coverage being provided by non-adjacent satellites.

Ultimately, the conditions and equations derived in Appendix C are compiled into separate tables for even and odd p. Eq. (C.1), Eqs. (C.4–C.6), Eqs. (C.24–C.29), and Eqs. (C.38–C.48) are used to populate Table 2.7 for odd p, while Eq. (C.1), Eqs. (C.4–C.6), and Eqs. (C.7–C.16) are used to populate Table 2.8 for even p. To keep Table 2.8 within the margins, the shorthand "LTAS" is adopted for the point $\left(r_l \sin\frac{\pi}{n}, r_l \cos\frac{\pi}{n}\right)$ and "UTAS" is adopted for the point $\left(r_u \sin\frac{\pi}{n}, r_u \cos\frac{\pi}{n}\right)$ in the Q_p column. The modified notation $(D_{21,21})_y = y_{D_{21,21}}$ for indicating the y-coordinate of a point is also used in Tables 2.7–2.9 to help keep the tables within

the margins. Each table should be read from left to right, following a particular chain of conditions to ultimately identify Q_p. For example, consider a test for 5-fold coverage in the range $r_l \leq r_s < r_u$, assuming that Eqs. (2.57–2.60) are satisfied. Suppose that $y_{L_{2_B},1} \leq y_{P_{2,13}} < r_s$, which is one of the three possible conditions in the first column of Table 2.7. Next, in the second column, $y_{D_{22,31}}$ must be compared with $y_{P_{2,13}}$. Suppose that $y_{P_{2,13}} < y_{D_{22,31}}$. Lastly, in the third column, $y_{D_{22,31}}$ must be compared with $y_{D_{21,1n}}$. If $y_{D_{21,1n}} \leq y_{D_{22,31}}$, then it is clear from the fourth column that $Q_5 = D_{22,31}$. Finally, if $|Q_5 S_3| < R$ (from Eq. (2.80)), then 5-fold coverage exists.

Table 2.7: Flow Chart — Conditions for Determining the Location of Q_p, Odd $p \geq 2$

	Conditions			Q_p
$r_t \leq \vert \vee \leq r_s \vee \leq r_l$	$\vert\overline{OD_{21,\iota\kappa}}\vert \leq r_l$			$(0, r_l)$
	$r_l < \vert\overline{OD_{21,\iota\kappa}}\vert$			$D_{21,\iota\kappa}$
$r_l \leq \vert \vee \leq r_s \vee \leq r_u$	$(P_{2,1\iota})_y < (L_{2_B,1})_y$	$(D_{22,\iota 1})_y \leq (L_{2_B,1})_y$	$(D_{21,1n})_y \leq (L_{2_B,1})_y$	$L_{2_B,1}$
			$(L_{2_B,1})_y < (D_{21,1n})_y$	$D_{21,1n}$
		$(L_{2_B,1})_y < (D_{22,\iota 1})_y$	$(D_{21,1n})_y \leq (D_{22,\iota 1})_y$	$D_{22,\iota 1}$
			$(D_{22,\iota 1})_y < (D_{21,1n})_y$	$D_{21,1n}$
	$(L_{2_B,1})_y \leq (P_{2,1\iota})_y < r_s$	$(D_{22,\iota 1})_y \leq (P_{2,1\iota})_y$	$(D_{21,1n})_y \leq (P_{2,1\iota})_y$	$P_{2,1\iota}$
			$(P_{2,1\iota})_y < (D_{21,1n})_y$	$D_{21,1n}$
		$(P_{2,1\iota})_y < (D_{22,\iota 1})_y$	$(D_{21,1n})_y \leq (D_{22,\iota 1})_y$	$D_{22,\iota 1}$
			$(D_{22,\iota 1})_y < (D_{21,1n})_y$	$D_{21,1n}$
	$r_s \leq (P_{2,1\iota})_y$	$\vert\overline{OD_{21,\iota\kappa}}\vert \leq r_s$		S_1
		$r_s < \vert\overline{OD_{21,\iota\kappa}}\vert$		$D_{21,\iota\kappa}$
$r_u \leq \vert \vee \leq r_s \vee \leq r_{s_3}$	$(P_{2,1\iota})_y < (L_{2_B,1})_y$	$(D_{22,\iota 1})_y \leq (L_{2_B,1})_y$	$(D_{21,1n})_y \leq (L_{2_B,1})_y$	$L_{2_B,1}$
			$(L_{2_B,1})_y < (D_{21,1n})_y$	$D_{21,1n}$
		$(L_{2_B,1})_y < (D_{22,\iota 1})_y$	$(D_{21,1n})_y \leq (D_{22,\iota 1})_y$	$D_{22,\iota 1}$
			$(D_{22,\iota 1})_y < (D_{21,1n})_y$	$D_{21,1n}$
	$(L_{2_B,1})_y \leq (P_{2,1\iota})_y < (U_{2_B,1})_y$	$(D_{22,\iota 1})_y \leq (P_{2,1\iota})_y$	$(D_{21,1n})_y \leq (P_{2,1\iota})_y$	$P_{2,1\iota}$
			$(P_{2,1\iota})_y < (D_{21,1n})_y$	$D_{21,1n}$
		$(P_{2,1\iota})_y < (D_{22,\iota 1})_y$	$(D_{21,1n})_y \leq (D_{22,\iota 1})_y$	$D_{22,\iota 1}$
			$(D_{22,\iota 1})_y < (D_{21,1n})_y$	$D_{21,1n}$
	$(U_{2_B,1})_y \leq (P_{2,1\iota})_y$			$U_{2_B,1}$

Table 2.8: Flow Chart — Conditions for Determining the Location of Q_p, Even $p \geq 2$

	Conditions			Q_p
$r_t \vee r_s \vee r_l$	$\lvert\overline{OD_{21,\iota\kappa}}\rvert \leq r_l$			LTAS
	$r_l < \lvert\overline{OD_{21,\iota\kappa}}\rvert$			$D_{21,\iota\kappa}$
$r_l \vee r_s \vee r_u$	$(M_{\iota\kappa})_y \leq r_l \cos\frac{\pi}{n}$	$\lvert\overline{OD_{21,\iota\kappa}}\rvert \leq r_l$	$\lvert\overline{OD_{21,21}}\rvert \leq r_l$	LTAS
			$r_l < \lvert\overline{OD_{21,21}}\rvert$	$D_{21,21}$
		$r_l < \lvert\overline{OD_{21,\iota\kappa}}\rvert$	$(D_{21,21})_y \leq (D_{21,\iota\kappa})_y$	$D_{21,\iota\kappa}$
			$(D_{21,\iota\kappa})_y < (D_{21,21})_y$	$D_{21,21}$
	$r_l \cos\frac{\pi}{n} < (M_{\iota\kappa})_y$		$(D_{21,21})_y \leq (M_{\iota\kappa})_y$	$M_{\iota\kappa}$
			$(M_{\iota\kappa})_y < (D_{21,21})_y$	$D_{21,21}$
$r_u \vee r_s \vee r_{s_3}$	$(M_{\iota\kappa})_y \leq r_l \cos\frac{\pi}{n}$	$\lvert\overline{OD_{21,\iota\kappa}}\rvert \leq r_l$	$\lvert\overline{OD_{21,21}}\rvert \leq r_l$	LTAS
			$r_l < \lvert\overline{OD_{21,21}}\rvert$	$D_{21,21}$
		$r_l < \lvert\overline{OD_{21,\iota\kappa}}\rvert$	$(D_{21,21})_y \leq (D_{21,\iota\kappa})_y$	$D_{21,\iota\kappa}$
			$(D_{21,\iota\kappa})_y < (D_{21,21})_y$	$D_{21,21}$
	$r_l \cos\frac{\pi}{n} < (M_{\iota\kappa})_y < r_u \cos\frac{\pi}{n}$		$(D_{21,21})_y \leq (M_{\iota\kappa})_y$	$M_{\iota\kappa}$
			$(M_{\iota\kappa})_y < (D_{21,21})_y$	$D_{21,21}$
	$r_u \cos\frac{\pi}{n} \leq (M_{\iota\kappa})_y$			UTAS

2.6.2 Partial Conditions on the Existence of 2-fold Coverage

From Eqs. (2.68) (also in Eq. (2.61)) and (2.80), the fundamental necessary condition for the existence of 2-fold coverage by adjacent satellites is

$$|\overline{Q_2 S_2}| < R \tag{2.87}$$

where Q_2 is an auxiliary point defined in Table 2.9, covering all possible parameter configurations. In short, the results are obtained from Table 2.8 by using $p = 2$. Greater detail and discussion is given in Appendix C for even p, but a brief

explanation follows. Notice in Figure 2.2 that a line drawn from the origin to $W_{3,12}$ bisects the region $C'_{2\times,12}$. By definition, 2-fold coverage by two adjacent satellites is created at a point Q_2 on this bisector and within the region of interest. In the absence of altitude shells, 2-fold coverage would be created at the midpoint $Q_2 = M_{12}$, but when altitude shells are taken into account, the location of Q_2 depends on the satellite altitude and other factors. Table 2.9 provides a simplified version of Table 2.8; simplifications are valid because for $p = 2$, clearly $D_{21,\iota\kappa} = D_{21,21}$, which creates redundant conditions. Thus, all redundant conditions involving $D_{21,\iota\kappa}$ are removed. The same does not hold for $M_{\iota\kappa}$ because even though $M_{\iota\kappa} = M_{12}$, no redundant conditions are created as a result. Also, note in Table 2.9 that $D_{12,12}$ is used instead of $D_{21,21}$, which is used in Tables 2.7–2.8. This change in notation is made to facilitate comparison to Figure 2.2 as well as to previous discussions of D intersections. M_{12} is then used instead of M_{21} for consistency, even though $\iota = 2$ and $\kappa = 1$.

Remaining necessary conditions for the existence of 2-fold coverage (or less) for adjacent satellites are

$$\begin{gathered} d_{12} < 2R \\ |\overline{OD_{12,12}}| < r_u \\ D_{12,12} \neq \varnothing \quad \Longleftrightarrow \quad \text{if } m_{1,1} = m_{2,2}, \text{ then } b_{1,1} = b_{2,2} \end{gathered} \tag{2.88}$$

which when coupled with Eq. (2.87) constitutes a set of necessary and sufficient conditions for existence.

Table 2.9: Flow Chart — Conditions for Determining the Location of Q_p, $p = 2$

	Conditions		Q_2
$r_l \vee r_s \vee r_l$	$\lvert\overline{OD_{12,12}}\rvert \le r_l$		$(r_l \sin\frac{\pi}{n}, r_l \cos\frac{\pi}{n})$
$r_l \vee\lvert r_s$	$r_l < \lvert\overline{OD_{12,12}}\rvert$		$D_{12,12}$
$r_l \vee\lvert r_s \vee r_u$	$(M_{12})_y \le r_l \cos\frac{\pi}{n}$	$\lvert\overline{OD_{12,12}}\rvert \le r_l$	$(r_l \sin\frac{\pi}{n}, r_l \cos\frac{\pi}{n})$
		$r_l < \lvert\overline{OD_{12,12}}\rvert$	$D_{12,12}$
	$r_l \cos\frac{\pi}{n} < (M_{12})_y$	$(D_{12,12})_y \le (M_{12})_y$	M_{12}
		$(M_{12})_y < (D_{12,12})_y$	$D_{12,12}$
$r_u \vee\lvert r_s \vee r_{s_3}$	$(M_{12})_y \le r_l \cos\frac{\pi}{n}$	$\lvert\overline{OD_{12,12}}\rvert \le r_l$	$(r_l \sin\frac{\pi}{n}, r_l \cos\frac{\pi}{n})$
		$r_l < \lvert\overline{OD_{12,12}}\rvert$	$D_{12,12}$
	$r_l \cos\frac{\pi}{n} < (M_{12})_y < r_u \cos\frac{\pi}{n}$	$(D_{12,12})_y \le (M_{12})_y$	M_{12}
		$(M_{12})_y < (D_{12,12})_y$	$D_{12,12}$
	$r_u \cos\frac{\pi}{n} \le (M_{12})_y$		$(r_u \sin\frac{\pi}{n}, r_u \cos\frac{\pi}{n})$

Chapter 3

Results and Validation

Much insight to the dependency of coverage area on the parameters can be gained by implementing the development in Chapter 2. The results given in this chapter serve that purpose in addition to validating the computational approach proposed by Takano and Marchand.[1,17] The discussion and presentation of results is preceded by a section establishing some constraints on the parameter space. Next, basic validation of the coverage area calculation is accomplished, followed by validation of an example optimal constellation design problem with a single independent variable. Lastly, sample parameter spaces are examined for constellation design with multiple independent variables.

3.1 Constraints on the Parameter Space

The development in Chapter 2 limits analytical simulations to constellations providing at most 2-fold coverage by adjacent satellites. To ensure that no coverage multiplicities greater than two exist for an arbitrary simulation, a condition can be imposed stating that triplets of adjacent satellites cannot intersect:

$$d_{2n} \geq 2R \tag{3.1}$$

which precludes the existence of coverage multiplicities $p \geq 3$ in general and $p = 2$ for non-adjacent satellites. This is a conservative constraint, however, because it is

possible for only 1-fold coverage and 2-fold coverage by adjacent satellites to exist with $d_{2n} < 2R$. Alternative constraints could also be devised.

3.2 Parameter Space and Validation of Numerical Methods

With the preceding analysis and development complete, initial exploration of the parameter space can be performed. The results in this section impose the constraint given by Eq. (3.1). Figures 3.1–3.3 show three possible types of behavior

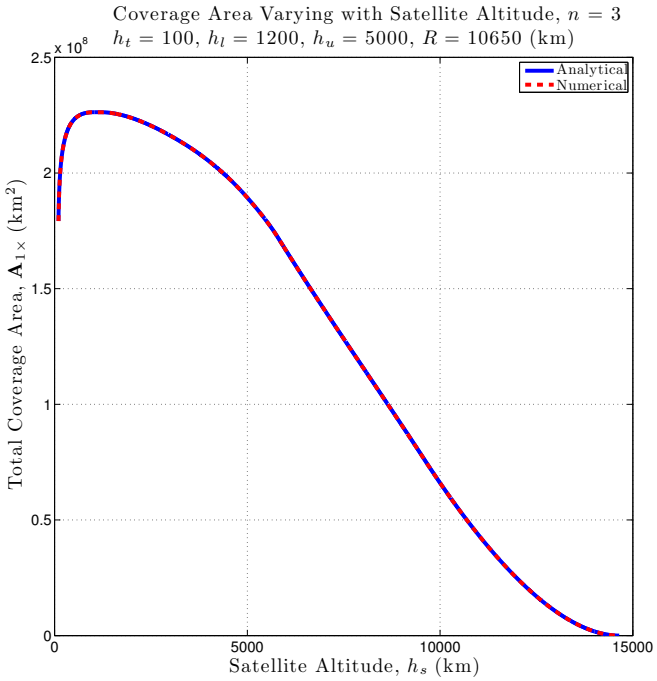

Figure 3.1: Total coverage area vs. satellite altitude (Example 1) is a continuous smooth curve: Optimal altitude corresponds to maximum coverage area

for how the total coverage area varies with satellite altitude, h_s, when all other parameters are held fixed. The tangent height, h_t, is conservatively chosen to be 100

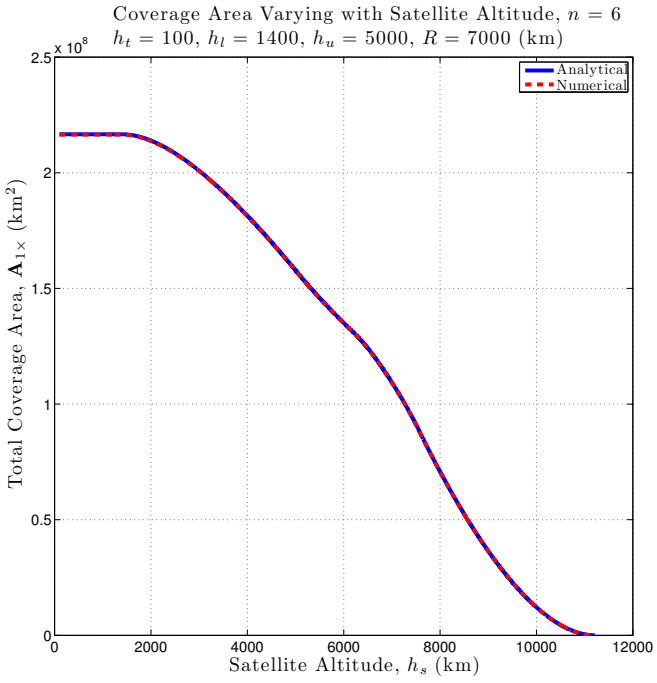

Figure 3.2: Total coverage area vs. satellite altitude (Example 2) is a continuous smooth curve: Maximum coverage area saturation observed at low altitudes

km for all of the following simulations to avoid line of sight penetration of the portion of the atmosphere that could contain Earth limb, airglow, and auroral effects.[15] Figure 3.1 shows a case where there is a clear optimal satellite altitude corresponding to a maximum coverage area provided by the constellation. Under other conditions, as shown in Figure 3.2, saturation can occur at low satellite altitudes; these are regimes in which varying h_s offers no coverage benefit. Another interesting artifact of total coverage area is observed in Figure 3.3, where a sharp corner is apparent near $h_s \approx 10,820$ km. The explanation for this is that the overlap area shape $C'_{2\times,12}$ changes type rapidly over a small range — approximately 70 km — of satellite

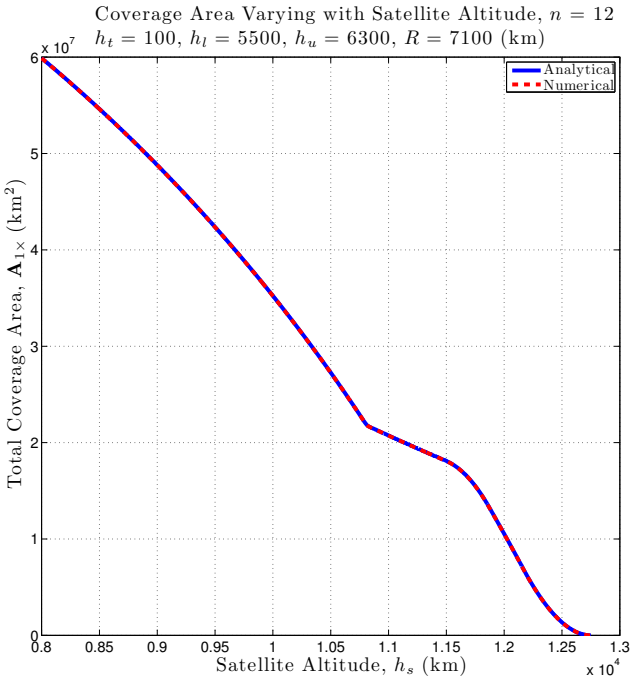

Figure 3.3: Total coverage area vs. satellite altitude (Example 3) is a continuous non-smooth curve: Global maximum exists only at the start of the altitude range considered

altitude.

Another purpose of this analysis is to provide an analytical means of validating the numerical process proposed by Takano and Marchand.[1,17] The numerical algorithm employed by these authors is generally applicable to the time-varying and the time-invariant case, with generalized sensor profiles. However, since closed form solutions are not available in the generalized case, an intermediate step is to validate a set of simplified cases, such as those discussed here. For example, the simulation results presented in Figures 3.1–3.3 do not encompass all possible scenarios, but

do validate a subset of satellite configurations in a single circular orbit against the numerical model derived by Takano and Marchand.[1,17] An even larger subset of

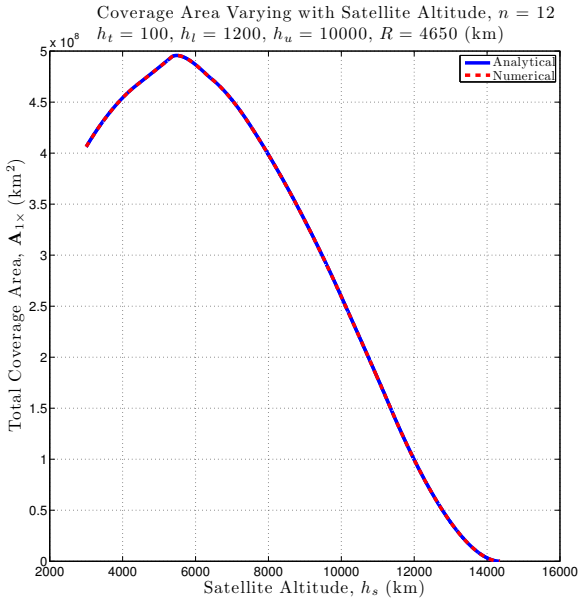

Figure 3.4: Example 4: Total coverage area vs. satellite altitude

satellite configurations is validated in Figures 3.4–3.7, which together with Figures 3.1–3.3 cover all 22 cases defined in Tables 2.5–2.6. Appendix D provides evidence in Figures D.1–D.10 that all 22 cases are indeed validated.

Figures 3.1–3.7 compare analytical and numerical results for continuous coverage area by fixing all parameters and then increasing the satellite altitude. Further notice that the values of the fixed parameters are different in each simulation. The present study seeks to provide complete validation of the numerical process under the stated simplified set of assumptions, including the constellation coverage area

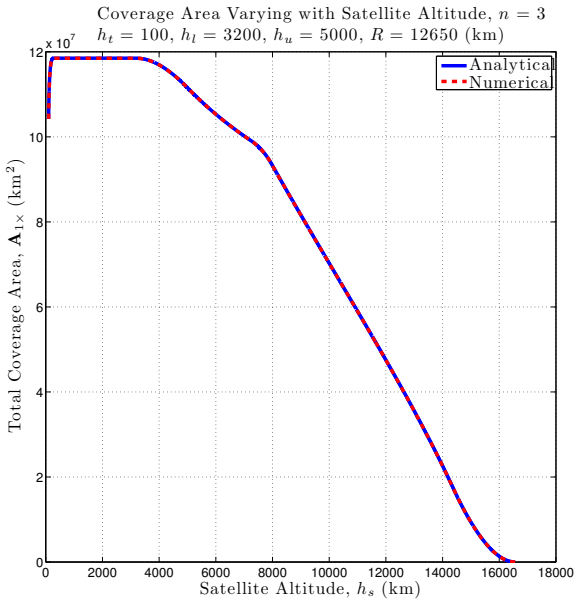

(a) Example 5

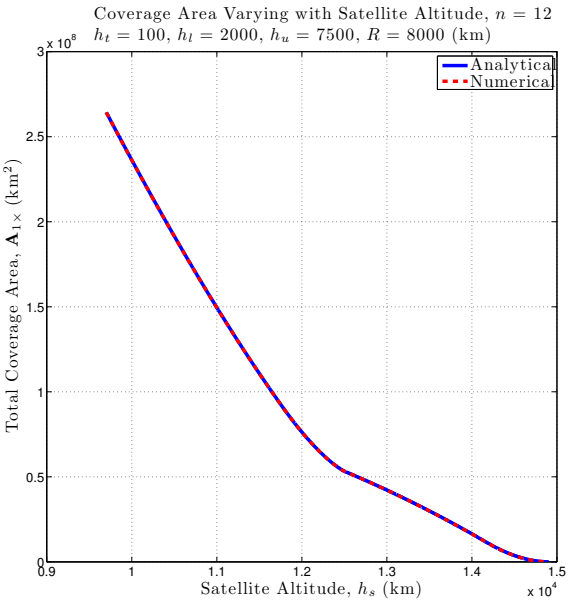

(b) Example 6

Figure 3.5: Total coverage area vs. satellite altitude

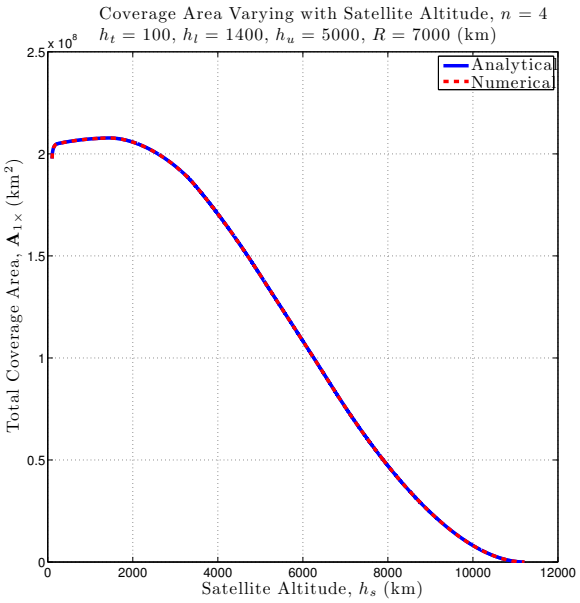

(a) Example 7

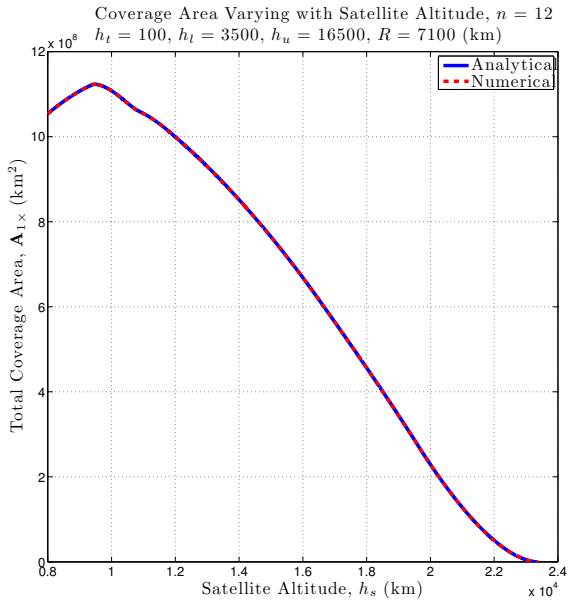

(b) Example 8

Figure 3.6: Total coverage area vs. satellite altitude

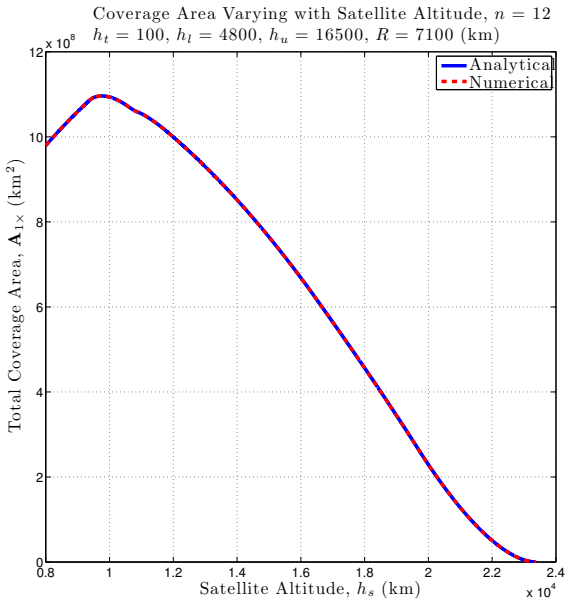

(a) Example 9

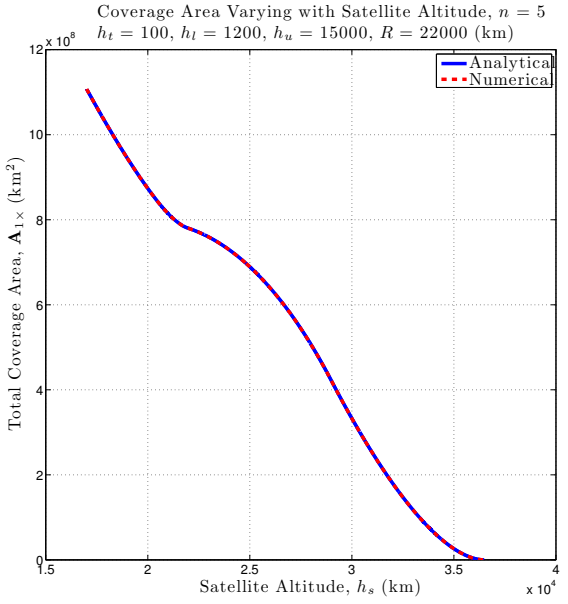

(b) Example 10

Figure 3.7: Total coverage area vs. satellite altitude

calculation and the 2-fold coverage constraint. The numerical approach[1,17] considers a cost index determined numerically through the synthesis of computer graphics methods. The process employed here, in contrast, provides validation with an analytically determined cost index.

3.3 Optimal Constellation Design

The analytical model's capabilities are more fully demonstrated when applied to optimal constellation design. The optimization problem posed in this example is to minimize the number of satellites required to achieve at least 99.9% single coverage of DABS over a range of satellite altitudes. This example is borrowed from Takano and Marchand[17] so that the analytical results obtained can be compared with his numerical results.

For simplicity, the problem is designed to have only one independent variable, so four of the parameters — h_t, h_l, h_u, and R — are fixed, with values given in Figure 3.8. Furthermore, the value employed in this example for the equatorial radius of the Earth is 6378.14 km, as opposed to 6378 km, which was used for all other analysis in this investigation. Although Takano and Marchand considered a satellite altitude range of 100 to 6000 km, this is not possible with the current analytical model, because the only coverage multiplicities with associated objective functions are 1-fold coverage and 2-fold coverage between adjacent satellites. Thus, the altitude range is limited in this study to be between 100 and 1212 km, which is the highest altitude for which a minimal number of satellites can be analytically determined with these four particular parameter values. The necessary and sufficient conditions

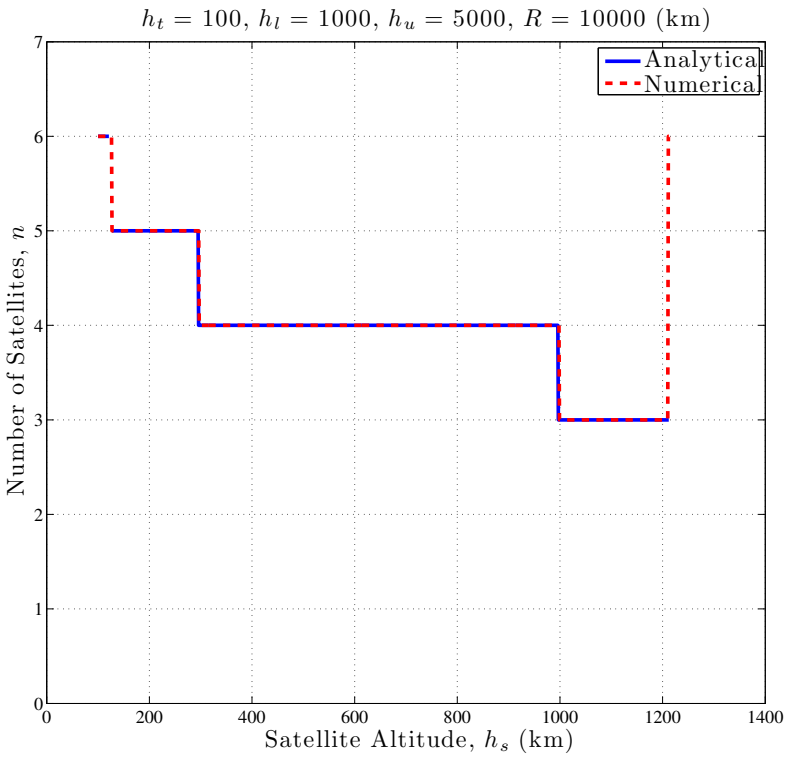

Figure 3.8: Minimum number of satellites vs. satellite altitude

in Section 2.6 are implemented to ensure proper restriction of the parameter space. For consistency with the numerical results, a 1 km resolution is employed over the constellation altitude range. To optimize the constellation, a grid search is performed at each altitude, ultimately affording the results in Figure 3.8. While the model implemented is strictly analytical, the results are still subject to roundoff and truncation error. Consequently, coverage area up to $10^{-10}\%$ greater than $\mathbf{A}_{\mathrm{DABS}}$ is also allowed to prevent loss of data or erroneous results. In other words, acceptable coverage area values are within the following range:

$$0.999\mathbf{A}_{\mathrm{DABS}} \leq \mathbf{A}_{1\times} \leq (1 + 10^{-12})\mathbf{A}_{\mathrm{DABS}}$$

The limits of the analytical model are also evident *within* the altitude range considered. Between altitudes of 121 and 127 km, no analytical result is available because triple coverage exists for those cases. The gap in data appears as a missing segment of the blue curve in Figures 3.8–3.10. The primary source of discrepancy between the analytical and numerical results are that Takano and Marchand did not use the true value of $\mathbf{A}_{\mathrm{DABS}}$; rather, they computed its value numerically, approximating each altitude shell as a regular polygon with 100 vertices. Thus, the valid range of $\mathbf{A}_{1\times}$ is not identical for the analytical and numerical methods. In Figure 3.8, this difference affects the satellite altitude at which the minimum number of satellites transitions to a higher or lower value. Figure 3.9 reveals that the primary source of error is a bias introduced by the numerical method in the calculation of $\mathbf{A}_{\mathrm{DABS}}$. For further error analysis, the relative error in $\mathbf{A}_{1\times}$ is computed as

$$\mathbf{A}_{1\times,\mathrm{err}} = \frac{|\mathbf{A}_{1\times} - \mathbf{A}_{1\times,\mathrm{num}}|}{\mathbf{A}_{1\times}} \tag{3.2}$$

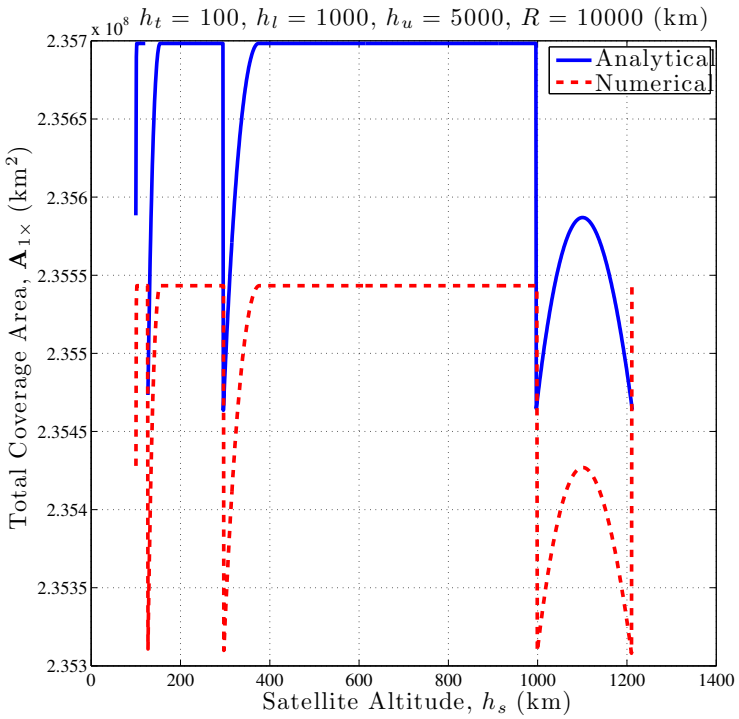

Figure 3.9: Maximum total coverage area vs. satellite altitude for the minimum number of satellites

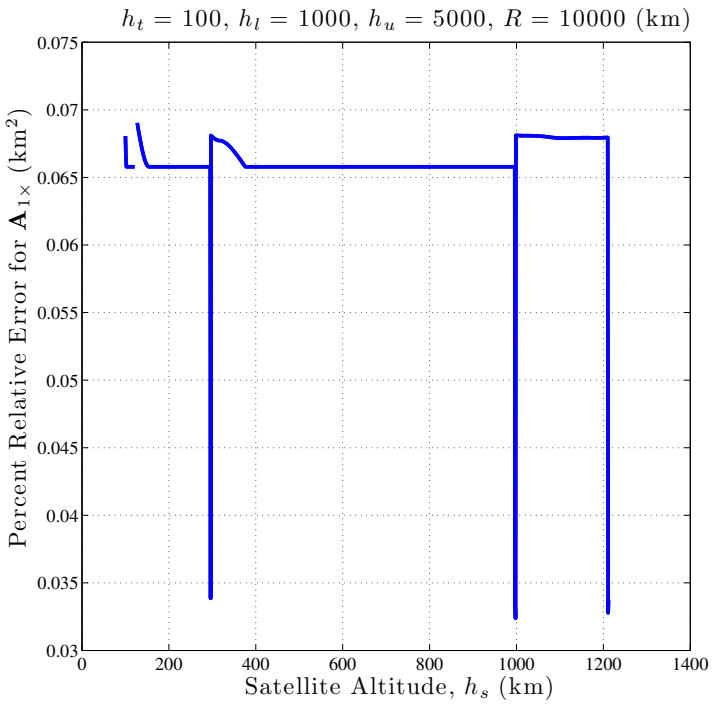

Figure 3.10: Percent relative error in maximum total coverage area vs. satellite altitude for the minimum number of satellites

and plotted in Figure 3.10 as a percentage, where $\mathbf{A}_{1\times,\text{num}}$ is the numerical approximation of $\mathbf{A}_{1\times}$. As expected, the error is below 0.1%, which is to the specifications of the algorithm proposed by Takano and Marchand.[1,17]

3.4 Multiple Independent Variables

A more realistic constellation design problem would consider optimization with a greater number of free parameters. For example, h_s could be varied together with R or h_u, where the minimum number of satellites required for 99.9% coverage of DABS is still the objective in either case. Sample parameter spaces are shown in Figures 3.11–3.12. A clearly defined maximum coverage area exists in Figure 3.11, while Figure 3.12 shows the same saturation characteristics seen in Figures 3.2 and 3.5(a), except now with a planar region of maximum coverage area saturation.

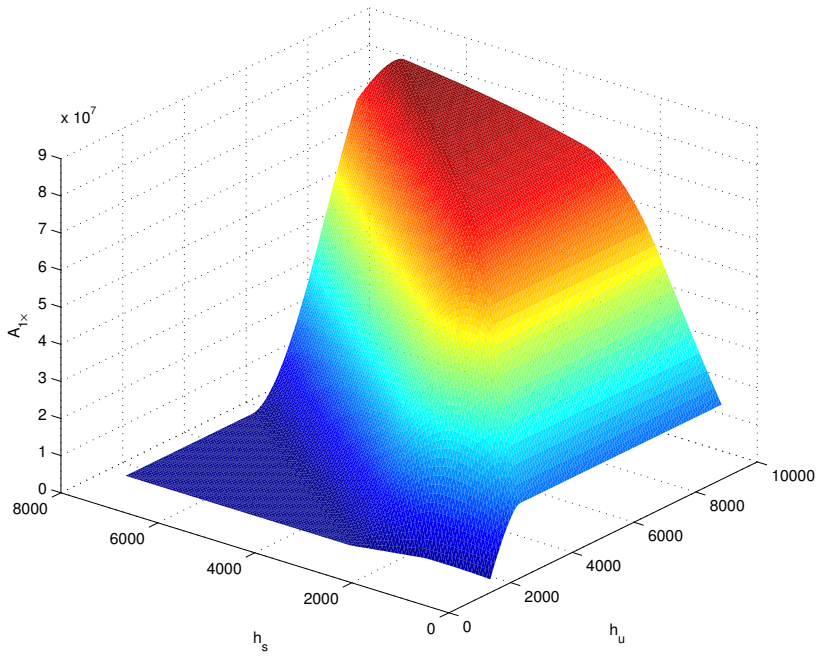

Figure 3.11: Example 1: $h_t = 100$ km, $h_l = 1400$ km, $R = 100$ km, $n = 6$

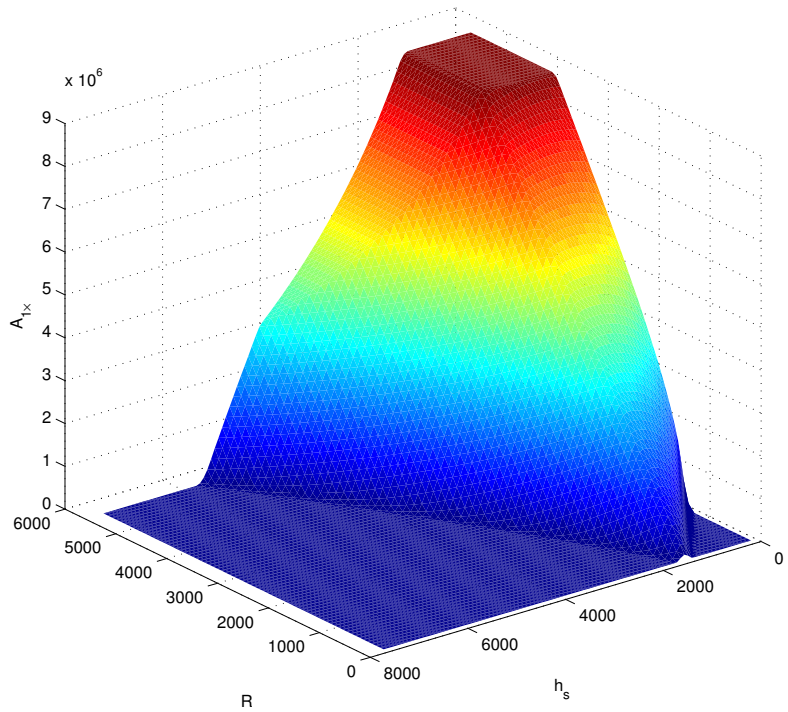

Figure 3.12: Example 2: $h_t = 100$ km, $h_l = 1400$ km, $h_u = 1500$ km, $n = 6$

Chapter 4

Conclusion

The problem of constellation design for space-based space situational awareness applications is considered from an analytical perspective. The model developed allows for computation of the above-the-horizon coverage area, where the region of interest — located within a pre-specified dual-altitude band — is subject to a maximum of 2-fold coverage by adjacent satellites. First, geometrical arguments are employed to establish an analytical formulation for coverage area provided by a planar, circular constellation of equally spaced satellites with omnidirectional sensors. This leads to a piecewise differentiable exact representation for the total coverage area provided by the constellation. Analytical conditions are also established for determining the existence of arbitrary coverage multiplicities manifested strictly between adjacent satellites.

While the results of this study are presently limited to simulating a maximum of 2-fold coverage between adjacent satellites, the method's utility is quite evident. By using the exact expression of the total coverage area as a cost index in an optimization process, it is demonstrated that under the given assumptions, this approach can be employed for optimal constellation design. The results of this investigation are also successfully validated against a generalized numerical algorithm developed under a parallel study.

Appendices

Appendix A

Modified Single Satellite ATH Coverage Model

This appendix serves two purposes. First, it restates the equations that define shell intersections for a single satellite as well as the geometrical elements that make up the coverage area $\mathbf{A}_{1\times,1}$ — all derived by Marchand and Kobel[16] — with updated notation employed in this thesis. Secondly, it combines results from Marchand and Kobel[16] with those of Takano and Marchand[1,17] to yield a representation of $\mathbf{A}_{1\times,1}$ (the area of the ATH coverage region visible to a single satellite and subject to 1-fold coverage or greater) that is not only compact, but which also, when possible, follows more closely the original formulas used by Marchand and Kobel. A major advantage to the representation given here is that the notation for Type I intersections, as described in Section 2.3, is used instead of the original notation for intersections developed by Marchand and Kobel. Surely this will alleviate any sources of confusion arising from comparing this thesis to previous work.

A.1 Type I Shell Intersections

The following Eqs. (A.1–A.14) define the coordinates of all 14 Type I intersections associated with S_j. Naturally, using $j = 1$ would give the original intersection points used for the single satellite model. The notation is updated from that of Marchand and Kobel to be consistent with that of this thesis.

A.1.1 Intersections of Altitude Shells with the Range Shell

$$\begin{aligned} x_{A_{1,j}} &= \sqrt{r_l^2 - y_{A_{1,j}}^2} \\ y_{A_{1,j}} &= \frac{r_l^2 + r_s^2 - R^2}{2r_s} \end{aligned} \tag{A.1}$$

$$\begin{aligned} x_{A_{2,j}} &= -x_{A_{1,j}} \\ y_{A_{2,j}} &= y_{A_{1,j}} \end{aligned} \tag{A.2}$$

$$\begin{aligned} x_{B_{1,j}} &= \sqrt{r_u^2 - y_{B_{1,j}}^2} \\ y_{B_{1,j}} &= \frac{r_u^2 + r_s^2 - R^2}{2r_s} \end{aligned} \tag{A.3}$$

$$\begin{aligned} x_{B_{2,j}} &= -x_{B_{1,j}} \\ y_{B_{2,j}} &= y_{B_{1,j}} \end{aligned} \tag{A.4}$$

A.1.2 Intersections of Tangent Lines with Altitude Shells

$$\begin{aligned} x_{L_{1_A,j}} &= \frac{-2m_{1,j}^2 r_s + \sqrt{4m_{1,j}^2 r_s^2 - 4(1+m_{1,j}^2)(r_s^2 - r_l^2)}}{2(1+m_{1,j}^2)} \\ y_{L_{1_A,j}} &= m_{1,j} x_{L_{1_A,j}} + r_s \end{aligned} \tag{A.5}$$

$$\begin{aligned} x_{L_{2_A,j}} &= -x_{L_{1_A,j}} \\ y_{L_{2_A,j}} &= y_{L_{1_A,j}} \end{aligned} \tag{A.6}$$

$$\begin{aligned} x_{L_{1_B,j}} &= \frac{-2m_{1,j}^2 r_s - \sqrt{4m_{1,j}^2 r_s^2 - 4(1+m_{1,j}^2)(r_s^2 - r_l^2)}}{2(1+m_{1,j}^2)} \\ y_{L_{1_B,j}} &= m_{1,j} x_{L_{1_B,j}} + r_s \end{aligned} \tag{A.7}$$

$$\begin{aligned} x_{L_{2_B,j}} &= -x_{L_{1_B,j}} \\ y_{L_{2_B,j}} &= y_{L_{1_B,j}} \end{aligned} \tag{A.8}$$

$$x_{U1_{A},j} = \frac{-2m_{1,j}^2 r_s + \sqrt{4m_{1,j}^2 r_s^2 - 4(1+m_{1,j}^2)(r_s^2 - r_u^2)}}{2(1+m_{1,j}^2)} \tag{A.9}$$

$$y_{U1_{A},j} = m_{1,j} x_{U1_{A},j} + r_s$$

$$x_{U2_{A},j} = -x_{U1_{A},j}$$

$$y_{U2_{A},j} = y_{U1_{A},j} \tag{A.10}$$

$$x_{U1_{B},j} = \frac{-2m_{1,j}^2 r_s - \sqrt{4m_{1,j}^2 r_s^2 - 4(1+m_{1,j}^2)(r_s^2 - r_u^2)}}{2(1+m_{1,j}^2)} \tag{A.11}$$

$$y_{U1_{B},j} = m_{1,j} x_{U1_{B},j} + r_s$$

$$x_{U2_{B},j} = -x_{U1_{B},j}$$

$$y_{U2_{B},j} = y_{U1_{B},j} \tag{A.12}$$

A.1.3 Intersections of Tangent Lines with the Range Shell

$$x_{T1_{A},jj} = \frac{R}{\sqrt{1+m_{1,j}^2}} \tag{A.13}$$

$$y_{T1_{A},jj} = m_{1,j} x_{T1_{A},jj} + r_s$$

$$x_{T2_{A},jj} = -x_{T1_{A},jj}$$

$$y_{T2_{A},jj} = y_{T1_{A},jj} \tag{A.14}$$

A.2 Fundamental Geometrical Elements

The area of the complex regions described in Section A.3 are most easily computed by decomposing them into more fundamental shapes. This section defines all of the shapes relevant to the development of the piecewise differentiable objective function for the coverage area $\mathbf{A}_{1\times,1}$.

A.2.1 Triangles

The area of a triangle is

$$\mathbf{A}_{\triangle}(q_1, q_2, q_3) = \sqrt{s(s-q_1)(s-q_2)(s-q_3)} \tag{A.15}$$

where s is the semiperimeter, defined as half the perimeter of a polygon. For a triangle, the semiperimeter is

$$s = \frac{q_1 + q_2 + q_3}{2} \tag{A.16}$$

A.2.2 Circular Segments

The area of a standard circular segment is

$$\mathbf{A}_{\Sigma}(r, c) = r^2 \sin^{-1}\left(\frac{c}{2r}\right) - \frac{c}{4}\sqrt{4r^2 - c^2} \tag{A.17}$$

where r is the radius of the circle and c is the chord length. The complement of the area of a circular segment is used instead of the result obtained from Eq. (A.17) when the angle subtended is larger than π. This complementary area is defined as

$$\tilde{\mathbf{A}}_{\Sigma}(r, c) = \pi r^2 - \mathbf{A}_{\Sigma}(r, c) \tag{A.18}$$

A.2.3 Circular Sectors

The area of a circular sector can be expressed as

$$\mathbf{A}_{\pi_1}(r, c) = \frac{1}{2}\beta r^2 \tag{A.19}$$

where r is the radius of the circle and β is the angle in radians subtended at the center. The input to $\mathbf{A}_{\pi_1}$ does not contain β because it can be expressed in terms

of r and a chord length c by using trigonometry:

$$\beta = 2\sin^{-1}\left(\frac{c}{2r}\right) \tag{A.20}$$

or

$$\beta = \cos^{-1}\left(1 - \frac{c^2}{2r^2}\right) \tag{A.21}$$

Thus, by substituting Eq. (A.20) into Eq. (A.19), the area of a circular sector can be rewritten as

$$\mathbf{A}_{\pi_1}(r, c) = r^2 \sin^{-1}\left(\frac{c}{2r}\right) \tag{A.22}$$

As with the circular segment, the complement of the area of a circular sector is simply

$$\tilde{\mathbf{A}}_{\pi_1}(r, c) = \pi r^2 - \mathbf{A}_{\pi_1}(r, c) \tag{A.23}$$

A.2.4 Composite Teardrop Sectors

A new quantity, $\tilde{R}$, is defined as the radius of an imaginary shell centered on a satellite, not to be confused with R, the radius of a satellite's range shell. The area of a composite teardrop sector is

$$\mathbf{A}_{\pi_2}(r, \tilde{R}, c, r_s) = \begin{cases} \mathbf{A}_{\triangle}(\tilde{R}, c, \tilde{R}) + \mathbf{A}_{\Sigma}(r, c) & r_s \leq \sqrt{\tilde{R}^2 - r^2} \\ \mathbf{A}_{\triangle}(\tilde{R}, c, \tilde{R}) + \tilde{\mathbf{A}}_{\Sigma}(r, c) & r_s > \sqrt{\tilde{R}^2 - r^2} \end{cases} \tag{A.24}$$

where $\tilde{R} \geq r$ in order for the conditions to be real. The conditions are derived from the Pythagorean theorem, where the equality $r_s = \sqrt{\tilde{R}^2 - r^2}$ corresponds to the case when the chord c passes through the origin O. Both cases arise in the construction of $\mathbf{A}_{1\times,1}$. For example, the condition $r_s \leq \sqrt{\tilde{R}^2 - r^2}$ is satisfied in case 3(e), while $r_s > \sqrt{\tilde{R}^2 - r^2}$ is satisfied in case 1(b).

Do not confuse $\mathbf{A}_{\pi_2}(r, \tilde{R}, c, r_s)$ with $\mathbf{A}_{\Lambda_5}(r_1, q_1, q_2, q_3)$, which assumes no symmetry about the shape and no relationship between the lengths of each side of the triangle or the satellite altitude. They are conceptually similar shapes, but have fundamentally different definitions.

A.2.5 Composite Triangles

The area of the composite triangle of the first kind, which was used by Marchand and Kobel, is

$$\mathbf{A}_{\Lambda_1}(r_1, r_2, q_1, q_2, q_3) = \mathbf{A}_{\triangle}(q_1, q_2, q_3) - \mathbf{A}_{\Sigma}(r_1, q_2) + \mathbf{A}_{\Sigma}(r_2, q_3) \tag{A.25}$$

though it is not needed or employed in the modified formulation of $\mathbf{A}_{1\times,1}$. The composite triangle of the second kind is used, however, and its area is computed as

$$\mathbf{A}_{\Lambda_2}(r_1, q_1, q_2, q_3) = \mathbf{A}_{\triangle}(q_1, q_2, q_3) - \mathbf{A}_{\Sigma}(r_1, q_2) \tag{A.26}$$

The subscript "2" for Λ_2 is retained for consistency and to prevent confusion.

A.2.6 Overlap Region of Two Circles

The result presented here describes the taxonomy of the region formed by the intersection of two circles. If the overlap region exists, the area is either that of a circle or of the sum of two circular segments, but complications arise when there is a lack of symmetry. If the radii are unequal, then for a circular segment, the angle subtended at the center could be a reflex angle, which means that the area of this circular segment would be greater than half the area of the associated circle.

The following results are given in terms of the application to the ATH coverage problem, where r is the radius of an altitude shell and R is the radius of a

satellite's range shell. The subscript "AS" stands for altitude shell and refers to the altitude shell of choice (LTAS or UTAS). If the LTAS is used, then $r = r_l$, while if the UTAS is used, then $r = r_u$.

$$\mathbf{A}_{\mathrm{AS}\cap\mathrm{RS}}(r, R, c, r_s) = 0 \quad r_s \geq R + r \tag{A.27}$$

$$\mathbf{A}_{\mathrm{AS}\cap\mathrm{RS}}(r, R, c, r_s) = \begin{cases} \pi R^2 & r \geq R + r_s \\ \pi r^2 & R \geq r + r_s \end{cases} \tag{A.28}$$

$$\mathbf{A}_{\mathrm{AS}\cap\mathrm{RS}}(r, R, c, r_s) = \begin{cases} \tilde{\mathbf{A}}_{\Sigma}(R, c) + \mathbf{A}_{\Sigma}(r, c) & r_s \leq \sqrt{r^2 - R^2} \\ \mathbf{A}_{\Sigma}(R, c) + \mathbf{A}_{\Sigma}(r, c) & r_s > \sqrt{r^2 - R^2} \end{cases} \tag{A.29}$$

The inequalities in Eq. (A.29) must be real, so it is also required that $r \geq R$.

$$\mathbf{A}_{\mathrm{AS}\cap\mathrm{RS}}(r, R, c, r_s) = \begin{cases} \mathbf{A}_{\Sigma}(R, c) + \tilde{\mathbf{A}}_{\Sigma}(r, c) & r_s \leq \sqrt{R^2 - r^2} \\ \mathbf{A}_{\Sigma}(R, c) + \mathbf{A}_{\Sigma}(r, c) & r_s > \sqrt{R^2 - r^2} \end{cases} \tag{A.30}$$

The inequalities in Eq. (A.30) must be real, so it is also required that $R \geq r$.

A.3 Piecewise Differentiable Representation of Coverage Area $\mathbf{A}_{1\times,1}$

Table A.1: Coverage Region $C_{1\times,1}$ Subcases for $r_t \leq r_s < r_l$

Conditions	Case no.
$R < \lvert\overline{L_{1_A,1}S_1}\rvert$	1(a)
$\lvert\overline{L_{1_A,1}S_1}\rvert \leq R < \lvert\overline{U_{1_A,1}S_1}\rvert$	1(b)
$\lvert\overline{U_{1_A,1}S_1}\rvert \leq R$	1(c)

Table A.2: Coverage Region $C_{1\times,1}$ Subcases for $r_l \leq r_s < r_u$

Conditions	Case no.
$R < \lvert\overline{L_{1_B,1}S_1}\rvert$	2(a)
$\lvert\overline{L_{1_B,1}S_1}\rvert \leq R < \lvert\overline{L_{1_A,1}S_1}\rvert$	2(b)
$\lvert\overline{L_{1_A,1}S_1}\rvert \leq R < \lvert\overline{U_{1_A,1}S_1}\rvert$	2(c)
$\lvert\overline{U_{1_A,1}S_1}\rvert \leq R$	2(d)

Table A.3: Coverage Region $C_{1\times,1}$ Subcases for $r_u \leq r_s < r_{s_3}$

Conditions	Case no.
$R < \lvert\overline{U_{1_B,1}S_1}\rvert$	3(a)
$\lvert\overline{U_{1_B,1}S_1}\rvert \leq R < \lvert\overline{L_{1_B,1}S_1}\rvert$	3(b)
$\lvert\overline{L_{1_B,1}S_1}\rvert \leq R < \lvert\overline{L_{1_A,1}S_1}\rvert$	3(c)
$\lvert\overline{L_{1_A,1}S_1}\rvert \leq R < \lvert\overline{U_{1_A,1}S_1}\rvert$	3(d)
$\lvert\overline{U_{1_A,1}S_1}\rvert \leq R$	3(e)

Table A.4: Coverage Area $\mathbf{A}_{1\times,1}$ for $r_t \leq r_s < r_l$

Case no.	Area Subject to 1-fold Coverage or Greater
1(a)	$\mathbf{A}_{1\times,1} = \mathbf{A}_{\mathrm{AS}\cap\mathrm{RS}}(r_u, R, \lvert\overline{B_{1,1}B_{2,1}}\rvert, r_s) - \mathbf{A}_{\mathrm{AS}\cap\mathrm{RS}}(r_l, R, \lvert\overline{A_{1,1}A_{2,1}}\rvert, r_s)$
1(b)	$\mathbf{A}_{1\times,1} = \mathbf{A}_{\mathrm{AS}\cap\mathrm{RS}}(r_u, R, \lvert\overline{B_{1,1}B_{2,1}}\rvert, r_s) - \pi r_l^2 - \mathbf{A}_{\pi_1}(R, \lvert\overline{T_{1_A,11}T_{2_A,11}}\rvert) + \mathbf{A}_{\pi_2}(r_l, \lvert\overline{L_{1_A,1}S_1}\rvert, \lvert\overline{L_{1_A,1}L_{2_A,1}}\rvert, r_s)$
1(c)	$\mathbf{A}_{1\times,1} = \pi r_u^2 - \pi r_l^2 - \mathbf{A}_{\pi_2}(r_u, \lvert\overline{U_{1_A,1}S_1}\rvert, \lvert\overline{U_{1_A,1}U_{2_A,1}}\rvert, r_s) + \mathbf{A}_{\pi_2}(r_l, \lvert\overline{L_{1_A,1}S_1}\rvert, \lvert\overline{L_{1_A,1}L_{2_A,1}}\rvert, r_s)$

Table A.5: Coverage Area $\mathbf{A}_{1\times,1}$ for $r_l \leq r_s < r_u$

Case no.	Area Subject to 1-fold Coverage or Greater
2(a)	$\mathbf{A}_{1\times,1} = \mathbf{A}_{\mathrm{AS}\cap\mathrm{RS}}(r_u, R, \lvert\overline{B_{1,1}B_{2,1}}\rvert, r_s) - \mathbf{A}_{\pi_1}(R, \lvert\overline{T_{1_A,11}T_{2_A,11}}\rvert)$
2(b)	$\mathbf{A}_{1\times,1} = \mathbf{A}_{\mathrm{AS}\cap\mathrm{RS}}(r_u, R, \lvert\overline{B_{1,1}B_{2,1}}\rvert, r_s) - \mathbf{A}_{\mathrm{AS}\cap\mathrm{RS}}(r_l, R, \lvert\overline{A_{1,1}A_{2,1}}\rvert, r_s)$ $- \mathbf{A}_{\Lambda_2}(r_l, \lvert\overline{L_{1_B,1}S_1}\rvert, \lvert\overline{L_{1_B,1}L_{2_B,1}}\rvert, \lvert\overline{L_{1_B,1}S_1}\rvert)$
2(c)	$\mathbf{A}_{1\times,1} = \mathbf{A}_{\mathrm{AS}\cap\mathrm{RS}}(r_u, R, \lvert\overline{B_{1,1}B_{2,1}}\rvert, r_s) - \pi r_l^2 - \mathbf{A}_{\pi_1}(R, \lvert\overline{T_{1_A,11}T_{2_A,11}}\rvert)$ $+ \mathbf{A}_{\pi_2}(r_l, \lvert\overline{L_{1_A,1}S_1}\rvert, \lvert\overline{L_{1_A,1}L_{2_A,1}}\rvert)$ $- \mathbf{A}_{\Lambda_2}(r_l, \lvert\overline{L_{1_B,1}S_1}\rvert, \lvert\overline{L_{1_B,1}L_{2_B,1}}\rvert, \lvert\overline{L_{1_B,1}S_1}\rvert)$
2(d)	$\mathbf{A}_{1\times,1} = \pi r_u^2 - \pi r_l^2 - \mathbf{A}_{\pi_2}(r_u, \lvert\overline{U_{1_A,1}S_1}\rvert, \lvert\overline{U_{1_A,1}U_{2_A,1}}\rvert, r_s)$ $+ \mathbf{A}_{\pi_2}(r_l, \lvert\overline{L_{1_A,1}S_1}\rvert, \lvert\overline{L_{1_A,1}L_{2_A,1}}\rvert, r_s)$ $- \mathbf{A}_{\Lambda_2}(r_l, \lvert\overline{L_{1_B,1}S_1}\rvert, \lvert\overline{L_{1_B,1}L_{2_B,1}}\rvert, \lvert\overline{L_{1_B,1}S_1}\rvert)$

Table A.6: Coverage Area $\mathbf{A}_{1\times,1}$ for $r_u \leq r_s < r_{s_3}$

Case no.	Area Subject to 1-fold Coverage or Greater
3(a)	$\mathbf{A}_{1\times,1} = 0$
3(b)	$\mathbf{A}_{1\times,1} = \mathbf{A}_{\mathrm{AS}\cap\mathrm{RS}}(r_u, R, \lvert\overline{B_{1,1}B_{2,1}}\rvert, r_s) - \mathbf{A}_{\pi_1}(R, \lvert\overline{T_{1_A,11}T_{2_A,11}}\rvert)$ $+ \mathbf{A}_{\Lambda_2}(r_u, \lvert\overline{U_{1_B,1}S_1}\rvert, \lvert\overline{U_{1_B,1}U_{2_B,1}}\rvert, \lvert\overline{U_{1_B,1}S_1}\rvert)$
3(c)	$\mathbf{A}_{1\times,1} = \mathbf{A}_{\mathrm{AS}\cap\mathrm{RS}}(r_u, R, \lvert\overline{B_{1,1}B_{2,1}}\rvert, r_s) - \mathbf{A}_{\mathrm{AS}\cap\mathrm{RS}}(r_l, R, \lvert\overline{A_{1,1}A_{2,1}}\rvert, r_s)$ $- \mathbf{A}_{\Lambda_2}(r_l, \lvert\overline{L_{1_B,1}S_1}\rvert, \lvert\overline{L_{1_B,1}L_{2_B,1}}\rvert, \lvert\overline{L_{1_B,1}S_1}\rvert)$ $+ \mathbf{A}_{\Lambda_2}(r_u, \lvert\overline{U_{1_B,1}S_1}\rvert, \lvert\overline{U_{1_B,1}U_{2_B,1}}\rvert, \lvert\overline{U_{1_B,1}S_1}\rvert)$
3(d)	$\mathbf{A}_{1\times,1} = \mathbf{A}_{\mathrm{AS}\cap\mathrm{RS}}(r_u, R, \lvert\overline{B_{1,1}B_{2,1}}\rvert, r_s) - \pi r_l^2 - \mathbf{A}_{\pi_1}(R, \lvert\overline{T_{1_A,11}T_{2_A,11}}\rvert)$ $+ \mathbf{A}_{\pi_2}(r_l, \lvert\overline{L_{1_A,1}S_1}\rvert, \lvert\overline{L_{1_A,1}L_{2_A,1}}\rvert, r_s)$ $- \mathbf{A}_{\Lambda_2}(r_l, \lvert\overline{L_{1_B,1}S_1}\rvert, \lvert\overline{L_{1_B,1}L_{2_B,1}}\rvert, \lvert\overline{L_{1_B,1}S_1}\rvert)$ $+ \mathbf{A}_{\Lambda_2}(r_u, \lvert\overline{U_{1_B,1}S_1}\rvert, \lvert\overline{U_{1_B,1}U_{2_B,1}}\rvert, \lvert\overline{U_{1_B,1}S_1}\rvert)$
3(e)	$\mathbf{A}_{1\times,1} = \pi r_u^2 - \pi r_l^2 - \mathbf{A}_{\pi_2}(r_u, \lvert\overline{U_{1_A,1}S_1}\rvert, \lvert\overline{U_{1_A,1}U_{2_A,1}}\rvert, r_s)$ $+ \mathbf{A}_{\pi_2}(r_l, \lvert\overline{L_{1_A,1}S_1}\rvert, \lvert\overline{L_{1_A,1}L_{2_A,1}}\rvert, r_s)$ $- \mathbf{A}_{\Lambda_2}(r_l, \lvert\overline{L_{1_B,1}S_1}\rvert, \lvert\overline{L_{1_B,1}L_{2_B,1}}\rvert, \lvert\overline{L_{1_B,1}S_1}\rvert)$ $+ \mathbf{A}_{\Lambda_2}(r_u, \lvert\overline{U_{1_B,1}S_1}\rvert, \lvert\overline{U_{1_B,1}U_{2_B,1}}\rvert, \lvert\overline{U_{1_B,1}S_1}\rvert)$

Appendix B

Details of the 22 Shape Types for $\mathbf{A}'_{2\times,12}$

Figures B.1–B.22 are included in this appendix to supplement the discussion and derivation in Sections 2.4 and 2.5 regarding the 22 shape types for $\mathbf{A}'_{2\times,12}$. While each shape type is depicted in Figures 2.6–2.7 and a sound understanding of the taxonomy of overlap regions can be extracted from them, the overlap regions are small, making it difficult to discern from the figures which intersection points are located at which vertices. For such a small size, it is also impossible to label each vertex of each of the 22 regions without cluttering the figures. To remedy the issue, this appendix contains enlarged versions of each of the 22 polygons and labels all the vertices of each one. The intention is that Figures B.1–B.22 will facilitate understanding the origin of the conditions and equations in Tables 2.5 and 2.6, respectively.

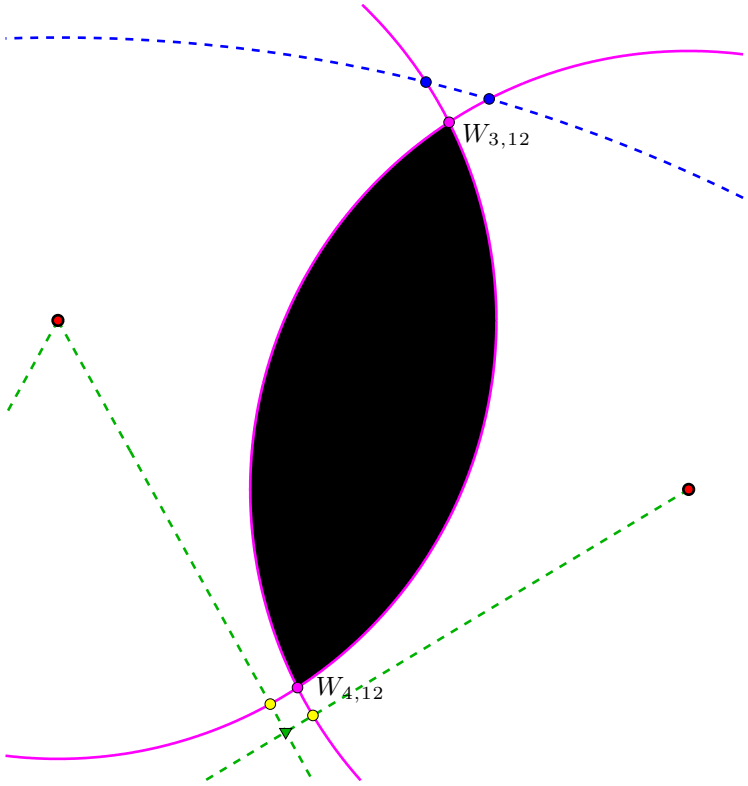

Figure B.1: Case 2

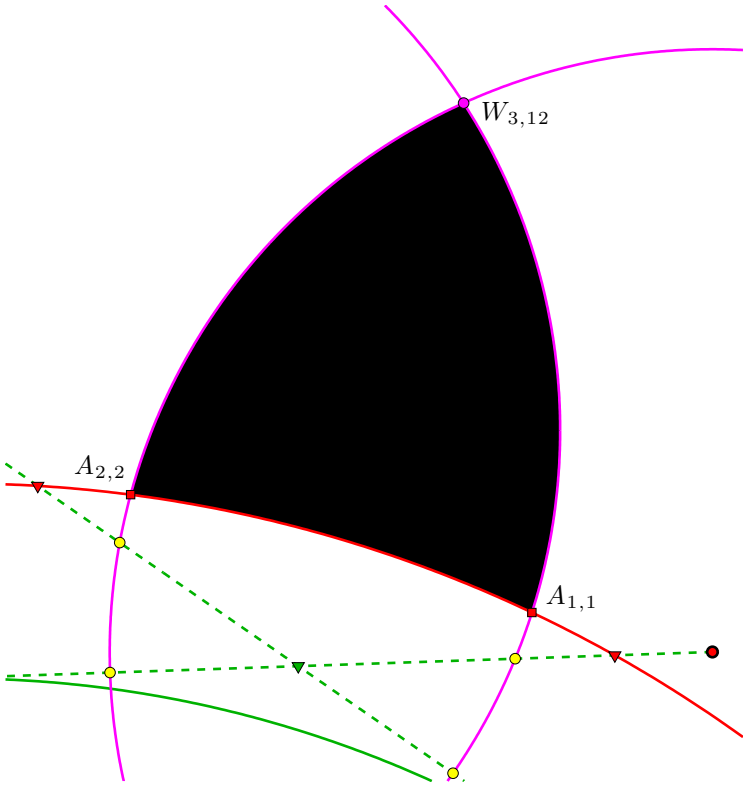

Figure B.2: Case 3.i

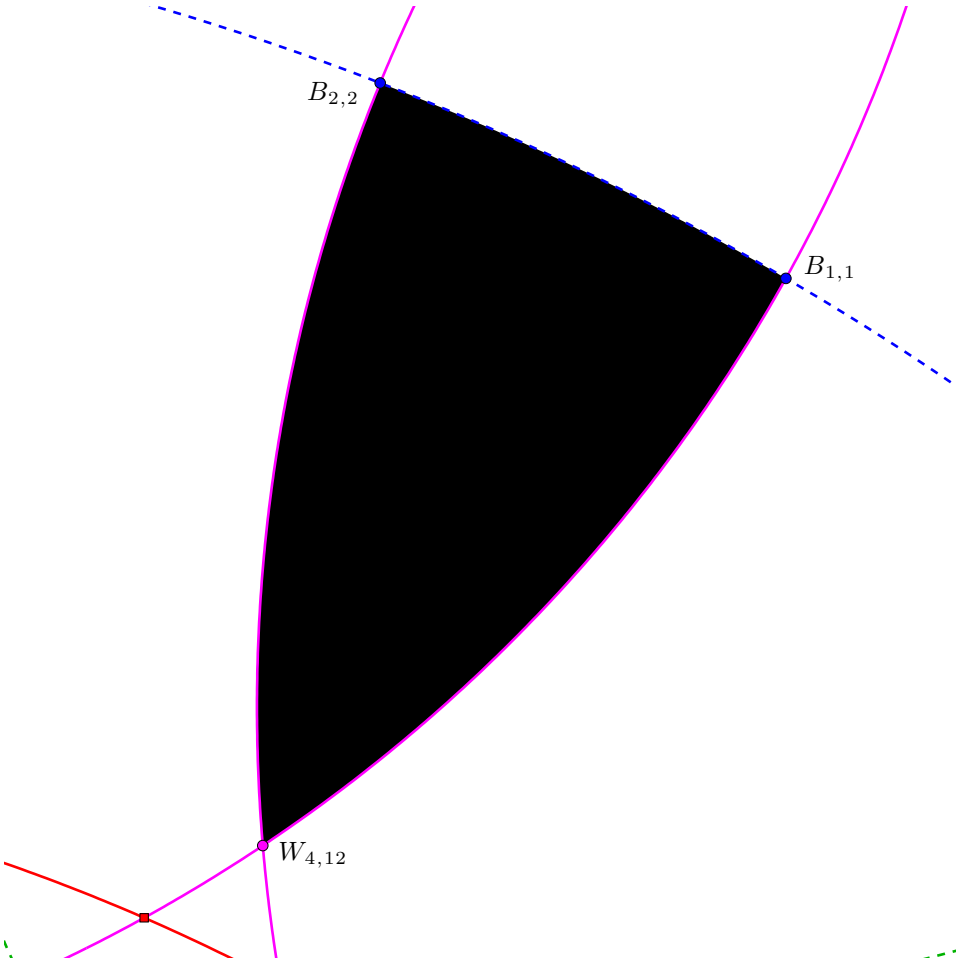

Figure B.3: Case 3.ii

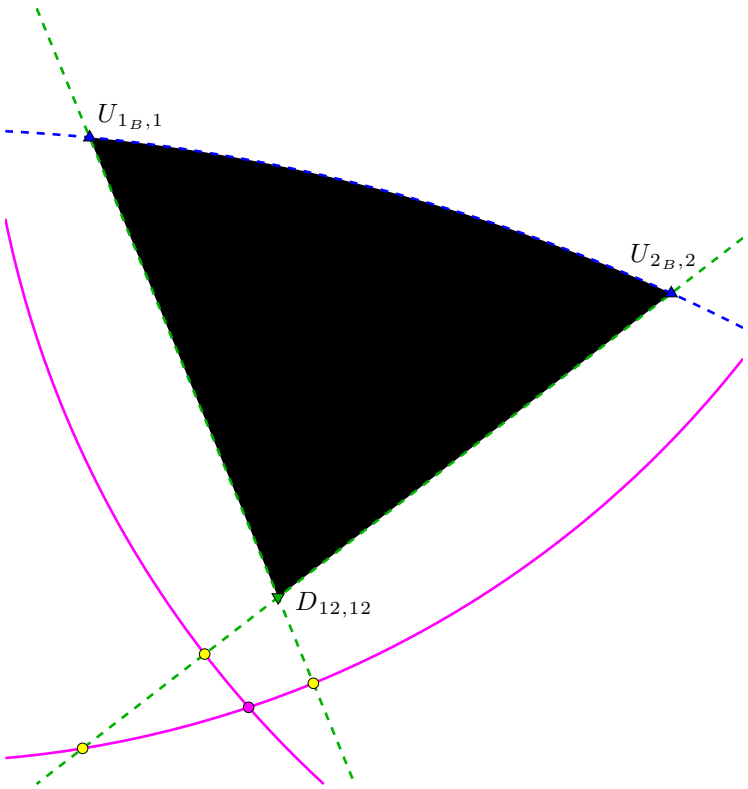

Figure B.4: Case 3.iii.a

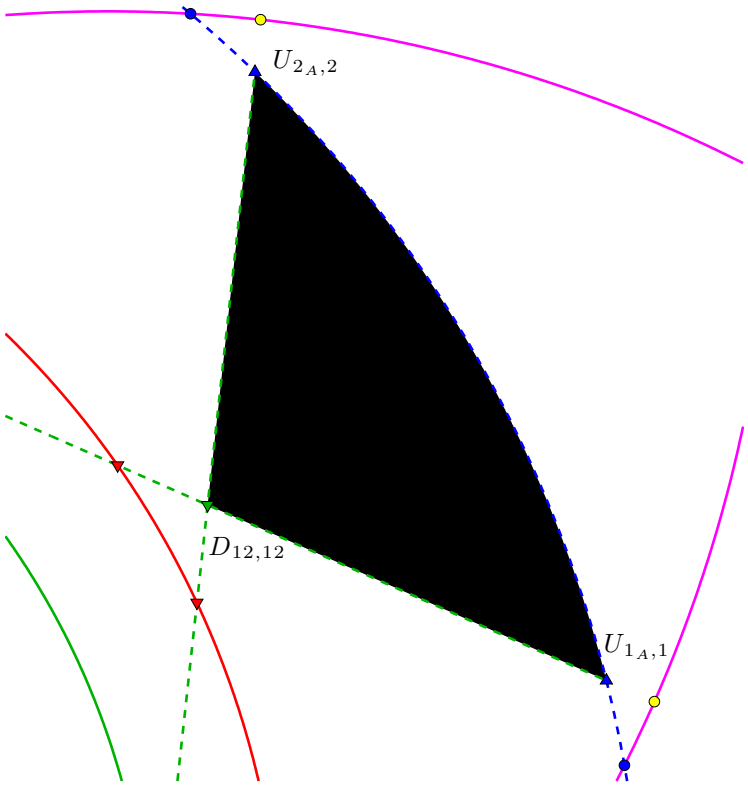

Figure B.5: Case 3.iii.b

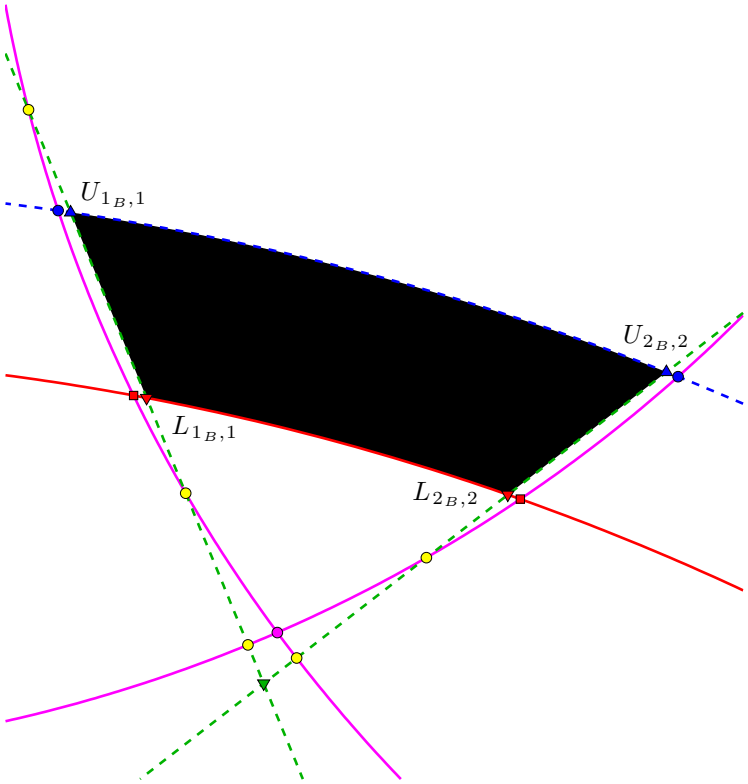

Figure B.6: Case 4.i.a

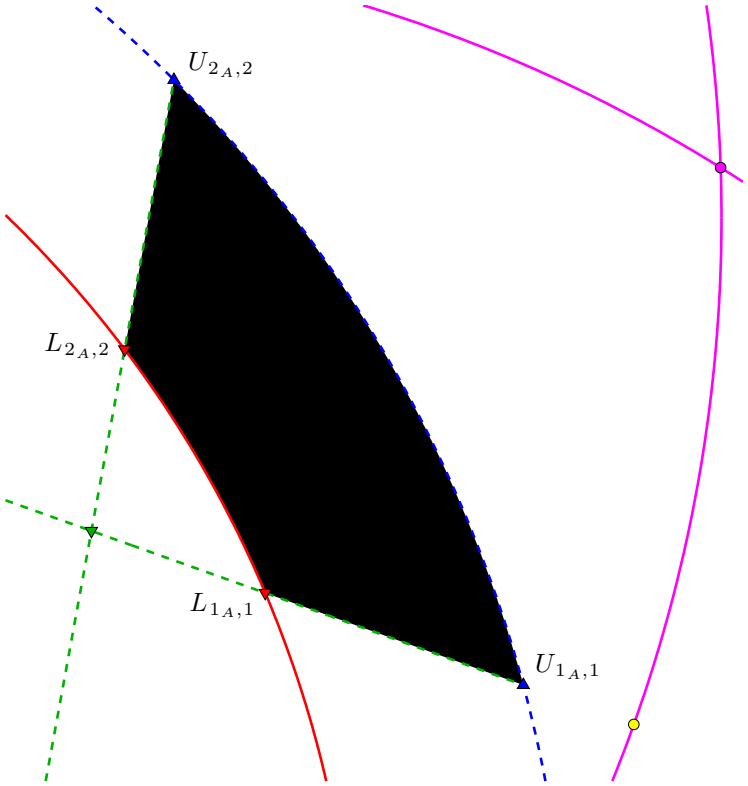

Figure B.7: Case 4.i.b

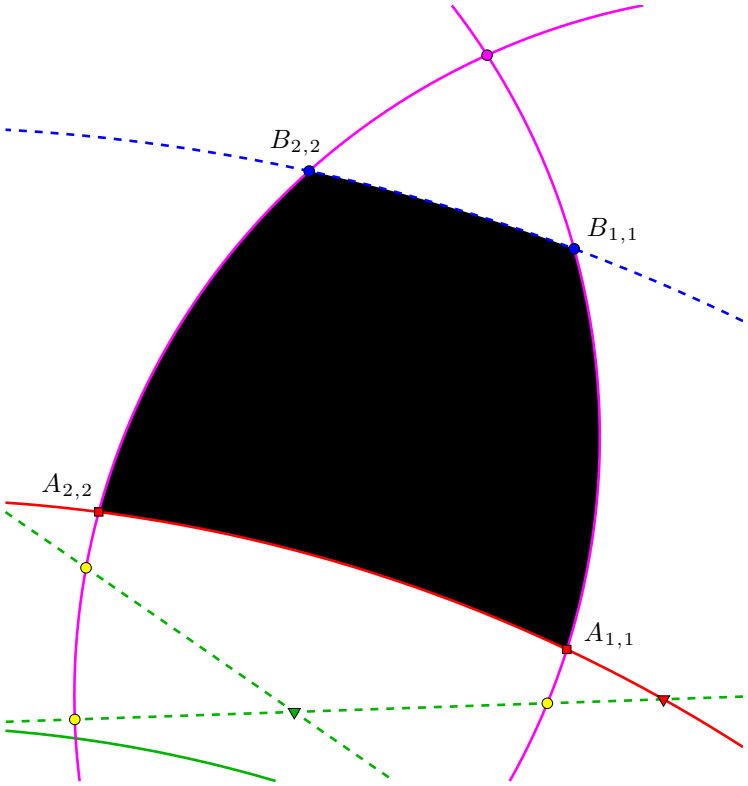

Figure B.8: Case 4.ii

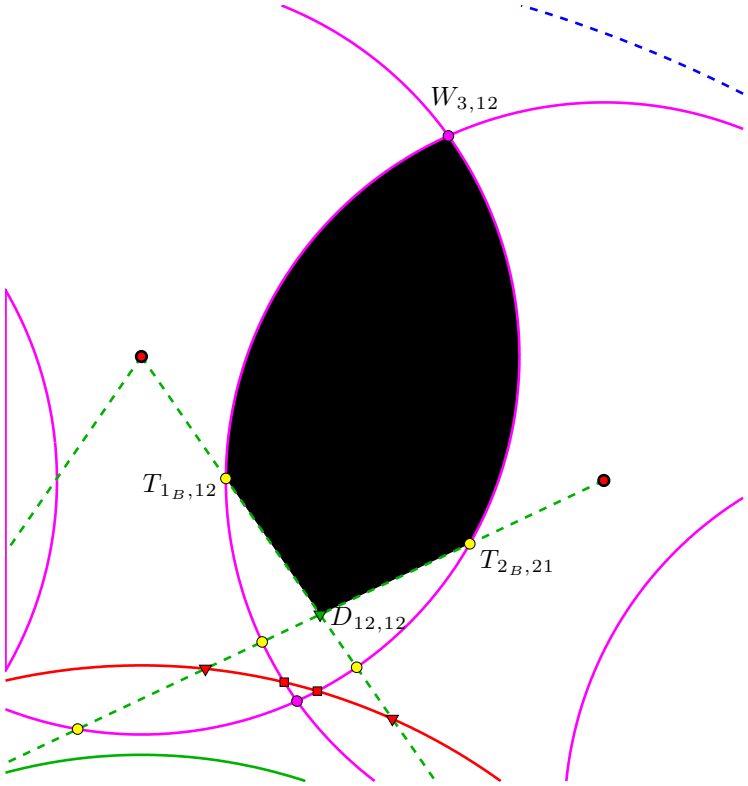

Figure B.9: Case 4.iii.a

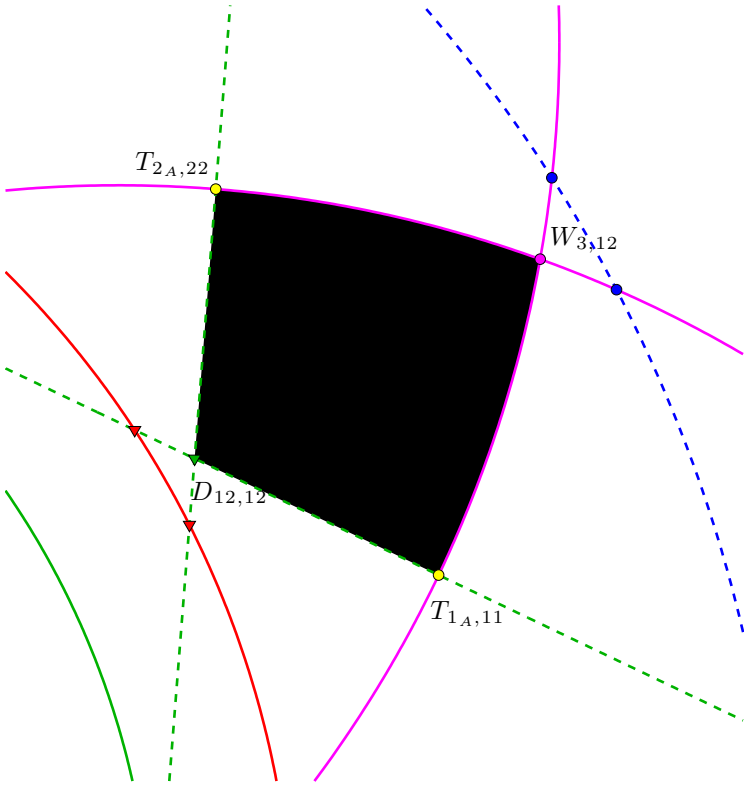

Figure B.10: Case 4.iii.b

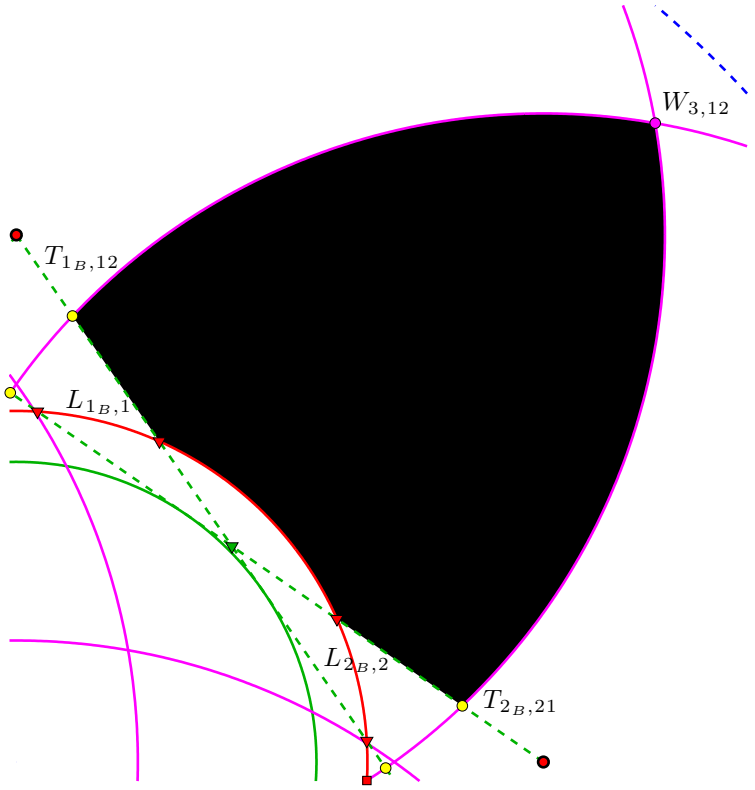

Figure B.11: Case 5.i.a

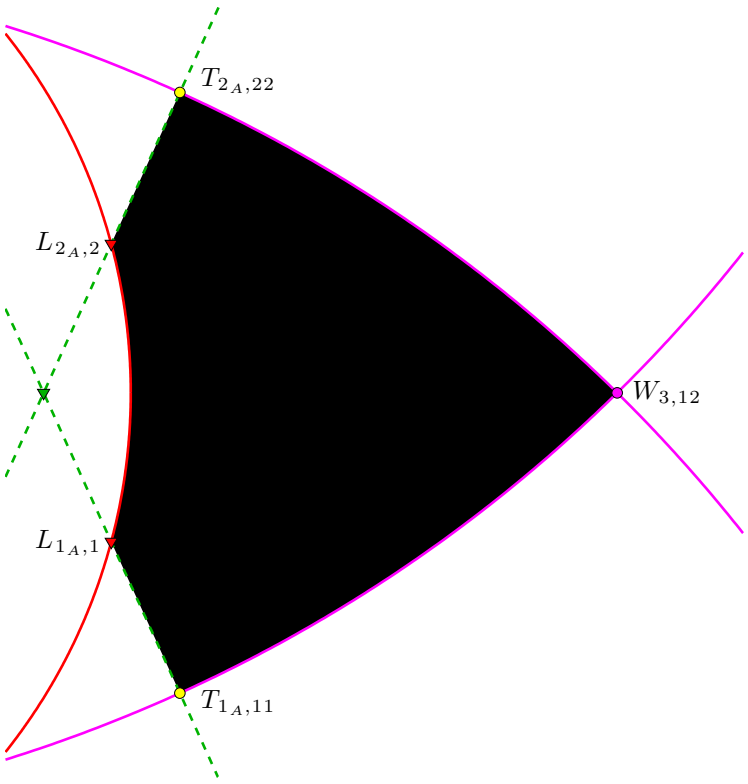

Figure B.12: Case 5.i.b

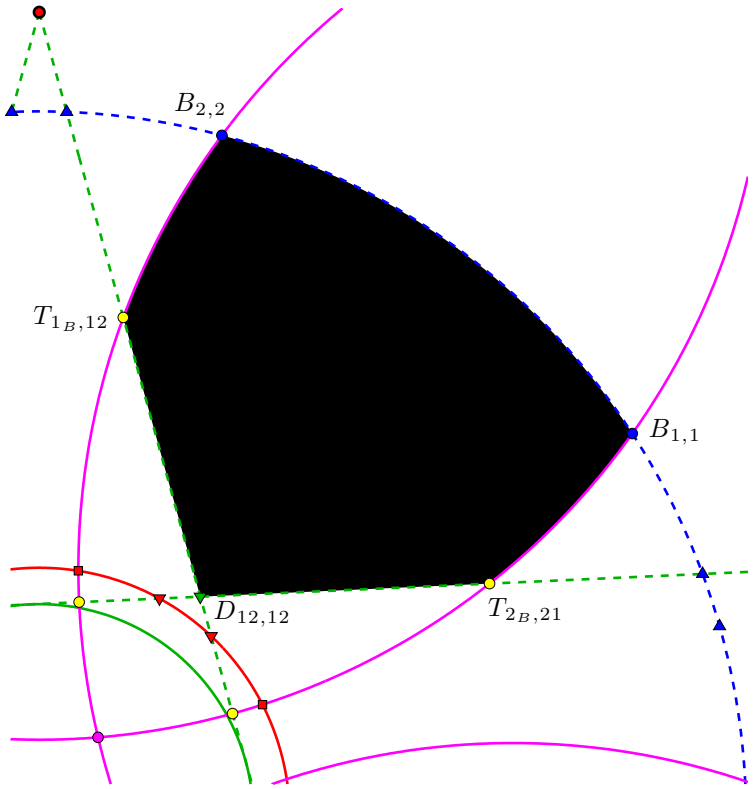

Figure B.13: Case 5.ii.a

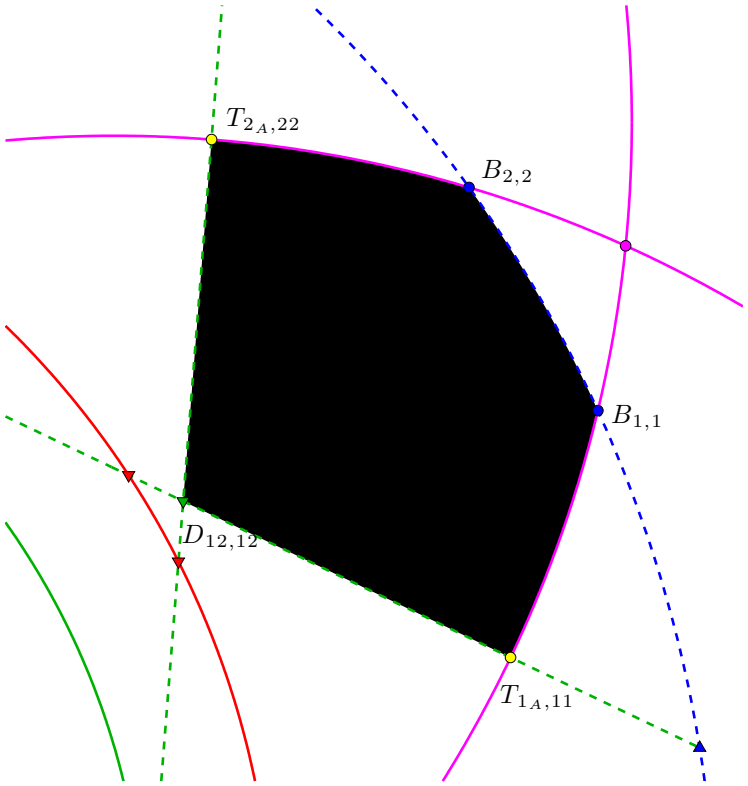

Figure B.14: Case 5.ii.b

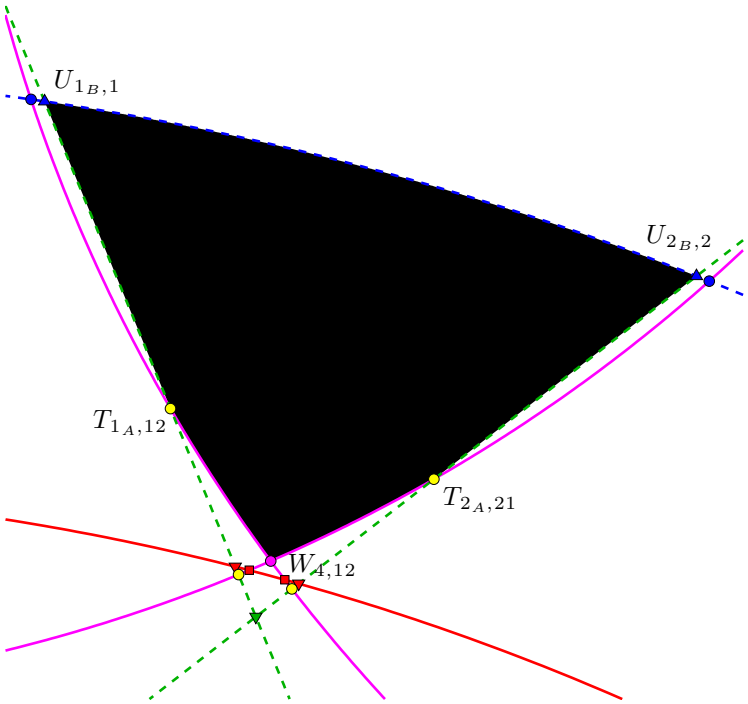

Figure B.15: Case 5.iii

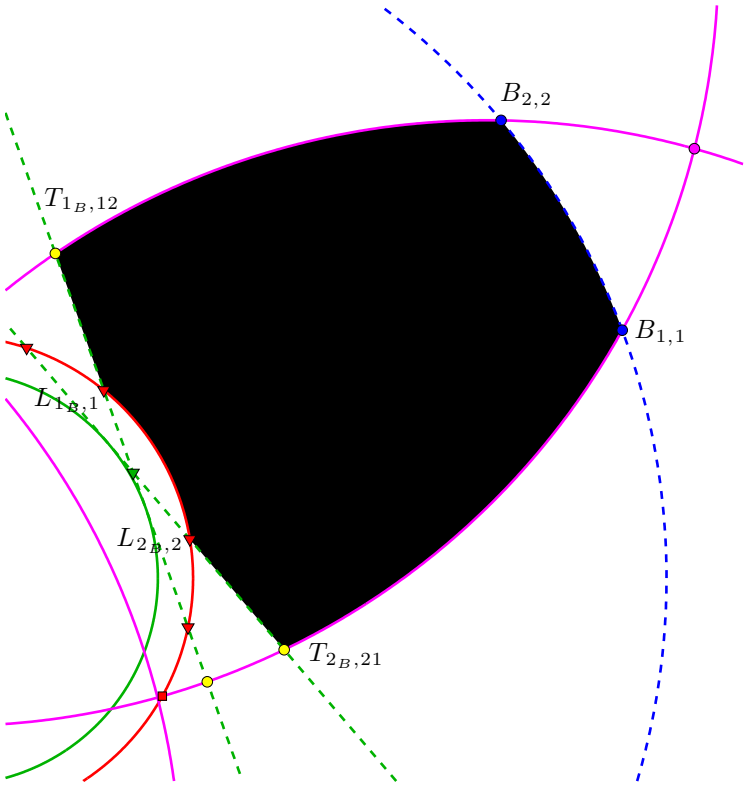

Figure B.16: Case 6.i.a

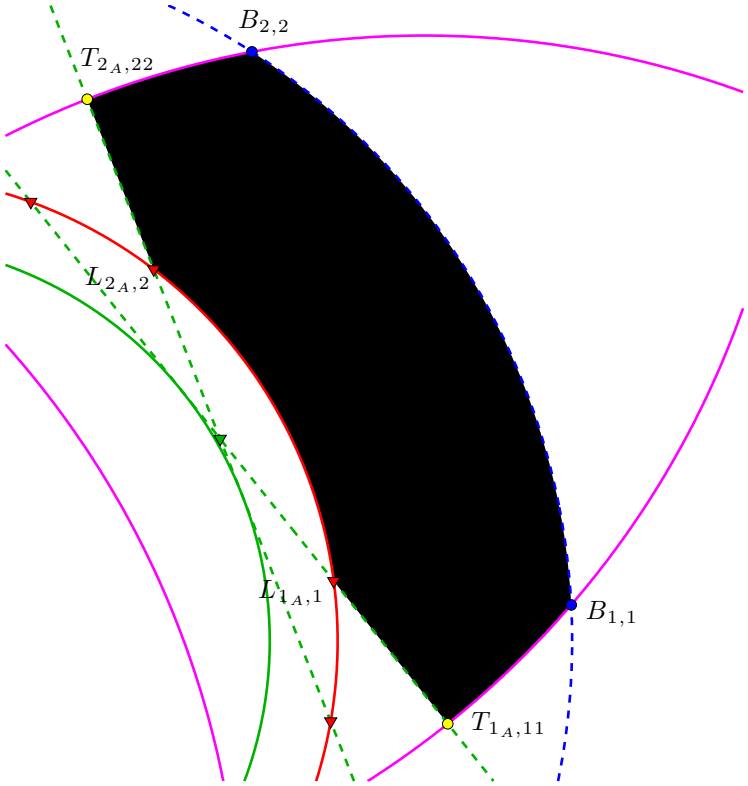

Figure B.17: Case 6.i.b

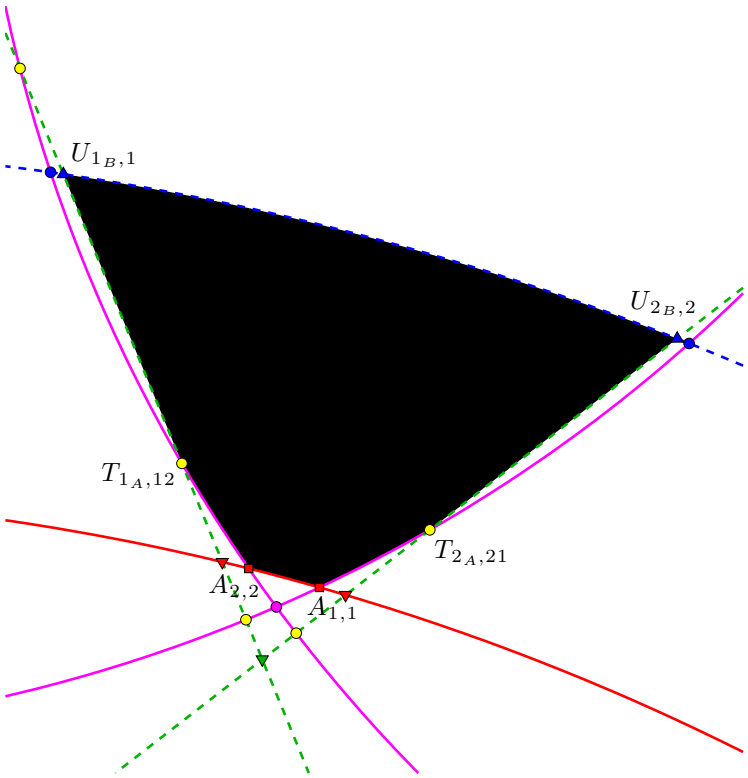

Figure B.18: Case 6.ii

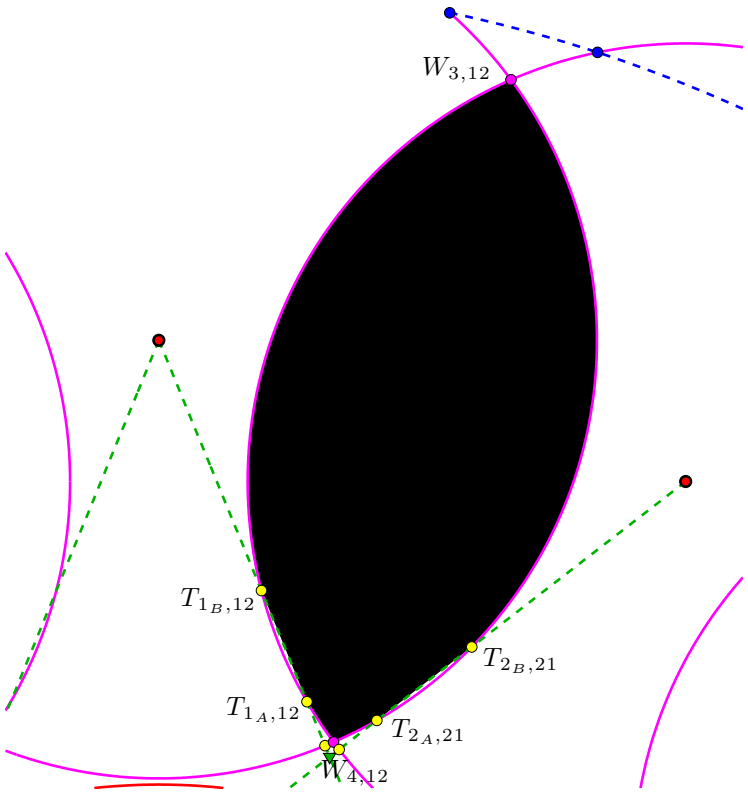

Figure B.19: Case 6.iii

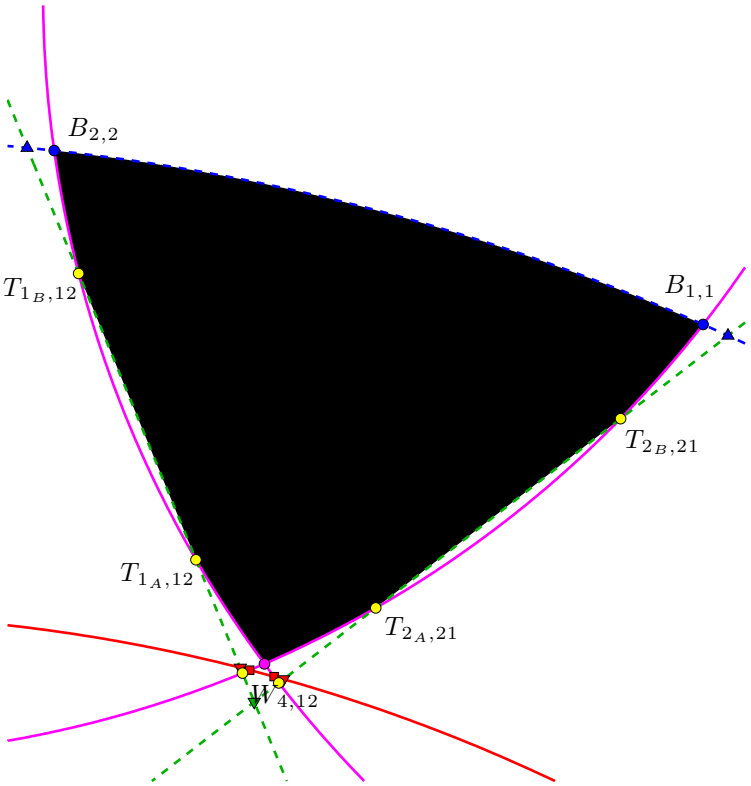

Figure B.20: Case 7.i

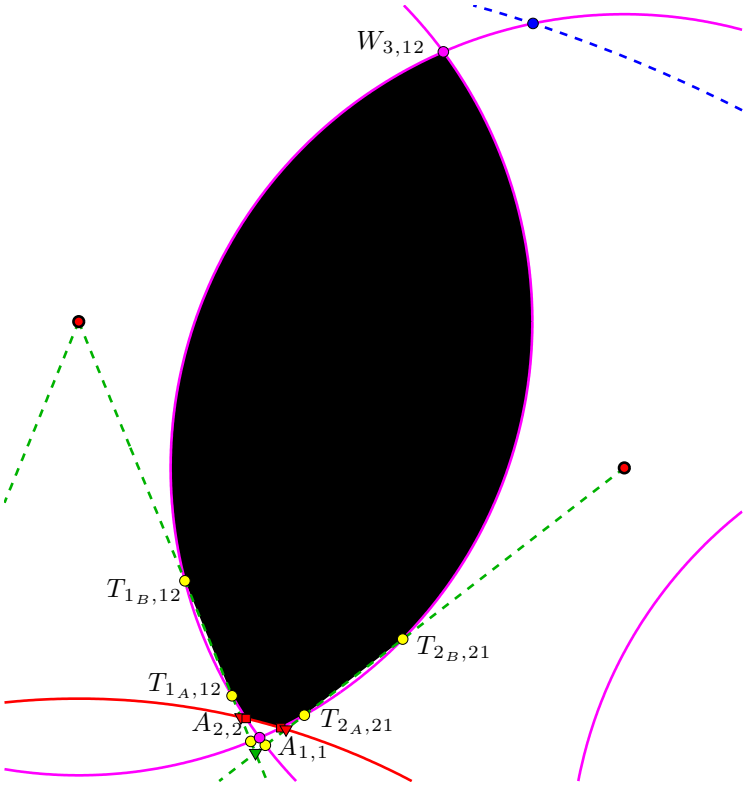

Figure B.21: Case 7.ii

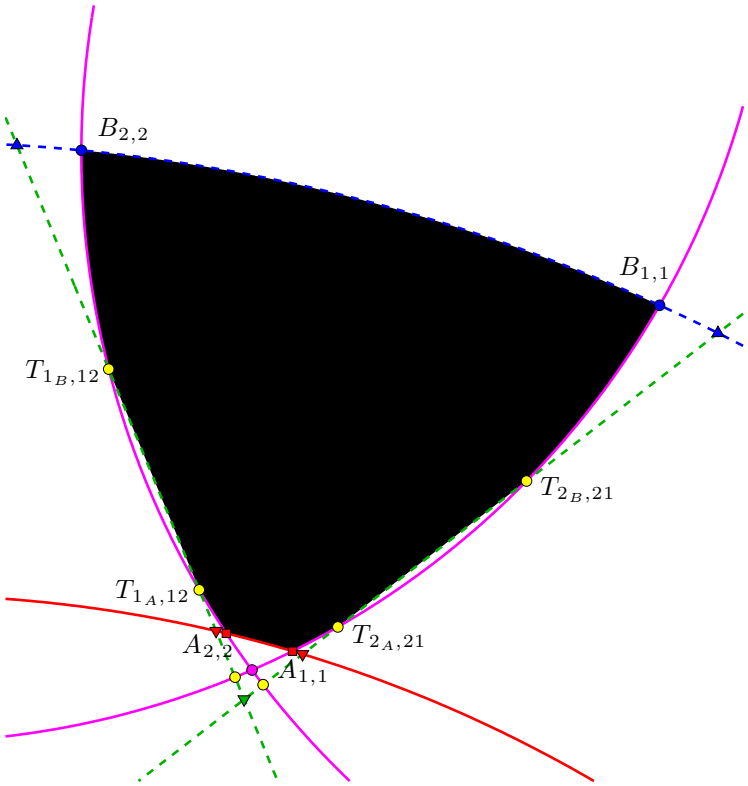

Figure B.22: Case 8

Appendix C

Derivation: Determining the Location of Q_p

Recall that the conditions in Tables 2.7–2.8 are divided into three major cases, each of which is a range of satellite altitude: $r_t \leq r_s < r_l$, $r_l \leq r_s < r_u$, and $r_u \leq r_s < r_{s_3}$. The easiest conditions to derive of the three satellite altitude ranges are in the range $r_t \leq r_s < r_l$. In fact, these conditions are the same for even and odd p. When the satellites are below the LTAS, intuition tells us that Q_p is located on the LTAS because, for example, 2-fold coverage would be created when $|\overline{OW_{3,12}}| > r_l$ in most circumstances. This implies

$$Q_p = \begin{cases} \left(r_l \sin\frac{\pi}{n}, r_l \cos\frac{\pi}{n}\right) & p \text{ even} \\ (0, r_l) & p \text{ odd} \end{cases} \tag{C.1}$$

In other words, a satellite's range shell need only be large enough for 2-fold coverage to occur. But the statement does not hold true when p increases beyond a certain point. Consider how $D_{21,\iota\kappa}$ varies for odd p, for instance. Figure C.1 attempts to illustrate geometrically how the location of $D_{21,\iota\kappa}$ changes by displaying the relevant TLs with progressively darker shades of green as p increases from 3. This particular image uses $n = 25$ because it provides the most clarity for explaining the point being made. There are two dramatic changes that can occur in the behavior and location

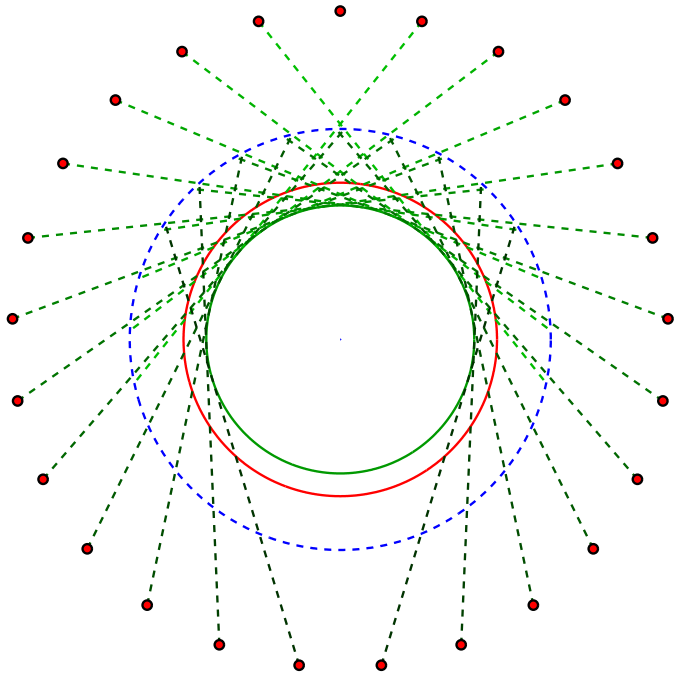

Figure C.1: For odd p, shows tangent lines associated with $D_{21,\iota\kappa}$, which moves first down the $\hat{\mathbf{y}}$-axis and then up the $\hat{\mathbf{y}}$-axis as p increases ($n = 25$)

of $D_{21,\iota\kappa}$, and they happen under the following conditions:

$$m_{2,\iota} = m_{1,\kappa}; \quad b_{2,\iota} = b_{1,\kappa} \quad \text{collinear TLs} \tag{C.2}$$

$$m_{2,\iota} = m_{1,\kappa}; \quad b_{2,\iota} \neq b_{1,\kappa} \quad \text{parallel but not collinear TLs} \tag{C.3}$$

which are derived from Eqs. (2.33–2.34). Eq. (C.2) is satisfied when the TLs are collinear (approximately $\iota = 6$ and $\kappa = 21$ in Figure C.1); Eq. (C.3) is satisfied when the TLs are parallel but not collinear (approximately $\iota = 12$ and $\kappa = 15$ in

Figure C.1). At first, as p increases from $p = 3$, $D_{21,\iota\kappa}$ moves down the $\hat{\mathbf{y}}$-axis until the theoretical geometry in Eq. (C.2) is reached such that the TLs are collinear. As p increases further, $D_{21,\iota\kappa}$ then begins to move up until the theoretical geometry in Eq. (C.3) is reached such that the TLs are parallel but not collinear. This is the only scenario for which $D_{21,\iota\kappa}$ does not exist. Beyond this value of p, computing $D_{21,\iota\kappa}$ from Eq. (2.32) would actually give a negative y-coordinate that slowly increases as it approaches the satellite altitude, which would be the theoretical limit. This limit is only close to attainable when the S_ι and S_κ pair with the most negative y-coordinates are extremely close to the THS or when n is unrealistically large so that the satellite separation angle, θ_s, is small. However, for the purposes of ascertaining the state of p-fold coverage, it is only important to observe that for these higher values of p (beyond the state defined by Eq. (C.3)), p-fold coverage does not exist for any R. Figure C.2 clearly shows how $D_{21,\iota\kappa}$ varies for odd p by plotting the y-coordinate as a function of coverage multiplicity.

With the preceding discussion in mind, it should be clear that $D_{21,\iota\kappa}$ has a role in determining where Q_p is located for any satellite altitude range and for both even and odd p. What makes the lowest satellite altitude range easy for analysis is that the entire region AS is above the horizon of the satellites. In other words, satellite location is not important within this range. The key to understanding the conditions for $r_t \leq r_s < r_l$ is that Eq. (C.1) is only valid in this range if part of the region above the horizon of S_ι and S_κ is below the LTAS. This condition can be expressed as

$$|\overline{OD_{21,\iota\kappa}}| \leq r_l \tag{C.4}$$

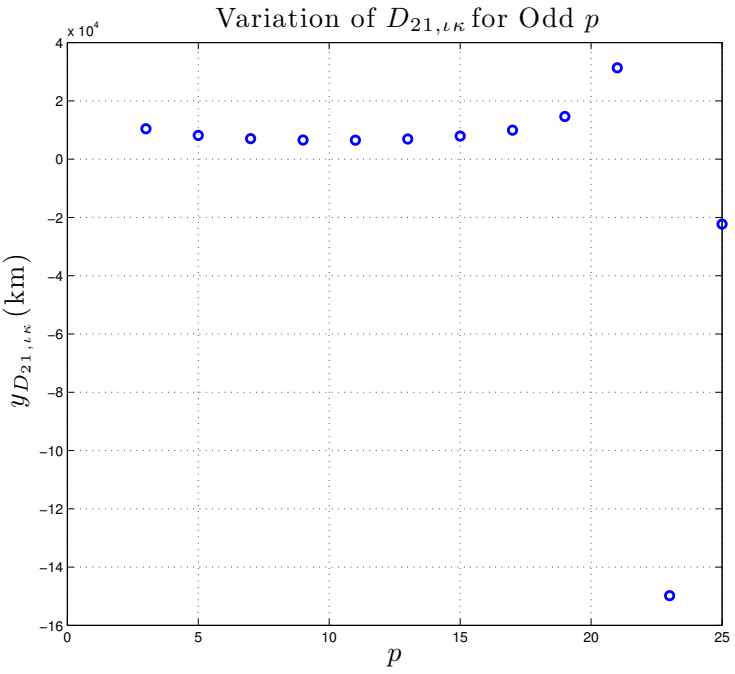

Figure C.2: Evidence that $D_{21,\iota\kappa}$ does not monotonically increase along the $\hat{\mathbf{y}}$-axis as p increases ($n = 25$, odd p)

which also says that $D_{21,\iota\kappa}$ is below the LTAS. If Eq. (C.4) is not satisfied, then

$$r_l < |\overline{OD_{21,\iota\kappa}}| \tag{C.5}$$

is satisfied and it follows that

$$Q_p = D_{21,\iota\kappa} \tag{C.6}$$

Realize that careful attention is given throughout this derivation to comparing radial distances to radial distances and coordinates to coordinates. Clearly, Eqs. (2.33) and (C.5) cannot be satisfied simultaneously for this satellite altitude range, so analysis of this altitude range is complete.

At this juncture, it is more logical to complete the derivation of these conditions for even p first because these conditions are more straightforward to derive. For the next satellite altitude range $r_l \leq r_s < r_u$, the location of $M_{\iota\kappa}$ is crucial; the same is actually true for the entire range $r_l \leq r_s < r_{s_3}$, whenever the satellites are above the LTAS. In fact, if

$$y_{M_{\iota\kappa}} \leq r_l \cos\frac{\pi}{n} \tag{C.7}$$

is satisfied, then the same conditions for $r_t \leq r_s < r_l$ (Eqs. (C.4) and (C.5)) apply with a modification. The modification is understood from Figures C.1 and C.2 and applies to almost all remaining conditions for even p: almost all candidate Q_p intersection points must be compared in some way to $D_{21,21}$ for $p > 2$. This is because $D_{21,\iota\kappa}$ could be below or above $D_{21,21}$. Let the term "pairs of interest" refer to the (S_ι, S_κ) pair and all preceding pairs. If $D_{21,\iota\kappa}$ is above $D_{21,21}$, then the region above the horizon of the (S_ι, S_κ) pair is above the horizon of all preceding pairs since $D_{21,\iota\kappa}$ has the greatest altitude of all pairs of interest. If $D_{21,\iota\kappa}$ is below $D_{21,21}$, then this is no longer the case. Instead, the region above the horizon of all pairs of interest must be above the horizon of the (S_2, S_1) pair since $D_{21,21}$ has the greatest altitude of all pairs of interest. It is interesting to note that if $D_{21,\iota\kappa}$ is below $D_{21,2n}$ and $|\overline{OD_{21,2n}}| \geq r_u$, as shown in Figure C.1 (or if $D_{21,\iota\kappa}$ is below $D_{21,21}$ and $|\overline{OD_{21,21}}| \geq r_u$), then the entire necessary and sufficient condition scheme breaks down in the sense that testing for p-fold coverage would not correspond to the expected satellite pair determined by Eqs. (2.75–2.76); the (S_ι, S_κ) pair would actually be offset according to how many preceding $D_{21,\iota\kappa}$ intersections are outside the UTAS. While this is an important observation, realize that it does not invalidate

the results because this scenario actually violates the assumption that this derivation considers coverage multiplicity strictly between adjacent satellites. If $D_{21,2n} \geq r_u$ for odd p or $D_{21,21} \geq r_u$ for even p, then it is *impossible* to provide coverage by adjacent satellites for $p \geq 2$. The previous statement is only true for those two satellite pairs, and even applies for $n = 2$ or $n = 3$.

Consider the scenario when $|\overline{OD_{21,\iota\kappa}}| \leq r_l$. Several subcases are possible. If

$$|\overline{OD_{21,21}}| \leq r_l \tag{C.8}$$

is also satisfied, then the region above the horizon of the (S_2, S_1) pair is above the horizon of all satellite pairs of interest and Eq. (C.1) applies. It does not matter whether $y_{D_{21,\iota\kappa}}$ is greater than or less than $y_{D_{21,21}}$. Alternatively, if

$$r_l < |\overline{OD_{21,21}}| \tag{C.9}$$

is satisfied, then the region above the LTAS is not above the horizon of all pairs of interest. Thus,

$$Q_p = D_{21,21} \tag{C.10}$$

since only the region above the horizon of the (S_2, S_1) pair — not the entire region above the LTAS — is above the horizon of all satellite pairs of interest and within the region AS. It turns out, in this case, that $y_{D_{21,\iota\kappa}} < y_{D_{21,21}}$, though it is not really relevant. If, instead, $r_l < |\overline{OD_{21,\iota\kappa}}|$, then direct comparison between $y_{D_{21,\iota\kappa}}$ and $y_{D_{21,21}}$ is essential because depending on where $y_{D_{21,\iota\kappa}}$ falls in the curve in Figure C.2, $y_{D_{21,\iota\kappa}}$ could be greater than or less than $y_{D_{21,21}}$. The region above the horizon of all satellite pairs of interest is equivalent to the region above the horizon

of whichever one of these two intersections has a greater y-coordinate. Thus,

$$Q_p = \begin{cases} D_{21,\iota\kappa} & \text{if } y_{D_{21,21}} \leq y_{D_{21,\iota\kappa}} \\ D_{21,21} & \text{if } y_{D_{21,\iota\kappa}} < y_{D_{21,21}} \end{cases} \tag{C.11}$$

If the midpoint $M_{\iota\kappa}$ is instead located such that

$$r_l \cos\frac{\pi}{n} < y_{M_{\iota\kappa}} \tag{C.12}$$

then $D_{21,\iota\kappa}$ is clearly below or equal to $D_{21,21}$, since S_ι and S_κ must be in the first quadrant for Eq. (C.12) to hold. In other words, the region above the horizon of $D_{21,21}$ is above the horizon of all satellite pairs of interest. Therefore, if $y_{D_{21,21}} \leq y_{M_{\iota\kappa}}$, then $M_{\iota\kappa}$ is in the region of interest, which means that for this particular scenario, Eq. (2.56) is both a necessary *and* sufficient condition for p-fold coverage when coupled with Eqs. (2.57–2.60). To show this, use Eqs. (2.68) and (2.80) with $Q_p = M_{\iota\kappa}$:

$$\begin{aligned} d_p &< R \\ |\overline{Q_p S_\iota}| &< R \\ |\overline{M_{\iota\kappa} S_\iota}| &< R \\ \frac{1}{2} d_{\iota\kappa} &< R \\ d_{\iota\kappa} &< 2R \end{aligned}$$

The result is identical to Eq. (2.56). Conversely, if $y_{M_{\iota\kappa}} < y_{D_{21,21}}$, then Eq. (C.10) applies. Thus, Q_p is equal to whichever of $D_{21,21}$ and $M_{\iota\kappa}$ is at a higher altitude:

$$Q_p = \begin{cases} M_{\iota\kappa} & \text{if } y_{D_{21,21}} \leq y_{M_{\iota\kappa}} \\ D_{21,21} & \text{if } y_{M_{\iota\kappa}} < y_{D_{21,21}} \end{cases} \tag{C.13}$$

For the final satellite altitude range $r_u \leq r_s < r_{s_3}$, it should be evident and not surprising that the same conditions and equations given in Eq. (C.7–C.13) still apply, as was hinted earlier, except that Eq. (C.12) must be modified to

$$r_l \cos\frac{\pi}{n} < y_{M_{\iota\kappa}} < r_u \cos\frac{\pi}{n} \tag{C.14}$$

since the satellite altitude range allows for $M_{\iota\kappa}$ to be outside the UTAS. In fact,

$$r_u \cos\frac{\pi}{n} \leq y_{M_{\iota\kappa}} \tag{C.15}$$

is the final condition for even p in determining the location of Q_p. If Eq. (C.15) is satisfied, then $y_{D_{21,21}} \leq y_{M_{\iota\kappa}}$ is implied because the necessary condition given by Eq. (2.57) must be satisfied. Thus, no comparison to $D_{21,21}$ is shown in the row of Table 2.8 corresponding to Eq. (C.15). In this scenario, however, $M_{\iota\kappa}$ is not in the region of interest even though it is at a higher altitude, setting this case apart from Eq. (C.13). This is a situation where it must be determined whether $W_{4,\iota\kappa}$ is below point Q_p in the sense that $x_{W_{4,\iota\kappa}} < x_{Q_p}$. Thus,

$$Q_p = \left(r_u \sin\frac{\pi}{n}, r_u \cos\frac{\pi}{n}\right) \tag{C.16}$$

Entirely different issues arise when considering the satellite altitude range $r_l \leq r_s < r_u$ for odd p. First, observe that $M_{\iota\kappa}$ is always below the satellite altitude. Next, define a new point $P_{2,1\iota}$, illustrated in Figures C.3 and C.4 for $\iota = 2$, as the intersection of the left TL of S_1 and a line emanating from S_ι that is perpendicular to the left TL of S_1. The coordinates of $P_{2,1\iota}$ are given by the solution to the following system of equations:

$$y_{P_{2,1\iota}} = m_{2,1} x_{P_{2,1\iota}} + y_{s_1}; \qquad y_{P_{2,1\iota}} = -\frac{1}{m_{2,1}} x_{P_{2,1\iota}} + b_{P_{2,1\iota}} \tag{C.17}$$

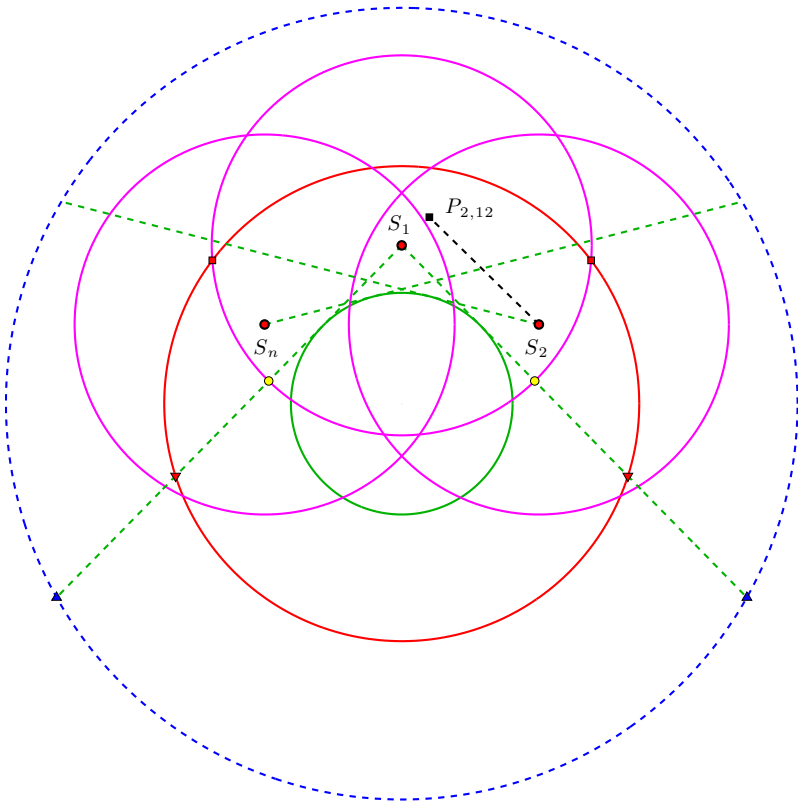

Figure C.3: Depiction of point $P_{2,12}$ with $y_{P_{2,12}} \geq r_s$ and $|\overline{P_{2,12}S_2}| < |\overline{S_1S_2}| < R$

where $b_{P_{2,1\iota}}$ is the y-coordinate of the point at which the line perpendicular to the right TL of S_1 intersects the $\hat{\mathbf{y}}$-axis, determined as

$$b_{P_{2,1\iota}} = y_{s_\iota} + \frac{1}{m_{2,1}} x_{s_\iota} \tag{C.18}$$

Setting the two equations in Eq. (C.17) equal to each other and rearranging, with $y_{s_1} = r_s$, gives

$$\left(m_{2,1} + \frac{1}{m_{2,1}}\right) x_{P_{2,1\iota}} + r_s = b_{P_{2,1\iota}} \tag{C.19}$$

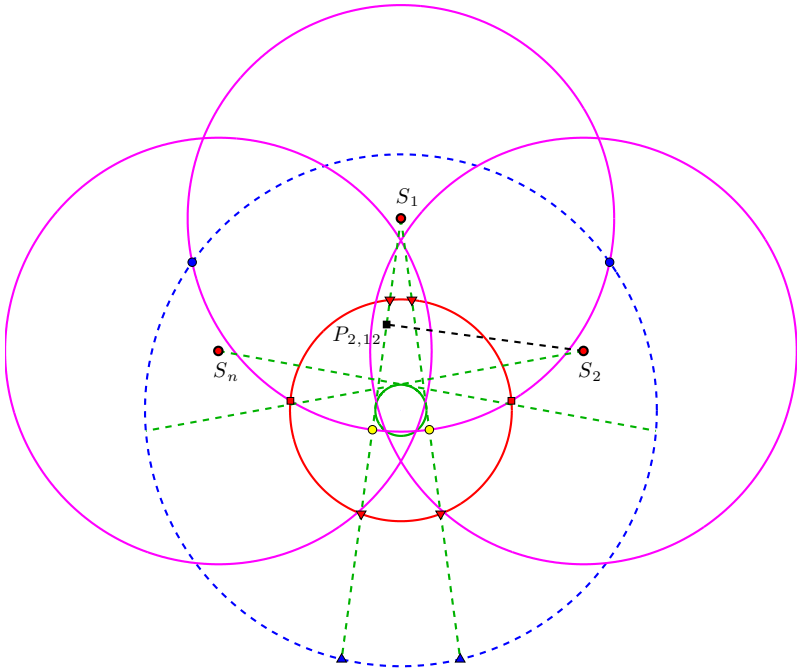

Figure C.4: Depiction of point $P_{2,12}$ with $y_{P_{2,12}} < r_s$ and $|\overline{P_{2,12}S_2}| < R < |\overline{S_1S_2}|$

Eq. (C.19) can be solved for $x_{P_{2,1\iota}}$ as

$$x_{P_{2,1\iota}} = \frac{m_{2,1}}{m_{2,1}^2 + 1} \left(b_{P_{2,1\iota}} - r_s \right) \tag{C.20}$$

Then, substituting Eq. (C.18) into Eq. (C.20) leads to

$$x_{P_{2,1\iota}} = \frac{m_{2,1}}{m_{2,1}^2 + 1} \left(\frac{x_{s_\iota}}{m_{2,1}} + y_{s_\iota} - r_s \right) \tag{C.21}$$

After determining the x-coordinate of $P_{2,1\iota}$ from Eq. (C.21), the y-coordinate can

then be computed from

$$y_{P_{2,1\iota}} = m_{2,1} x_{P_{2,1\iota}} + r_s \tag{C.22}$$

Now that $P_{2,1\iota}$ is defined, notice in Figures C.3–C.4 that the location of $P_{2,1\iota}$ and the distance $|\overline{P_{2,1\iota}S_\iota}|$ are crucial to determining p-fold coverage. First, note that the condition

$$|\overline{P_{2,1\iota}S_\iota}| \leq |\overline{S_1S_\iota}| \tag{C.23}$$

always holds because $|\overline{S_1S_\iota}|$ is the hypotenuse of the triangle $S_\iota P_{2,1\iota} S_1$. Obviously, in the degenerate case when $|\overline{P_{2,1\iota}S_\iota}| = |\overline{S_1S_\iota}|$, there is no triangle formed — only a line, because $P_{2,1\iota}$ collapses onto S_1. Secondly, observe that if

$$y_{P_{2,1\iota}} \geq r_s \tag{C.24}$$

and

$$|\overline{OD_{21,\iota\kappa}}| \leq r_s \tag{C.25}$$

then the region above the horizon of all satellite pairs of interest overlaps with the region above the horizon of S_1, creating p-fold coverage for odd p. Thus,

$$Q_p = S_1 \tag{C.26}$$

While the behavior illustrated in Figure C.2 occurs, it is not important for this scenario because it is always true that

$$y_{D_{21,2n}} < r_s \tag{C.27}$$

If, instead,

$$r_s < |\overline{OD_{21,\iota\kappa}}| \tag{C.28}$$

is satisfied, then only the region above the horizon of the (S_ι, S_κ) pair is above the horizon of all satellite pairs of interest, so Eq. (C.6) applies ($Q_p = D_{21,\iota\kappa}$).

Earlier in the derivation, it states that, in general, the changes in intersection points occur along the bisector of a line segment $\overline{S_2 S_n}$ for odd p. This has been the case so far, but the exception to this rule appears in the remaining few conditions. Consider the case when

$$y_{P_{2,1\iota}} < r_s \tag{C.29}$$

Now, it is possible for

$$|\overline{P_{2,1\iota} S_\iota}| < R < |\overline{S_1 S_\iota}| \tag{C.30}$$

to be satisfied while still achieving p-fold coverage whereas before, when $r_s \leq y_{P_{2,1\iota}}$, p-fold coverage is only possible if

$$|\overline{P_{2,1\iota} S_\iota}| \leq |\overline{S_1 S_\iota}| < R \tag{C.31}$$

is satisfied. The easiest way to continue is to just write the conditions required without giving thought to the concept of coverage threshold, which was used previously. It is evident from Figure C.3 that

$$r_l < |\overline{OT_{2_B,1\iota}}| \tag{C.32}$$

must be satisfied so that the region of p-fold coverage is within the region AS, and that

$$\begin{cases} |\overline{OD_{21,1n}}| < |\overline{OT_{2_B,1\iota}}| & \text{if } y_{D_{22,\iota 1}} < y_{D_{21,1n}} \\ |\overline{OD_{22,\iota 1}}| < |\overline{OT_{2_B,1\iota}}| & \text{if } y_{D_{21,1n}} \leq y_{D_{22,\iota 1}} \end{cases} \tag{C.33}$$

must also be satisfied so that the region visible to S_1 is also visible to the (S_ι, S_κ) satellite pair and all other satellite pairs of interest. The conditions in Eq. (C.33)

are derived from Figure C.2 by observing that $D_{21,1n}$ is analogous to $D_{21,21}$ and that $D_{22,\iota 1}$ is analogous to $D_{21,\iota\kappa}$. This occurs because of how certain D intersections move along the left TL of S_1 (symmetric intersections move in the same way along the right TL of S_1). First, realize that the point $D_{21,1n}$ is associated with S_κ. For $y_{s_\kappa} > r_t$, the slope of the right TL of S_κ is negative and the slope of the left TL of S_ι is positive, and, consequently, $y_{D_{22,\iota 1}} < y_{D_{21,1\kappa}}$. But for $y_{s_\kappa} < r_t$, the slopes of the respective TLs have reversed signs, so that $y_{D_{21,1\kappa}} \leq y_{D_{22,\iota 1}}$. From these arguments and Figures C.2 and C.3, it should be clear that $y_{D_{21,1\kappa}} \leq y_{D_{21,1n}}$ for all κ, so $y_{D_{21,1n}}$ need only be compared against $y_{D_{22,\iota 1}}$. Eq. (C.33) will likely only be violated for higher coverage multiplicities.

For odd p, when the satellite altitude range is $r_u \leq r_s < r_{s_3}$, p-fold coverage is only possible when Eq. (C.30) (the exception to the rule) is satisfied simply because now the region above S_1 is also above the UTAS and thus outside the region AS. It turns out that the conditions in Eqs. (C.32–C.33) are still valid, except that the condition designed to ensure that the region of p-fold coverage is within the region AS must be modified. These modifications only involve T intersections and their positions relative to the LTAS and UTAS. If

$$r_u < |\overline{OT_{2_B,1\iota}}| \tag{C.34}$$

is satisfied, then

$$|\overline{OT_{2_A,1\iota}}| < r_u \tag{C.35}$$

is also required, and Eq. (C.32) is automatically satisfied. If Eq. (C.34) is not satisfied and instead

$$r_u > |\overline{OT_{2_B,1\iota}}| \tag{C.36}$$

holds, then Eq. (C.32) must also be satisfied. If

$$r_u = |\overline{OT_{2_B,1\iota}}| \tag{C.37}$$

is satisfied, then both Eqs. (C.32) and (C.35) are automatically satisfied.

Converting Eqs. (C.29–C.37) to the coverage threshold representation is much less challenging upon realizing that the threshold conditions are analogous in every way — with $P_{2,1\iota}$ replacing $M_{\iota\kappa}$ — to the satellite altitude range $r_l \leq r_s < r_{s_3}$ for even p with one exception: The condition chains beginning with $y_{L_{2_B},1} \leq y_{P_{2,1\iota}} < r_s$ for $r_l \leq r_s < r_u$ and $y_{L_{2_B},1} \leq y_{P_{2,1\iota}} < y_{U_{2_B},1}$ for $r_u \leq r_s < r_{s_3}$ cannot be simplified. Previously, with reference to Eq. (C.12) for even p, the statement could be made that $D_{21,\iota\kappa}$ is clearly below or equal to $D_{21,21}$, since S_ι and S_κ must be in the first quadrant, so $D_{21,\iota\kappa}$ had no effect on the coverage threshold. But the analogous statement for odd p would be that $D_{22,\iota 1}$ is clearly below or equal to $D_{21,1n}$, which is false. Rather, $P_{2,1\iota}$ must be compared against $D_{22,\iota 1}$. Furthermore, notice that $y_{L_{2_B},1}$ and $y_{U_{2_B},1}$ are used instead of $r_l \cos\frac{\pi}{n}$ and $r_u \cos\frac{\pi}{n}$ to compare y-coordinates of other points against the LTAS and UTAS, respectively. This is because for even p, the points being compared to the LTAS and UTAS vary radially with satellite altitude, whereas for odd p, the points being compared to the LTAS and UTAS vary along the left TL of S_1 as satellite altitude varies.

Analogous arguments used to derive Eqs. (C.8–C.11) lead to the following conditions. If

$$y_{D_{22,\iota 1}} \leq y_{P_{2,1\iota}} \tag{C.38}$$

is satisfied, then $D_{21,1n}$ must still be compared against $P_{2,1\iota}$ to determine Q_p. If

$$y_{D_{21,1n}} \leq y_{P_{2,1\iota}} \tag{C.39}$$

then

$$Q_p = P_{2,1\iota} \tag{C.40}$$

Otherwise,

$$y_{D_{21,1n}} > y_{P_{2,1\iota}} \tag{C.41}$$

must be satisfied instead of Eq. (C.39), requiring the threshold

$$Q_p = D_{21,1n} \tag{C.42}$$

Similarly, if Eq. (C.38) is not satisfied, then

$$y_{D_{22,\iota 1}} > y_{P_{2,1\iota}} \tag{C.43}$$

must be satisfied instead, and $D_{22,\iota 1}$ must then also be compared against $D_{21,1n}$. If

$$y_{D_{21,1n}} \leq y_{D_{22,\iota 1}} \tag{C.44}$$

then the threshold becomes

$$Q_p = D_{22,\iota 1} \tag{C.45}$$

Otherwise, Eq. (C.42) applies. Eqs. (C.38–C.45) are the result of transforming the formulation in Eqs. (C.29–C.37) to one involving the threshold concept, which requires defining Q_p.

Lastly, for the satellite altitude range $r_l \leq r_s < r_u$, it is also helpful to discuss one of the finer details of the first condition in each of the three chains.

First, note that the chain beginning with Eq. (C.24) ($r_s \leq y_{P_{2,1\iota}}$) does not have an analogous counterpart for even p. Since no satellite is located on the bisector of $\overline{S_1 S_2}$, satellite altitude has no direct impact on the coverage threshold for even p. But satellite altitude does for odd p because S_1 is located on the bisector of $\overline{S_2 S_n}$. Each of the three chains is concerned with how $P_{2,1\iota}$, $L_{2_B,1}$, and r_s are related to each other, specifically the y-coordinates. It is valid to compare $y_{P_{2,1\iota}}$ and $y_{L_{2_B,1}}$ to the radial distance r_s because r_s is also the y-coordinate of S_1. The other two chains are concerned with the case when Eq. (C.29) ($y_{P_{2,1\iota}} < r_s$) is satisfied. By definition, $y_{L_{2_B,1}} \leq r_s$, so this is not always explicitly stated in Table 2.7. This is also why there are only three and not six permutations of these inequalities:

$$y_{P_{2,1\iota}} < y_{L_{2_B,1}} \leq r_s \tag{C.46}$$

$$y_{L_{2_B,1}} \leq y_{P_{2,1\iota}} < r_s \tag{C.47}$$

$$y_{L_{2_B,1}} \leq r_s \leq y_{P_{2,1\iota}} \tag{C.48}$$

where care is taken to ensure that only one of these conditions can be satisfied for some given geometry.

In addition to all of these preceding conditions relating to the coverage threshold, recall that Eq. (2.33) may need to be considered for even or odd p if any TLs of interest are collinear. But even if Eq. (2.33) were satisfied for any satellite altitude range, then $D_{21,\iota\kappa}$ and $M_{\iota\kappa}$ would be located on the THS — outside the region of interest. Thus, entries in the Q_p column of Tables 2.7–2.8 would be unchanged.

Appendix D

Relating the 22 Shape Types to Satellite Altitude

Figures D.1–D.10 correspond to Figures 3.1–3.7, respectively. It is not clear from Figures 3.1–3.7 that all 22 shape types for $\mathbf{A}'_{2\times,12}$ are validated because the graphs only illustrate the consistency in results. Therefore, Figures D.1–D.10 are given in this appendix to demonstrate that all 22 shape types are accounted for in the validation process. They also show patterns in the occurrence of certain shape types. For example, shape type 3.ii seems to always occur in the satellite altitude range after the altitude corresponding to maximum total coverage area. Shape type 0, as indicated in Figures D.1–D.10, refers to a situation in which 2-fold coverage does not exist. This happens when some or all of the conditions for identifying a particular shape type in Table 2.5 are not satisfied for each shape type. The maximum coverage area is indicated with a red circle on each of the following 10 figures. In three cases, the global maximum exists only at the start of the altitude range considered, a consequence of the constraint on the parameter space discussed in Section 3.1.

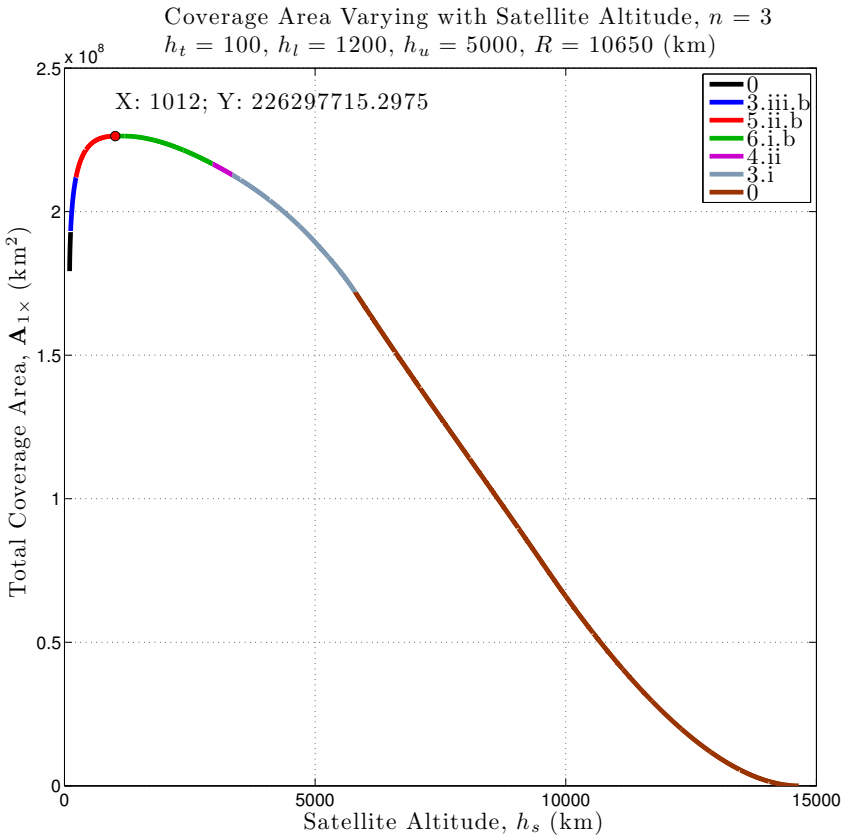

Figure D.1: Total coverage area vs. satellite altitude, five new cases: 3.iii.b, 5.ii.b, 6.i.b, 4.ii, 3.i

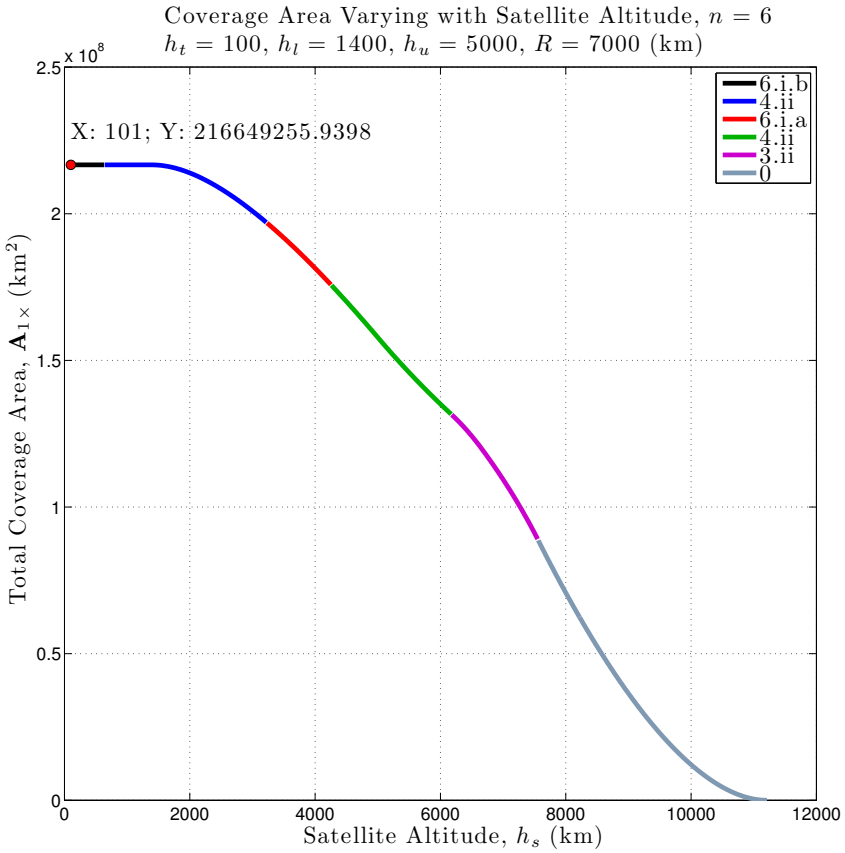

Figure D.2: Total coverage area vs. satellite altitude, two new cases: 6.i.a, 3.ii

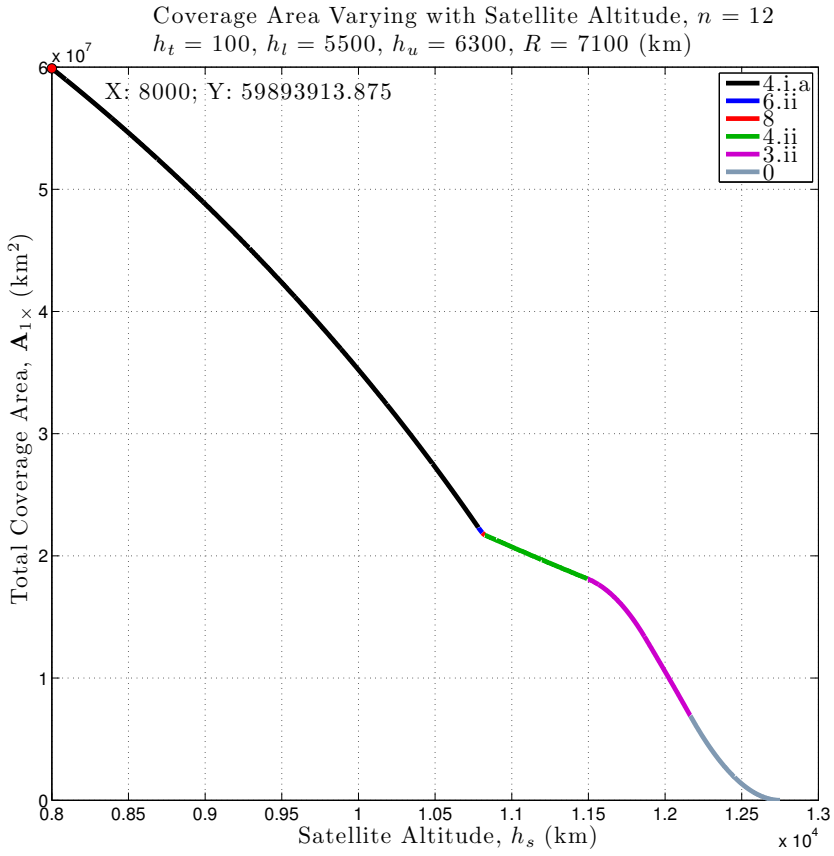

Figure D.3: Total coverage area vs. satellite altitude, three new cases: 4.i.a, 6.ii, 8

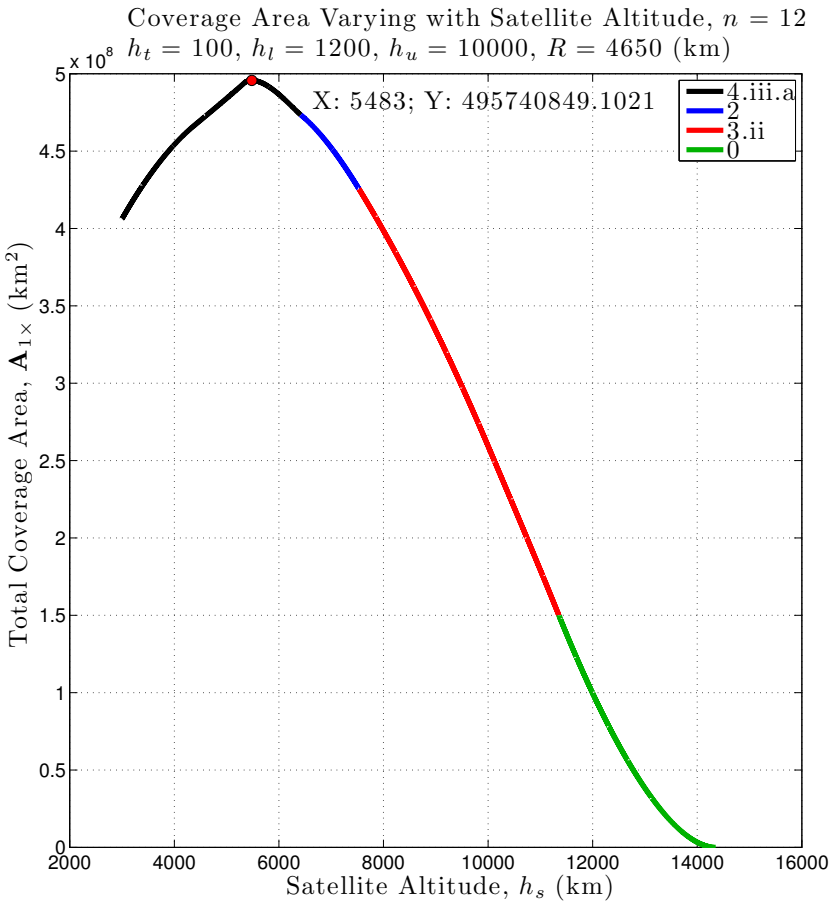

Figure D.4: Total coverage area vs. satellite altitude, two new cases: 4.iii.a, 2

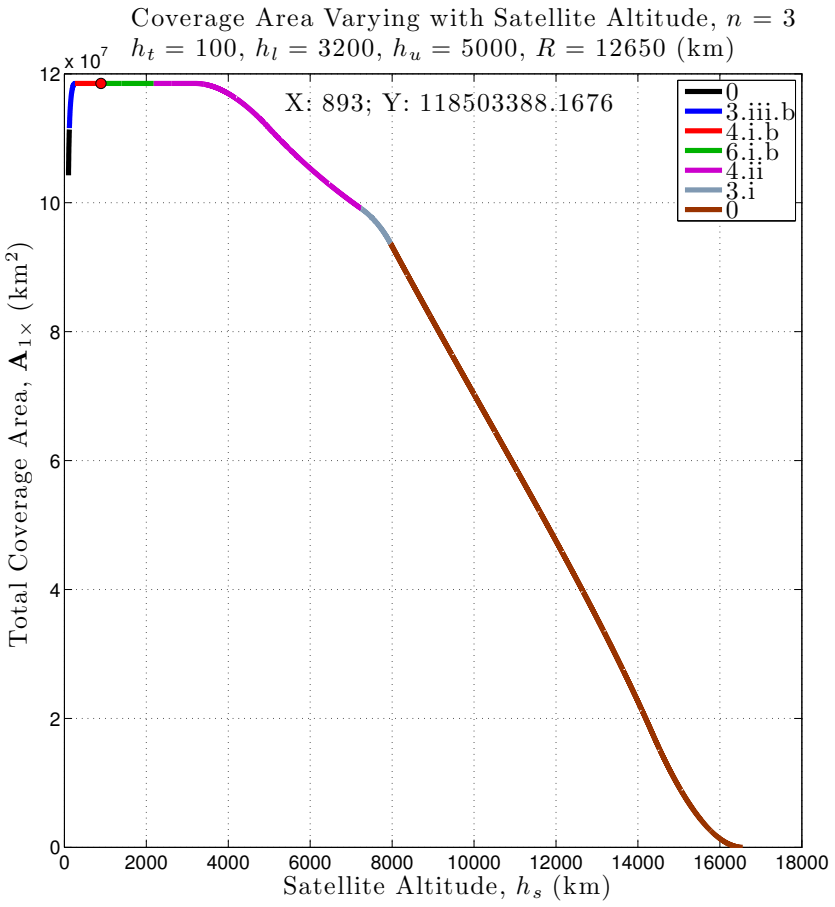

Figure D.5: Total coverage area vs. satellite altitude, one new shape: 4.i.b

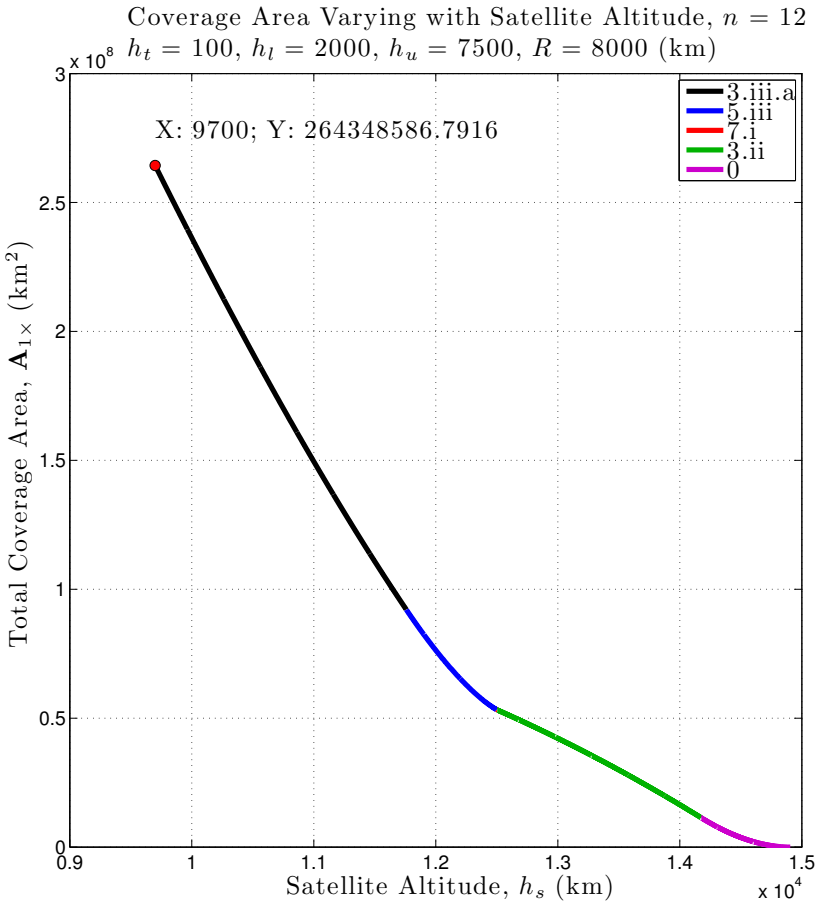

Figure D.6: Total coverage area vs. satellite altitude, three new cases: 3.iii.a, 5.iii, 7.i

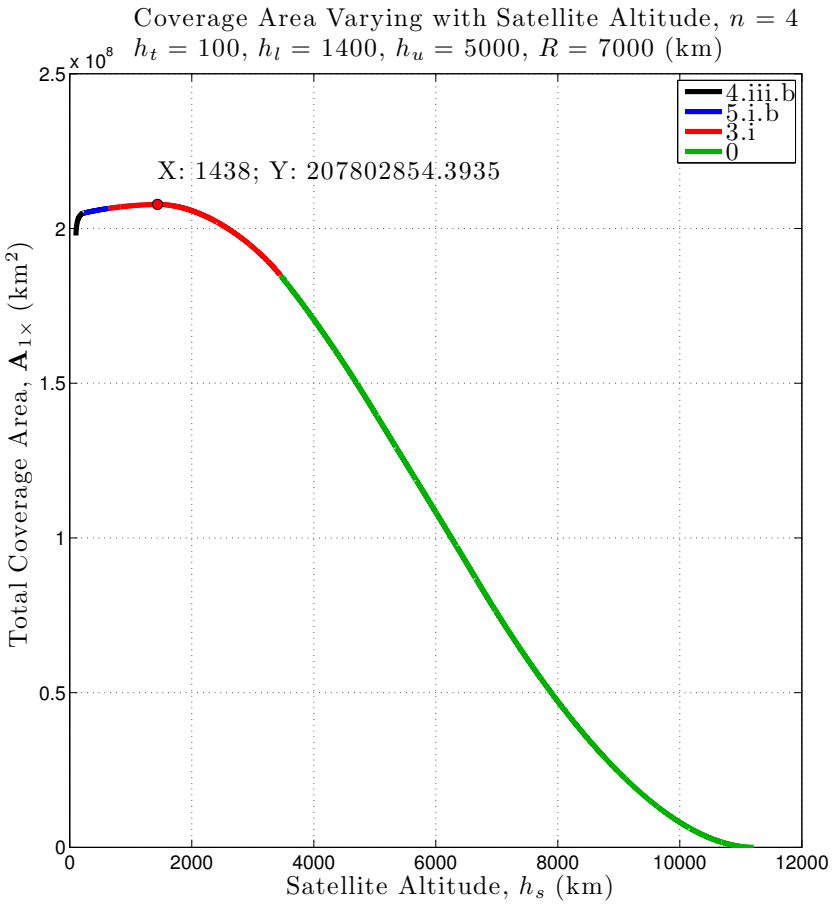

Figure D.7: Total coverage area vs. satellite altitude, two new cases: 4.iii.b, 5.i.b

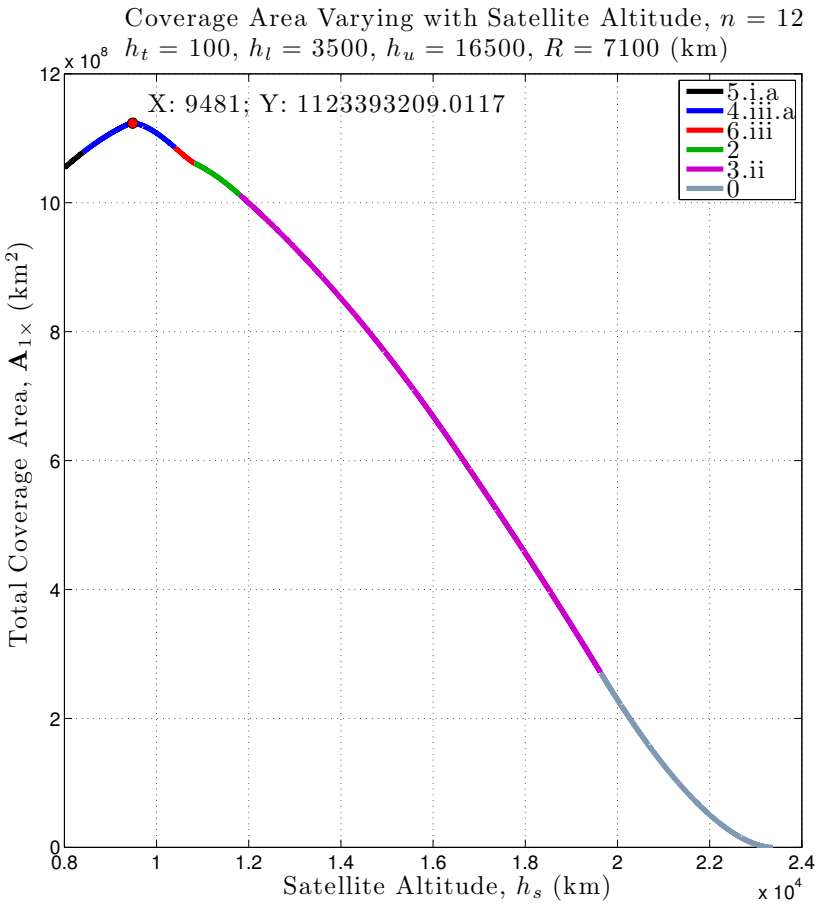

Figure D.8: Total coverage area vs. satellite altitude, two new cases: 5.i.a, 6.iii

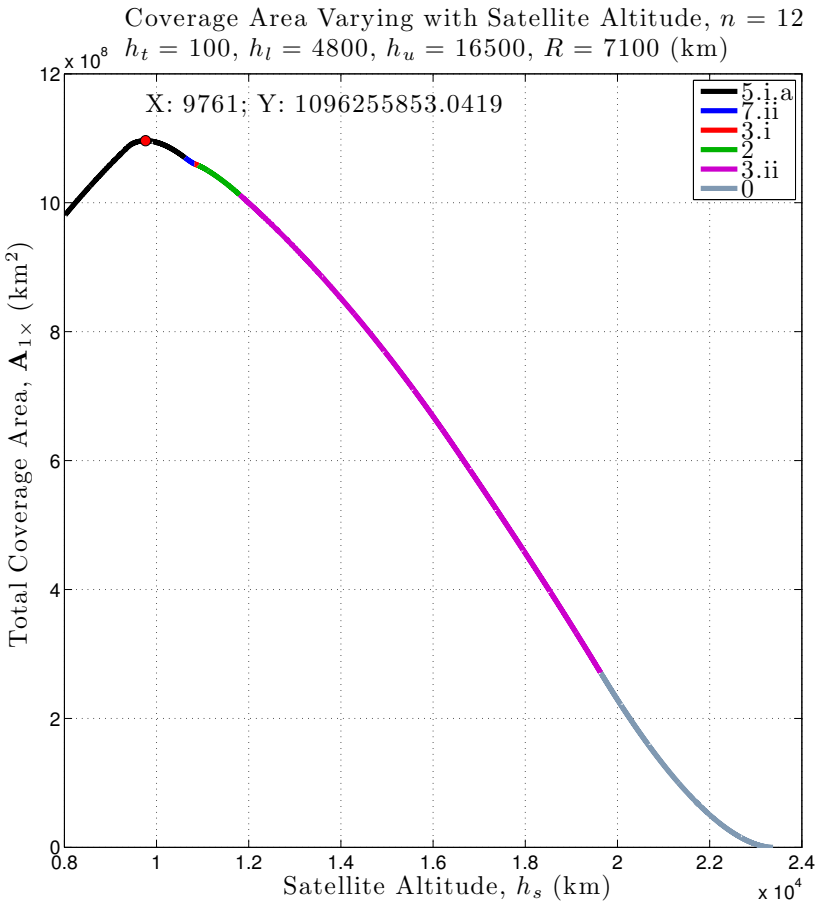

Figure D.9: Total coverage area vs. satellite altitude, one new shape: 7.ii

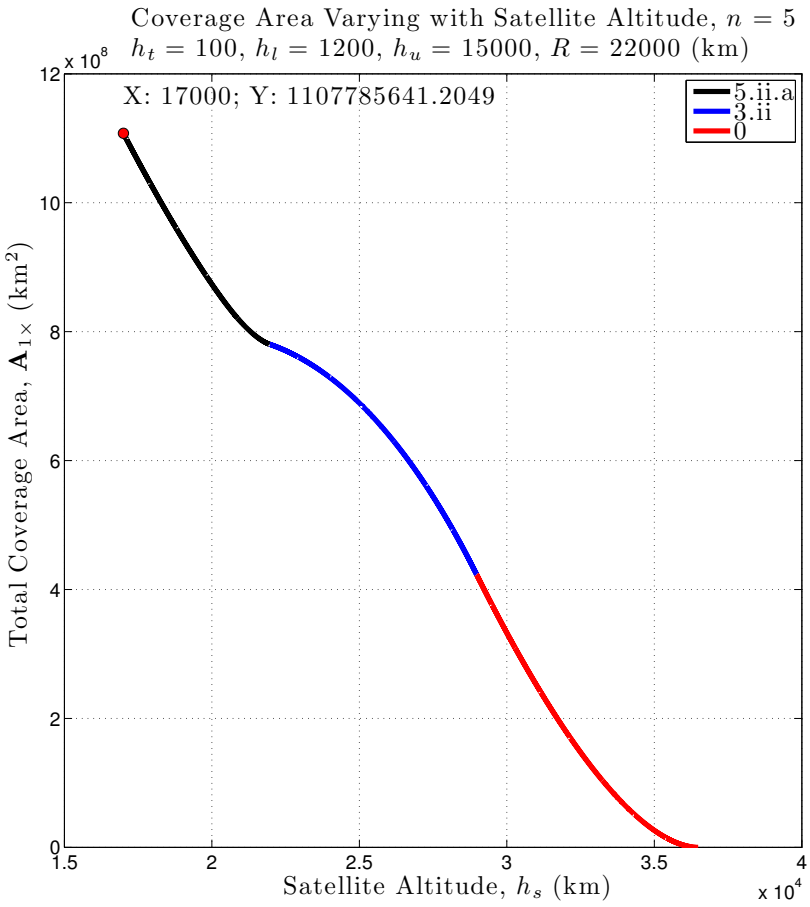

Figure D.10: Total coverage area vs. satellite altitude, one new shape: 5.ii.a

Bibliography

[1] Takano, A. T., *Numerical Analysis and Design of Satellite Constellations for Above the Horizon Coverage*, Master's thesis, Supervisor: Dr. Belinda G. Marchand, The University of Texas at Austin, December 2010.

[2] Lüders, R. D., "Satellite Networks for Continuous Zonal Coverage," *American Rocket Society Journal*, Vol. 31, No. 2, February 1961, pp. 179–184.

[3] Grinter, K., "NASA'S Tracking and Data Relay Satellite," http://www-pao.ksc.nasa.gov/kscpao/nasafact/tdrs.htm, Accessed October 25, 2011.

[4] Wertz, J. R. and Larson, W. J., editors, *Space Mission Analysis and Design*, Microcosm Press / Springer, 3rd ed., 1999.

[5] Misra, P. and Enge, P., *Global Positioning System: Signals, Measurements, and Performance*, Ganga-Jamuna Press, 2nd ed., 2006.

[6] Draim, J. E., "Three- and Four-Satellite Continuous-Coverage Constellations," *Journal of Guidance, Control, and Dynamics*, Vol. 8, No. 6, November–December 1985, pp. 725–730.

[7] Draim, J. E., "A Common-Period Four-Satellite Continuous Global Coverage Constellation," *Journal of Guidance, Control, and Dynamics*, Vol. 10, No. 5, September–October 1987, pp. 492–499.

[8] Draim, J. E., "Continuous Global N-Tuple Coverage with $(2N + 2)$ Satellites," *Journal of Guidance, Control, and Dynamics*, Vol. 14, No. 1, January–February 1991, pp. 17–23.

[9] Rider, L., "Optimal Orbital Constellations for Global Viewing of Targets against a Space Background," *Optical Engineering*, Vol. 19, No. 2, March/April 1980, pp. 219–223.

[10] Hanson, J. M. and Linden, A. N., "Improved Low-Altitude Constellation Design Methods," *Journal of Guidance, Control, and Dynamics*, Vol. 12, No. 2, March–April 1989, pp. 228–236.

[11] Gordon, K. J., "The Computation of Satellite Constellation Range Characteristics," *AIAA/AAS Astrodynamics Conference*, Scottsdale, AZ, August 1994, pp. 1–9.

[12] Beste, D. C., "Design of Satellite Constellations for Optimal Continuous Coverage," *IEEE Transactions on Aerospace and Electronic Systems*, Vol. AES-14, No. 3, May 1978, pp. 466–473.

[13] Adams, W. S. and Rider, L., "Circular Polar Constellations Providing Continuous Single or Multiple Coverage Above a Specified Latitude," *The Journal of the Astronautical Sciences*, Vol. 35, No. 2, April–June 1987, pp. 155–192.

[14] Walker, J. G., "Continuous Whole-Earth Coverage by Circular-Orbit Satellite Patterns," Tech. Rep. 77044, Royal Aircraft Establishment, March 1977.

[15] Rider, L., "Design of Low to Medium Altitude Surveillance Systems Providing Continuous Multiple Above-the-Horizon Viewing," *Optical Engineering*, Vol. 28, No. 1, January 1989, pp. 25–29.

[16] Marchand, B. G. and Kobel, C. J., "Above the Horizon Satellite Coverage with Dual-Altitude Band Constraints," *Journal of Spacecraft and Rockets*, Vol. 46, No. 4, July–August 2009, pp. 845–857.

[17] Takano, A. T. and Marchand, B. G., "Optimal Constellation Design for Space Based Situational Awareness Applications: A Numerical Approach," *Proceedings of the AAS/AIAA Astrodynamics Specialist Conference*, Girdwood, AK, August 2011.

[18] Fewell, M. P., "Area of Common Overlap of Three Circles," Tech. rep., Maritime Operations Div., Defence Science and Technology Organisation, October 2006, TN DSTO-TN-0722.

[19] Weisstein, E. W., "Quadrilateral," From MathWorld — A Wolfram Web Resource, http://mathworld.wolfram.com/Quadrilateral.html, Accessed July 4, 2011.

[20] Weisstein, E. W., "Bretschneider's Formula," From MathWorld — A Wolfram Web Resource, http://mathworld.wolfram.com/BretschneidersFormula.html, Accessed July 4, 2011.

Vita

Ashley Darius Biria was born in Seattle, Washington. He received the Bachelor of Science degree in Mechanical Engineering from Cornell University in May 2009. In August 2009, he entered graduate school in the Department of Aerospace Engineering and Engineering Mechanics at the University of Texas at Austin.

Permanent address: biria@utexas.edu

This thesis was typeset with LaTeX[†] by the author.

[†]LaTeX is a document preparation system developed by Leslie Lamport as a special version of Donald Knuth's TeX Program.